**Title**
Chlorophyll and Suspended Sediment Exchange between Central San Francisco Bay and the Coastal Pacific Ocean



**Author**
Martin, Maureen A.

**Publication Date**
2006

Peer reviewed

# Chlorophyll and Suspended Sediment Exchange between Central San Francisco Bay and the Coastal Pacific Ocean

by

Maureen Ann Martin

B.A. (Boston University) 2000
M.S. (University of California Berkeley) 2003

A dissertation submitted in partial satisfaction of the

requirements for the degree of

Doctorate of Philosophy

in

Engineering – Civil and Environmental Engineering

in the

Graduate Division

of the

University of California, Berkeley.

Committee in charge:

Professor Mark Stacey, chair

Professor James Hunt

Professor Thomas M. Powell

Fall 2006

# ABSTRACT

Chlorophyll and Suspended Sediment Exchange between Central San Francisco Bay and the Coastal Pacific Ocean

By

Maureen Ann Martin

Doctorate of Philosophy in Engineering – Civil and Environmental Engineering

University of California, Berkeley.

Professor Mark T. Stacey, chair

We measured suspended sediment and chlorophyll-a fluxes between San Francisco Bay and the coastal ocean for two days in March 2002, October/November 2002, and June 2003, one day during neap tide and one during spring tide. We applied a harmonic analysis to velocity and chlorophyll-a data to model scalar and velocity fields during a spring-neap cycle. We then integrated these modeled data over the fortnightly period to calculate net dispersive fluxes. The net flux consisted of an advective and a dispersive component. Dispersive flux was decomposed into physical mechanisms such as tidal pumping, steady circulation and unsteady circulation.

Net flux of both sediment and chlorophyll changed seasonally. The net chlorophyll flux was out of the bay during spring and fall, but in during summer. The net flux of suspended sediment was large and in during the fall and out during spring and summer. The direction of advective flux was always out of the estuary and the magnitude depended on advective speed and mean scalar concentration. Dispersive flux

was of similar magnitude as advective flux each season and changed direction seasonally. The dispersive flux was larger than the advective flux, contributing over 63% to the net flux of both scalars across season. Tidal pumping was the dominant dispersive process year round.

The dominance of tidal pumping implies that seasonal variability of ocean-estuary exchange is set almost entirely by variation in the east-west gradient of scalar concentrations between the ocean and the estuary. If concentrations are higher during flood tide compared to ebb tide, the tidal pumping flux will be into the estuary, whereas the converse is true if the concentration is higher on ebb tide.

The average chlorophyll and sediment concentrations are governed by different processes. During the summer while coastal upwelling occurs, chlorophyll concentration is higher in the ocean than in the estuary creating a gradient driven dispersive flux of coastal phytoplankton into the estuary. The opposite is true during spring when estuarine concentration is higher and the dispersive flux is driven out of the estuary. During fall there were relatively low gradients and the net dispersive chlorophyll flux was relatively small. The seasonal direction of chlorophyll fluxes measured in this study are consistent with physical and biological processes of a typical year, though, the magnitude and timing of these fluxes may change annually or inter-annually depending on the specific physical and biological conditions .

While the spatial and temporal distribution of favorable growth conditions determines the direction of the chlorophyll flux, growth within Central Bay plays a relatively small role in the local chlorophyll balance. Blooms or the accumulation of phytoplankton within Central Bay are limited by the large dispersive transport rates.

During times when the dispersive transport is small, such as fall, growth becomes relatively more important and local blooms could conceivably occur. However, when the dispersion is large, such as during spring and summer, most of the phytoplankton observed in Central Bay has been transported in from other basins, such as the coastal ocean or South Bay.

Although the net sediment flux was also dominated by tidal pumping, processes occurring at both longer and shorter timescales are important as well. The net sediment flux was out of the estuary during spring and summer, but was in during the fall. The direction of the fall flux is mostly driven by a large pulse of sediment that occurred during a maximum flood. We compared our fall flux results to tidal pumping fluxes estimated from a suspended sediment timeseries collected from 1996-1997 at the Golden Gate Bridge. These flux estimates were out of the estuary and similar in magnitude to our spring and summer flux calculations. From this longer record, we concluded that suspended sediment concentration is positively correlated with the absolute magnitude of velocity for all season. Because the system is ebb dominated, we can assume over sufficiently long times (> a year), that the flux is out of the estuary, but that there may be intermittent perturbations on shorter timescales. The average of these flux measurements compared to previously estimated inputs suggests that the amount of sediment entering the bay annually is balanced by the amount leaving.

# Acknowledgments

I would like to give my greatest thanks my research partner Jon Fram who helped collect and process all field data, especially for all of the MATLAB assistance he has given me over the years. I would also like to thank Nathaniel Hallinan for his moral support and his mathematical expertise. I would like to thank Mark Stacey, for his patience, inspiration, and tremendous help in collecting and analyzing data.

The work described in this dissertation was made possible with the crew of the USGS R/V Turning Tide, captained by Jay Cuetara, and operated with John Yokomizo, Curtis Smith, and Chris Battenfield. Field support was provided by Dave Ralston, James Grey, Stefan Talke, and Deanna Sereno. This research was funded by the following grants: California SeaGrant, #R/CZ-170 to Mark T. Stacey and Thomas Powell; NSF, #OCE-0094317 to Mark Stacey; and a Bay Area Water Quality Fellowship.

# Table of contents

# 1 INTRODUCTION

The San Francisco Bay and Delta region of California is an estuary bounded by the eastern coastal Pacific Ocean and the confluence of the Sacramento and San Joaquin rivers (Figure 1). It is the largest bay on the west coast of California and the 3rd largest estuary in the United States (Conomos et al. 1985; Knowles and Cayan 2002). Since the California Gold Rush in 1848, the watershed and estuary have undergone many changes, in particular vast urbanization. The subsequent land use changes have resulted in alteration of the hydrology, the loss of wetlands, contamination of water, sediments and biota, and declines of fish and wildlife species (http://sfbay.wr.usgs.gov/).

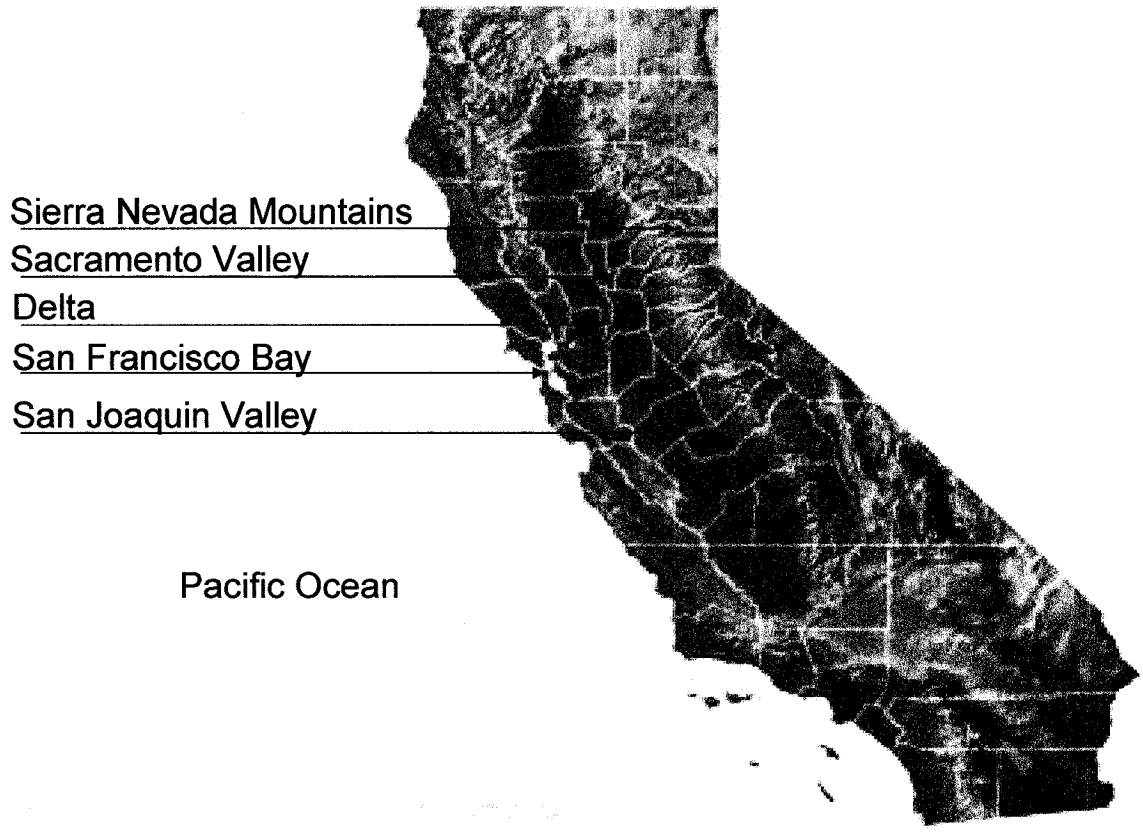


**Figure 1-1 Shaded relief map of major geographical features in Central and Northern California.**

One of the most difficult challenges in managing the San Francisco Bay is finding an appropriate balance between ecosystem health and human demands. San Francisco estuary is a critical resource for the flora, fauna and residents of California. Over 20 million people depend on the Delta for drinking water; 4.5 million acres of cropland are irrigated with Delta water; and several native threatened or endangered fish species reside in or migrate through the Delta (http://science.calwater.ca.gov). As the population of California continues to increase, resource demands increase, which in turn can increase the "stress" (pollution, further alterations to regional hydrology, invasive species, etc) on the ecosystem. Understanding how the ecosystem functions and responds to alterations is a top management priority. Through projects such as CALFED and the South Bay Salt Pond Restoration, San Francisco Bay is increasingly subject to scientific investigations

that attempt to meet ecosystem demands by improving the synthesis of science and policy.

Despite the increasing number of scientific studies conducted in the estuary as a whole, the Central San Francisco Bay has received little attention (Figure 1-2). Central Bay is the confluence of North Bay, South Bay and the ocean; it is often considered the mixing basin of the bay. Alterations in any one of the surrounding water masses will eventually affect the entire system but they will be mediated by the dynamics in Central Bay. In the north, the Delta levee system is changing and sunken islands are being restored. In the south, the Cargill salt ponds will be restored to tidal marshes. Climate change and global warming will alter sea level, sea surface temperature, and possibly regional weather patterns. These changes will affect freshwater flows, water circulation, transport of dissolved constituents, sediment transport and likely alter the floral and faunal community composition of the estuary. Understanding the dynamics of Central Bay will elucidate the connectivity of North Bay, South Bay and coastal waters and provides a management tool to determine how changes in one will affect the others. Quantifying exchange between Central San Francisco Bay and the coastal Pacific Ocean is a first step to understanding how changes in environmental conditions may propagate through the ecosystem.

Historically ocean-estuary exchange has been estimated using salinity (Hansen & Rattray 1965, Fischer 1972, Largier 1996). One of the benefits of using salinity to measure ocean-estuary exchange is the relative stability of ocean salinity and salt is a passive tracer water. In San Francisco Bay, as in most urbanized estuaries, salinity exchange is particularly important because the freshwater upstream is used for drinking

water and even low levels of salinity intrusion can affect the taste and aesthetic quality. Salinity exchange determines the density structure in the vertical, lateral, and longitudinal directions. The density fields, integrated with tidal forcing, determine the net ocean-estuary exchange of other scalars and particles.

There are many other ecologically important scalar constituents in the water such as: sediment and sorbed contaminants, planktonic plants and animals, nutrients, and dissolved contaminants. While most of these constituents are not passive tracers like salinity, their transport is largely due to physical forcing. The two constituents we focus on for the remainder of the text are sediment and phytoplankton.

Understanding sediment exchange between the ocean and estuary will improve management decisions regarding dredging, restoration projects and contaminant transport. Suspended sediment transport is correlated with several types of contaminant transport such as lead, mercury, PCBs and organochlorine pesticides (Leatherbarrow et al. 2005). Approximately 57% of sediment delivered to San Francisco Bay originates in the Central Valley and is delivered to the estuary through the Sacramento/ San Joaquin Delta system; the rest is delivered by local tributaries (McKee et al 2006). Recent changes in quantities dredged in the bay may reflect decreases in loading from the watershed. Dredging estimates from 1955-1990 indicate that 4.5 Mt/yr of sediment were removed during that period and in recent years (1995-2002) the rate has decreased to 3.1 Mt/yr (McKee et al 2006). Although the suspended sediment concentrations in the estuary are relatively high, terragenious sediment loading has decreased due to sediment accumulation behind dams upstream. Large amounts of sediment may initially be required for many of the large scale restoration projects in the estuary, such as reversing

the subsidence of islands in the Delta. Once tidal wetland restoration projects have reached a new equilibrium they will trap sediments, further decreasing the suspended load (Williams 2001). A decrease in the suspended load would mean a decrease in turbidity throughout the estuary. Turbidity in San Francisco Bay is relatively high and presently limits primary productivity in the bay.

Continual declines of suspended sediment concentration may increase the magnitude and frequency of problematic phytoplankton blooms in the future. Phytoplankton is the base of most aquatic food webs and has a large impact on biogeochemical cycles in the estuary. One of the most politically relevant chemical cycles in the modern world is that of $CO_2$, a greenhouse gas related to global warming. Worldwide, phytoplankton fix 50 Gtons of carbon annually (Falkowski et al. 1998). The efficiency of this carbon fixing depends on the species; diatom production is a net sink for $CO_2$, whereas coccolithophorid production is a net source (Harrison 2000). Phytoplankton also play a role in other chemical cycles such as selenium, mercury, and PCBs. Just as there are species-specific differences in the carbon cycle, species specific uptake efficiencies exist for these chemicals. *Procentrum minimum,* a dinoflagellate, concentrates selenium 6000 times more efficiently than *Skeletonema costatum,* a diatom, (Baines and Fisher 2001). Fertilizers administered to crops in the Central valley and effluent from sewage treatment plants are the main sources of nutrients in the estuary. Although nutrient concentrations are generally high enough to consider San Francisco Bay eutrophic, high turbidity and benthic grazing limit the amount primary production so the estuary does not currently experience problematic plant growth or related benthic

anoxia. However, there has been an increase in the frequency harmful algal species are observed in San Francisco Bay (Cloern et al. 2005).

Both suspended sediment concentration and phytoplankton are important to the entire ecosystem. San Francisco Bay is an open ecosystem connected to the Pacific Ocean through the Golden Gate channel. As more people come to rely on the resources of San Francisco Bay and the adjacent coastal ocean, it is important to understand how long term changes, such as increases in sea level, in flora and fauna composition, sea surface temperature, and nutrient loading will affect the future of the ecosystem. To appreciate the complexity of transport and exchange between San Francisco Bay and the Pacific Ocean, we first consider the physical characteristics of Central Bay as well as climatic influences.

### 1.1 Physical Setting of Central San Francisco Bay

Generally Central San Francisco Bay is considered to extend from Point San Pablo in the north, to the San Bruno Shoal in the south, and a small region to the west of Golden Gate (Figure 1-2). There is a small semi-enclosed sub-embayment (Richardson Bay) within Central Bay due north of Golden Gate and there are several islands within the region; namely, Angel Island, Treasure Island, and Alcatraz Island. Because of the complicated basin bathymetry, the tidal circulation patterns are very complex in this region.

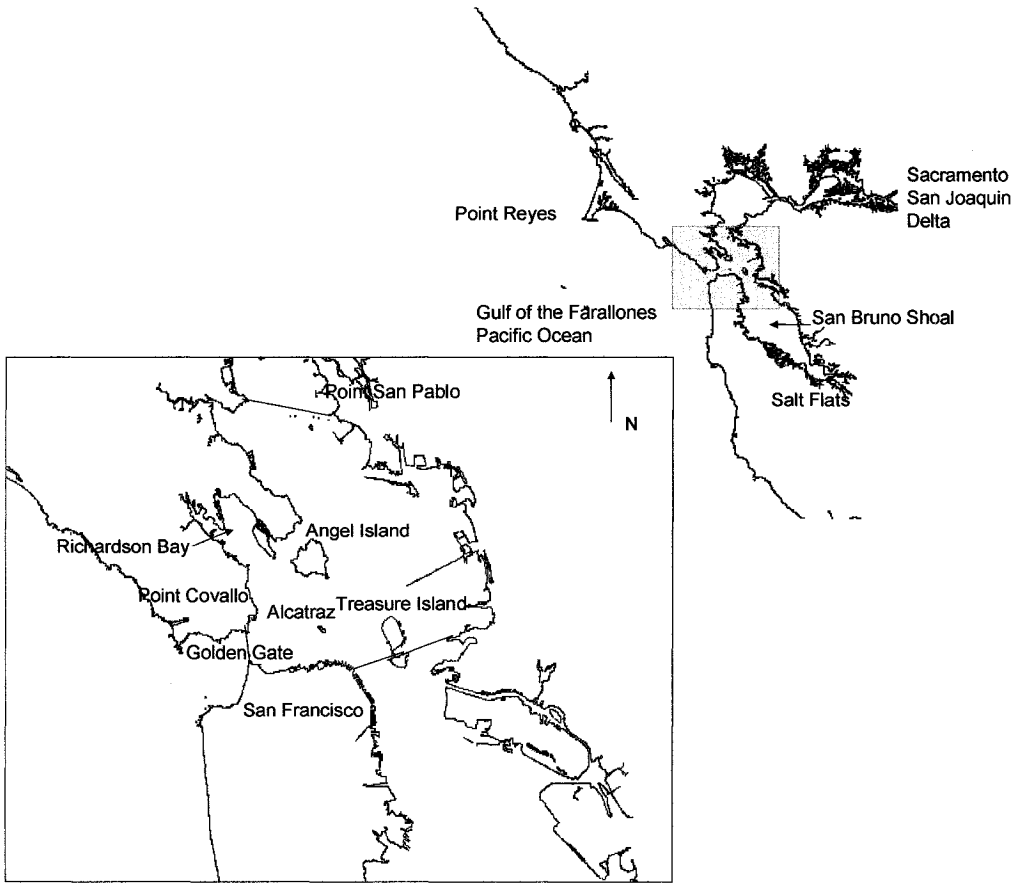


**Figure 1-2. Entire San Francisco Bay in the upper corner. The gray box outlines the expanded view Central San Francisco Bay.**

Approximately half of the entire bay's 8,446 $Mm^3$ of water is in Central Bay. Central Bay is the deepest sub-embayment in the estuary, with an average depth of 13.5m (http://sfbay.wr.usgs.gov/sediment/sfbay/geostat.html). The surface area of Central Bay is about 326.3 $Mm^2$, and the cross sectional area of the mouth at the Golden Gate is 177,000 $m^2$. As in many estuaries, freshwater flow, tides, wind, and coastal conditions are the most important physical factors determining circulation and dynamics in San Francisco Bay. Each of these factors affects the exchange between Central San Francisco Bay and the coastal ocean.

### 1.1.1 Freshwater Flow

An annual average of about 30 $km^3$ of freshwater enter the estuary from the watershed, generally with peak flows coming in early March (Knowles and Cayan 2002). About 90% of the freshwater delivered to the estuary comes through the Sacramento-San Joaquin river system. Other smaller tributaries such as Coyote Creek and the Napa River contribute about 10% (Conomos 1985). The annual average of river flow to San Francisco Bay is 600 $m^3/s$ (Conomos 1985). Although freshwater flows through the estuary are relatively large, they are small compared to tidal flows, especially in Central San Francisco Bay. Freshwater flows are approximately 0.04% of tidal flows measured near the narrow constriction of the Golden Gate channel.

The winter season of high river discharge is characterized by: large-scale compression of the salinity field and a seaward migration of salinity intrusion; enhanced stratification and gravitational circulation; decreased residence time; and increased inputs of river-borne materials such as dissolved inorganic nutrients, and suspended sediments (Cloern and Nichols 1985).

### 1.1.2 Winds

The strongest winds are generally during the summer but the wind intensifies during winter storms as well. The summer season of high winds affects conditions within the estuary and along the coast. Within the estuary summer conditions are characterized by enhanced evaporation, enhanced sediment resuspension and high water temperature (Conomos 1985). In contrast, surface temperature in the coastal ocean decreases. During the summer, northwest winds drive coastal upwelling. The Coriolis force and subsequent Ekman transport cause surface water moving away from the continental margin to be

replaced by waters upwelled from deeper regions. Upwelled water is typically cool and relatively nutrient rich (Mann & Lazier 1996). The cool coastal waters actually enhance density induced circulation in Central Bay during the summer when the rest of the bay is characterized by weak residual circulation (Largier 1996, Conomos 1985).

During the winter, winds shift to the south and southeast, the northerly-flowing Davidson Current moves near shore and upwelling ceases (Conomos 1985). The winter shift in wind patterns corresponds with the onset of winter storms. Although winter storms are responsible for maximum local rainfall, the high river flow conditions described above usually occur later in the season when the snowpack in the Sierras begins to melt.

### 1.1.3 Tides

In San Francisco Bay, as in many estuarine systems, tidal flows are the dominant forcing mechanism defining the velocity field. The tidal prism for San Francisco Bay is approximately $1.59 \times 10^9$ $m^3$ (Conomos 1985). The tidal excursion or how far a water parcel travels within a tidal cycle, in Central Bay is on the order 10-15 km, so only Central Bay waters are exchanged during a given tidal cycle (Walters et al 1985). The tides are variable on a daily, fortnightly and seasonal timescales. The tide is a mixture of semidiurnal and diurnal components (Cheng and Gartner 1985). When the oceanic water level is high, a flood tide results in water entering the estuary from the Pacific; the converse is true during low, or ebb tide, when waters leave the estuary. The relationship between tidal height and currents varies throughout the estuary. In Central Bay tides are a mixing of a standing and progressive wave. In Central Bay, the currents are ebb dominated and maximum tidal current velocities are on average 100 cm/s.

There is also a strong fortnightly spring-neap cycle: spring tides occur near the times of full and new moons and have the highest tidal range of the lunar month, whereas during the first and third quarters the neap tides occur when the tidal range is least (Conomos 1985). Spring tides correspond to larger water level differences between rising and falling stages of the tide, which in turn means velocities are greatest during that period. The opposite is true during neap tides when velocities are smallest. These variations in seasonal freshwater flows, winds and tides combine to create net transport of scalars such as sediment and phytoplankton.

## 1.2 Physical Estuarine Transport Mechanisms: Residual Flux Processes

Vertical, lateral, and temporal variations in both the velocity and scalar fields define a complex, potentially three-dimensional, flux field, which must be averaged over long timescales to define the residual scalar flux. Studies of estuarine salt fluxes (Fischer et al. 1979) have identified several dominant mechanisms that determine the residual flux of salt; in the remainder of this section, these mechanisms reviewed in the context of Central San Francisco Bay. To clarify the spatial descriptions in the subsequent sections, the longitudinal direction is the east-west direction and the x-direction, the lateral direction is the north-south and y-direction, and vertical direction is parallel to the direction of gravity and the z-direction.

### 1.2.1 Tidal Pumping and Trapping

When tidal flows interact with bathymetry, ebb-flood asymmetries develop in both the flow structures and the scalar concentrations. Stommel and Farmer (1952) described "tidal pumping" as a jet that enters an embayment during the flood tide, and

radial return flow during the ebb (Figure 1-3). The result is a net exchange of water, where some oceanic waters remain within the embayment after the ensuing ebb tide.

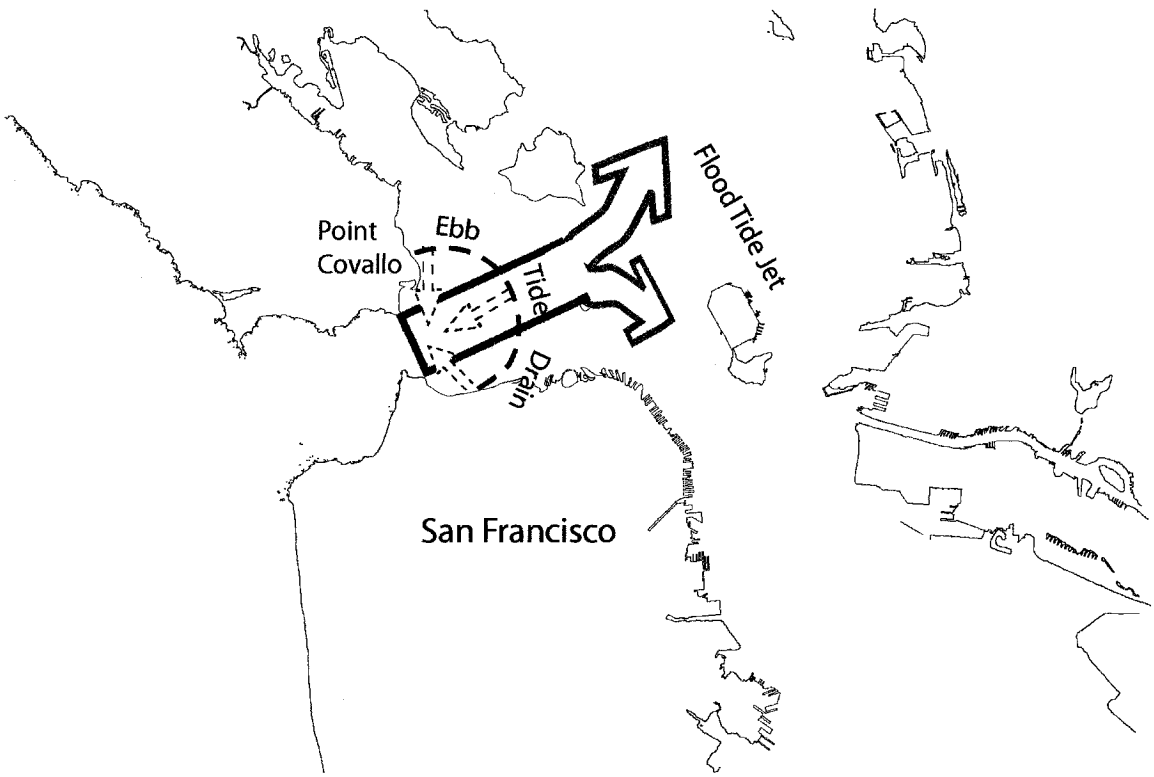


**Figure 1-3 Tidal pumping schematic in Central San Francisco Bay. The volume of water leaving the bay does not consist of entirely the same waters entering the bay, creating net exchange over the tidal cycle.**

A second transport mechanism that involves tidal interaction with bathymetry was analyzed by Okubo (1973), and has become known as "tidal trapping"(Figure 1-4). Tidal trapping is created by differences in frictional phasing between ebb and flood tides. A common example is a system with shallow shoals adjacent to a deep channel. In the shallower regions more energy is lost to friction than in the deep region so the tide turns earlier in the shoals (Okubo 1973). This has the cumulative effect of diffusing scalars and mixing water masses so that the same water masses that enter the estuary during one flood tide are not leaving the ensuing ebb tide. Tidal trapping in Richardson Bay (Figure

1-2) likely affects the timing and distribution of scalars in the northern reach of Central Bay

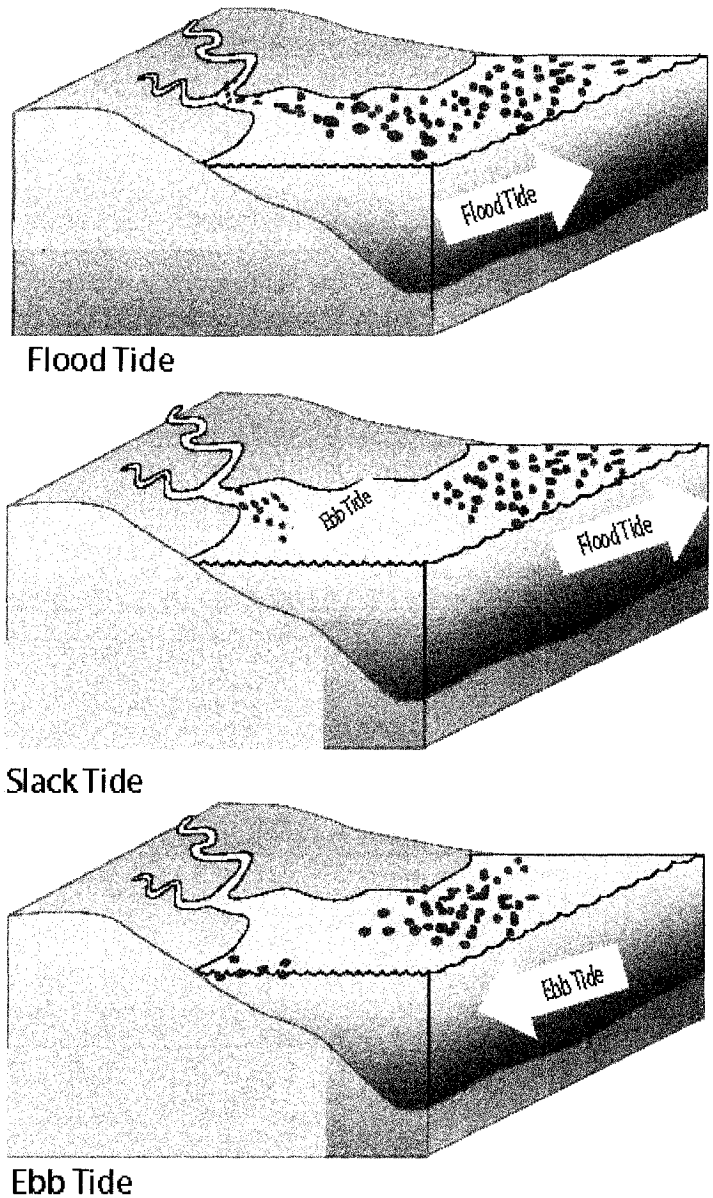


**Figure 1- 4 Schematic of tidal trapping in an idealized channel and shoal system. The tide begins to turn earlier in the shallows, creating greater dispersion within the tidal cycle.**

Our observations at the Golden Gate have established that both of these mechanisms are important for net scalar exchange and will collectively be referred to as tidal pumping henceforth. For our purposes we can consider velocity and scalar concentration signals to vary as some combination of sine functions. If tidal currents and scalar concentration are a quarter-cycle out of phase, then the net transport of the scalar by the tides would be zero due to the symmetry of flood and ebb tide concentrations. If this phasing is shifted slightly, such that, for example, flood tides have higher concentrations than ebbs, then a net flux of scalar is created that is directed into the estuary and reversed if ebbs have higher concentrations.

Tidal exchange processes are further modified at the Golden Gate by the formation of a headland eddy during the flooding tide on the north side of the channel (Fram et al. 2006). This eddy is retained in the shallow region between the primary tidal channel, Angel Island, and Point Covallo (Figure 1-2). On the ensuing ebb tide, this eddy makes its way back out of the estuary, maintaining its distinct scalar character such that water that entered the estuary early on the flood tide exits early in the ebb, rather than late as would be expected in a symmetric tidal flow. This leads to a phase shift between the salinity and velocity signals, which in turn, create a net flux (Fram et al. 2006).

### 1.2.2 Steady Exchange Flows

In addition to tidal forcing, a fundamental characteristic of estuaries is the density gradient created by differences in river and ocean salinities. This gradient establishes a residual flow through a baroclinic pressure gradient (Hansen and Rattray 1965). Combined with a seaward barotropic pressure gradient, the net flow consists of seaward

surface flow and landward bottom flow (Figure 1-5). This residual flow is generally termed estuarine circulation. However, because we will consider both lateral and vertical density induced flows, we will henceforth refer to this particular residual flux as steady exchange.

In Central Bay, Largier (1996) found that there was a seasonal intensification of both longitudinal and vertical density gradients during winter/spring and oceanic upwelling during summer. Subsequently steady vertical exchange was enhanced during those times too. The timing and magnitude of steady flows are influenced to great extent by tidally-induced turbulent mixing, creating variability in the estuarine exchange at the spring-neap timescales (Geyer et al. 2000; Ribeiro 2004 and even tidal Stacey et al. 2001).

Steady vertical scalar fluxes depend on the vertical structure of the scalar. If the scalar is well-mixed vertically, the net flux will be close to zero, with the upper and lower layer fluxes canceling one another. If, however, there is a vertical gradient in the scalar, then baroclinic exchange flows can create a net flux along the axis of the estuary. This is frequently invoked to explain the landward flux of salt that acts in opposition to seaward freshwater flow.

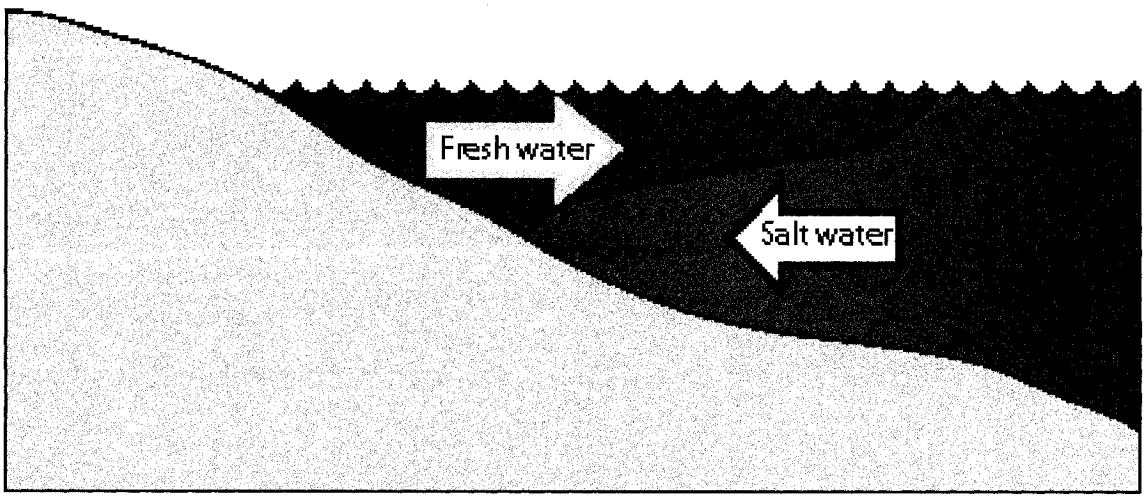


**Figure 1-5 Steady vertical circulation pattern induced by the density gradients.**

Lateral density gradients, the north-south direction in our case, create a similar type of bi-directional flow structure. Due to the geometry of San Francisco Bay and the fact that freshwater flow primarily enters through the northern reach of the Bay, the north side of the Golden Gate channel is fresher than the south side. Lateral baroclinic forcing creates residual flow directed into the estuary on the south and out on the north side of channel in Central Bay (Fram et al 2006). Additionally, the jet-drain geometry of tidal pumping (Figure 1-3) creates later asymmetries in the flow structure such that flow is outwards on the sides of the channel and inwards in the center. The net flux direction will depend on the lateral distribution of the scalar; i.e., if the scalar concentration is greatest on the north side, transport will be out of the estuary.

## 1.3 Estuarine Particle Dynamics

While the processes described above are most easily applied to conservative tracers such as salinity, they can also be extended to other passive particles. Because phytoplankton and sediment are not truly conservative, the processes affecting their distribution and transport are more complicated than that of salinity. Both sediment and

phytoplankton have additional complexity due to processes such as flocculation, growth, respiration, predation, deposition, and burial that affects their fate and transport. We will first consider factors that affect both phytoplankton and sediment: sinking and suspension.

In a quiescent fluid, a particle will settle if the density of the particle is greater than that of the fluid. A typical way to define the settling velocity for spherical particles is using Stokes law:

$$w_s = \frac{D^2}{18}\left(\frac{\rho_s - \rho}{\mu}\right)g \qquad \text{Eqn 1-1}$$

where $w_s$ is the settling velocity, $D$ is the diameter of the particle, $\rho_s$ is the density of the particle, $\rho$ is the density of the fluid, $\mu$ is the viscosity of the fluid, and $g$ is gravity. This equation was first introduced by Stokes in 1851 and is the balance between the drag force, and the immersed weight of the particle. One of the key assumption in this equation is that the Reynolds number of the particle, $\mathrm{Re}_s = \frac{w_s D}{\nu}$, is less than one so the flow is laminar. A typical grain size diameter of unflocculated sediment found in suspension found in San Francisco Bay is 14 μm and the density is ~2 g/cm$^3$ (Ganju et al. 2003). The sediment settling velocity would be 9x10$^{-3}$ cm/s. For a diatom, the dominant type of phytoplankton in San Francisco Bay, the diameter is in the range of 10μm (Cloern and Dufford 2005), and a typical density of the silica cell walls is 2.6 g/cm$^3$ (K.H. Mann 1996). This yields a diatom settling velocity ~5x10$^{-3}$ cm/s.

If a particle settles to the bed, it may either be buried or resuspended. To suspend a particle off the bed, the shear stress at the bed must be sufficient to overcome the body force acting on the particle. The Shields parameter is a common way to define the

critical shear threshold, over which, the sediment particle will be lifted off the bed. For turbulent flow the Shields parameter is defined as follows:

$$\text{Shields Parameter} = \frac{\tau_c}{(\rho_s - \rho_f)gD} = f\left(\frac{u_* D}{\nu}\right) \qquad \text{Eqn 1-2}$$

where $\tau_c$ is the critical shear, above which the particle will be suspended above the bed, $\rho_s$ is the density of the particle, $\rho_f$ is the density of the fluid, $g$ is gravity and $D$ is the diameter of the particle. The Shields parameter is a function of a slightly different Reynolds number, defined by the turbulent velocity scale of the fluid, $u_*$, particle diameter, $D$, and the water viscosity, $\nu$. The particle will remain in suspension as along as the turbulent velocity is maintained above the critical threshold. However, in an environment with semi-diurnal tides such as San Francisco Bay, there are slack tides approximately four times a day when the velocity is zero. During these times, particle settling can be quite rapid (Dyer 1986). Asymmetries in sinking and resuspension during the tidal cycle are a major focus in estuarine particle dynamics. Understanding the physical mechanisms creating the sinking and resuspension patterns of natural particles remains one of the most challenging aspects of particle transport in estuaries.

### 1.3.1 Implications for Sediment Transport

To create a tidal pumping flux of suspended sediment there must be differences between oceanic and estuary concentrations and timing asymmetries between peak concentration and peak velocity. To create a steady flux of suspended sediment, there must be gradients either vertically or laterally in concentration. Spatial gradients and

timing asymmetries in concentration can result from gradients or timing differences in stratification, shear and turbulence, grain size distribution, flocculation, bed availability and biological transformation. Local acceleration can create a phase shift between maximum bed stress and peak sediment concentrations at points above the bed. This lag represents the time required for sediment to diffuse vertically (Jay and Musiak 1994). Maximum sediment concentration may lead or lag the local maximum bed stress because advection from locations of higher mean concentration (resulting from greater bed stress, greater bed availability or both) will determine timing of maximum concentration (Jay and Musiak 1994).

The direction of net transport within the estuary may vary depending on the location within the estuary. Sediment accumulation in estuaries is a balance between local vertical processes and horizontal advection. Transport induced by the vertically sheared velocity is dependent on the vertical distribution of sediment relative to the velocity shear. The most common way to represent the vertical profile of suspended sediment is using the Rouse equation, where sediment concentration increases towards the bed.

This profile is derived by assuming steady state, negligible upward or downward fluid velocity, no horizontal gradients, and a constant settling velocity. The flux of sinking particles, $w_s C$, is balance by turbulent diffusion, $-K_z \frac{d\overline{C}}{dz}$. that can be represented by a parabolic diffusivity, , such that

$$w_s C = -K_z \frac{dC}{dz} \qquad \text{Eqn 1-3}$$

The diffusion coefficient is dependent on depth and has a parabolic form:

$$K_z = \beta \kappa u_* z(h - z)/h \qquad \text{Eqn 1-4}$$

where β is a proportionality constant between the diffusion coefficients for the sediment and fluid mass, κ is the Von Karman constant, $z$ is the depth, $h$ is the total water column height. Integrating equation 1-3 from $a$, the reference height with a known reference concentration, $C_a$, to $h$ yields the Rouse profile:

$$C(z) = C_a \left( \frac{h - z}{z} \frac{a}{h - a} \right)^{\frac{w_s}{\beta \kappa u_*}} \qquad \text{Eqn 1-5}$$

In many partially mixed estuaries, such as San Francisco Bay, estuarine circulation is often credited for creating an estuary turbidity maximum (ETM). Very small particles that remain well mixed in the water column and never settle out will tend to be transported out of the estuary by freshwater advection and baroclinic circulation. Transport of sediment that is heavy enough to settle but light enough to be resuspended will be up estuary on the seaward side of the ETM and out of the estuary on the landward side of the ETM (Jay and Musiak 1994). The ETM location changes depending on freshwater flows, tidal currents, wind, sediment availability and size.

Asymmetries in vertical mixing between ebb and flood tide may also cause landward transport of sediment. The interaction of the longitudinal density gradient in estuaries with the vertical shear in the tidal current leads to a forcing mechanism termed strain-induced periodic stratification (SIPS) (Simpson et al. 1990). During the ebb phase of the tide, higher seaward velocity at the surface moves lighter water over slower moving denser water to induce stratification. On the flood, this process is reversed so that the effect of vertical shear is to reduce stratification. Sinking particles in such a flow will

tend to be suspended higher in the water column during the flood than the ebb tide. This difference in vertical position, combined with the vertical shear of the tidal currents (faster the farther away from the bed), lead to a net transport into the estuary (Pringle and Franks 2001).

For our purposes, we are primarily concerned with the transport of particles in suspension. Bed transport of larger materials is beyond the scope of our investigation, primarily because it is so difficult to measure in comparison to suspended sediment. Nevertheless, the direction of the bed load transport is assumed to be out of the estuary. The presence of an ebb tidal bar on the Pacific side of the Golden Gate channel and recently discovered large sand waves just outside of the Golden Gate indicate that sand is transported out of the estuary (Hanes 2006).

### 1.3.2 Implications for Phytoplankton Transport

Dynamics of phytoplankton can be interpreted as responses to changes in processes that regulate the total biomass (total quantity, or by proxy, chlorophyll concentration), species composition, and spatial distribution of phytoplankton (Cloern 1996). In situ processes control populations within a water parcel, and physical transport processes mix water parcels and their phytoplankton. Cloern (1996) has reviewed the phytoplankton dynamics of San Francisco Bay and found

"in situ processes of population change include (1) the production of new biomass, which is controlled by the availability of visible light energy required for photosynthesis and nutrient resources required for the biosynthesis of new algal cells, (2) mortality, including that caused by parasites or viruses, (3) grazing losses to pelagic and benthic consumer animals, (4) turbulent mixing by tide and wind-induced motions in the

water column, (5) sinking and deposition of phytoplankton biomass on the bottom sediments, and (6) resuspension of bottom-deposited microalgae by tidal currents and wind waves" .

The aforementioned in situ processes are all spatially and temporally dependent, so as phytoplankton are transported within the estuary they experience different conditions (Malone et al. 1986; Lucas et al. 1999). Longitudinal (along the primary flow axis) and lateral (perpendicular to the primary axis) transport are determined by water circulation which is driven by tidal currents, freshwater advection, density gradients and wind. Vertical transport is also important and is determined by density stratification, and turbulent mixing.

In most of San Francisco Bay, accumulation of phytoplankton biomass is controlled by vertical transport. In South San Francisco Bay blooms are light limited because bottom sediments are tidally re-suspended, creating an environment too dark for photosynthesis (Alpine & Cloern 1988). In North San Francisco Bay, blooms are now limited by predation by an exotic Asian clam introduced around 1989 (Cloern 1996). Benthic grazers filter water and rely on vertical mixing and phytoplankton sinking for a constant supply of food. When the water column is stratified, the upper water column is separated from the benthos. Phytoplankton retained in the upper layer receive sufficient light for photosynthesis and escape benthic grazing. Stratification is strongest in North and South Bay after high freshwater flows. The spring-neap tidal cycle also contributes to the stratification, where spring tides have larger currents and therefore promote mixing, decreasing stratification, whereas the opposite is true during neap tides when currents are diminished.

Central San Francisco Bay is very different from North and South Bay because it is approximately 6-10 times deeper than the other embayments. This means that vertical stratification dynamics are very different. Tidal currents are always much stronger in Central Bay than elsewhere in the estuary. The strength of tidal currents combined with the complex bathymetry potentially leads to the most well mixed sub-basin within the estuary. Finally, this region is unique within the estuary because it exchanges directly with the adjacent coastal waters. All these factors make Central Bay a challenging and unique environment in which to measure scalar exchange.

In subsequent chapters we describe the methods used to calculate scalar exchange between San Francisco bay and the coastal ocean. We then present a qualitative analysis of the field data collected followed by the quantification of the fluxes. The ultimate goal is to determine which physical processes contribute to scalar exchange and how those processes vary throughout the course of our study.

# 2 Methods

Challenging oceanic conditions in Central San Francisco Bay have hindered historical exploration and scientific investigations in the area. The site is characterized by complex bathymetry, fast current speeds, and 3-D circulation patterns. Cargo ships, recreational boaters, and wind surfers are frequently in the area, further complicate the logistics of sustained scientific investigations. Initially, we attempted to measure the fluxes was in the narrowest part of the shipping channel, just west of the Golden Gate. However, current conditions and boat traffic made this location too difficult to reasonably collect data. The data reported in subsequent chapters, were collected along a transect east of the Golden Gate Bridge Other challenges faced during this investigation included: 1) instrument interactions with the bed, during the spring the instrument package hit the bed; 2) interactions with flora and fauna, the cage housing our instruments occasionally skewered fish and seaweed; 3) during the fall, the communication cable between the instruments and the boat was severed but repaired within an hour; 4) bubbles at the surface interfering with surface measurements; and 5) finding the balance between the best spatial and temporal coverage and reliable control of the boat and instruments.

### 2.1.0 Field Observations

To calculate net fluxes between the coastal Pacific and Central San Francisco Bay we measured cross-sectional velocity and scalar concentrations (salinity, chlorophyll and sediment) across the mouth of the estuary. The transect path was located just east of the

Golden Gate bridge and followed a 55m bathymetric contour (Figure 2-1). Data were collected during each of three seasons: spring runoff (March 6-7$^{th}$ &13-14$^{th}$ 2002), fall relaxation (October 29$^{th}$ & November 6-7$^{th}$ 2002), and summer upwelling (June 3$^{rd}$-4$^{th}$ & 10-11$^{th}$ 2003). During the summer and fall experiments, 12 minute transects across the channel were repeated continuously for 25 hours, one day during spring tide and one day during neap tide. Due to inadequate navigation equipment, overnight work was not possible during the first winter/spring experiment so data was collected only during daylight hours.

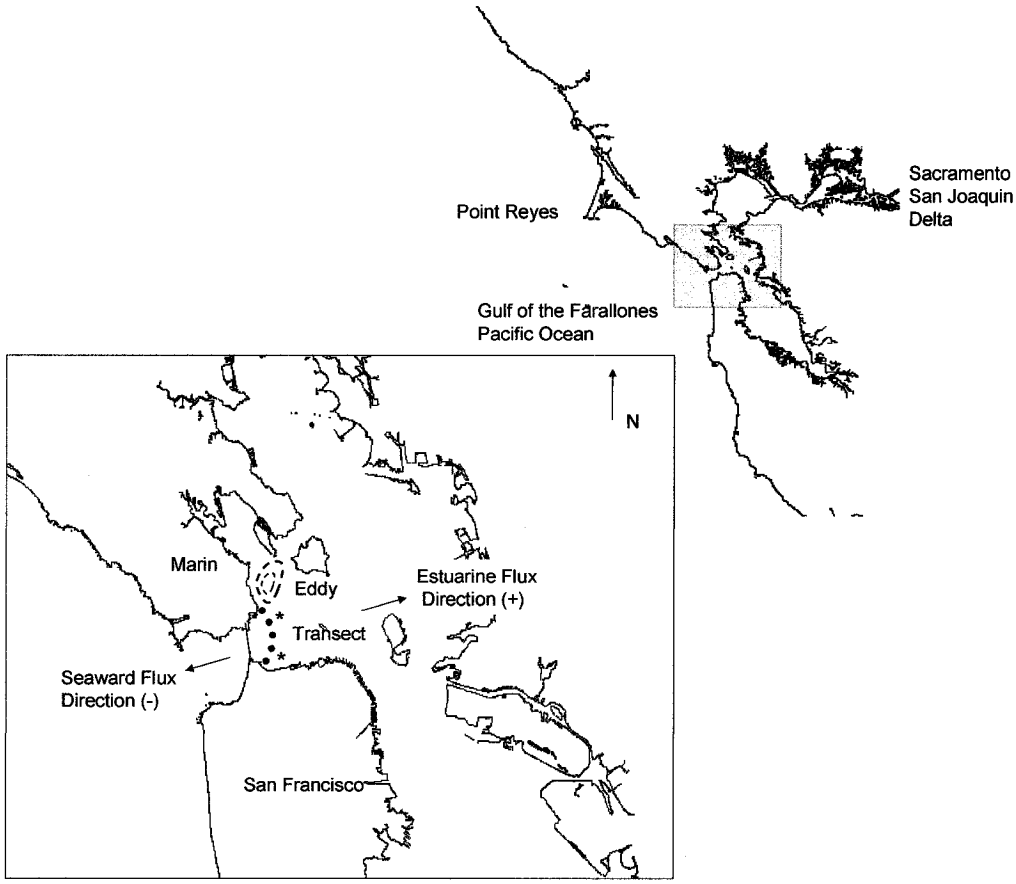


**Figure 2-1 The entire San Francisco Bay is featured in the upper corner and Central San Francisco Bay is marked by the shadowed box and enlarged in the lower map. The dotted line is the transect location following a 55 m bathymetry contour. Dashed circles to the north of the transect represent the eddy location. The eddy is a transient feature when tide turns from flood to ebb that enhances scalar exchange. The stars represent approximate locations where vertical profiles were taken. A flux out of the estuary is negative and a flux into the estuary is positive.**

Velocity and scalar concentrations were measured aboard the USGS R/V Turning Tide. The average boat speed was approximately 4m/s. Velocity was measured by a boat-mounted 300 kHz acoustic Doppler profiler (RDI ADCP), which was configured to have 1 meter vertical resolution. Scalar concentrations were obtained from an undulating towed vehicle (Sea-Sciences Acrobat) as well as a boat-mounted CTD (RBR). The instrument packaged on the Acrobat included a CTD (SeaBird Electronics), optical backscatter (D&A OBS), UVA chlorophyll fluorescence (Turner SCUFA), and spherical photosynthetic active radiation (PAR) sensor (LICOR). These data channels were relayed at 4 Hz to onboard computers, a sampling frequency smaller than any of the individual instrument sampling rates. The Acrobat was able to profile reliably from a depth of about 10 meters to about 50 meters (Figure 2-2). Each transect took about 12 minutes and within that time we were able to fly instruments up and down about three times (Figure 2-3).

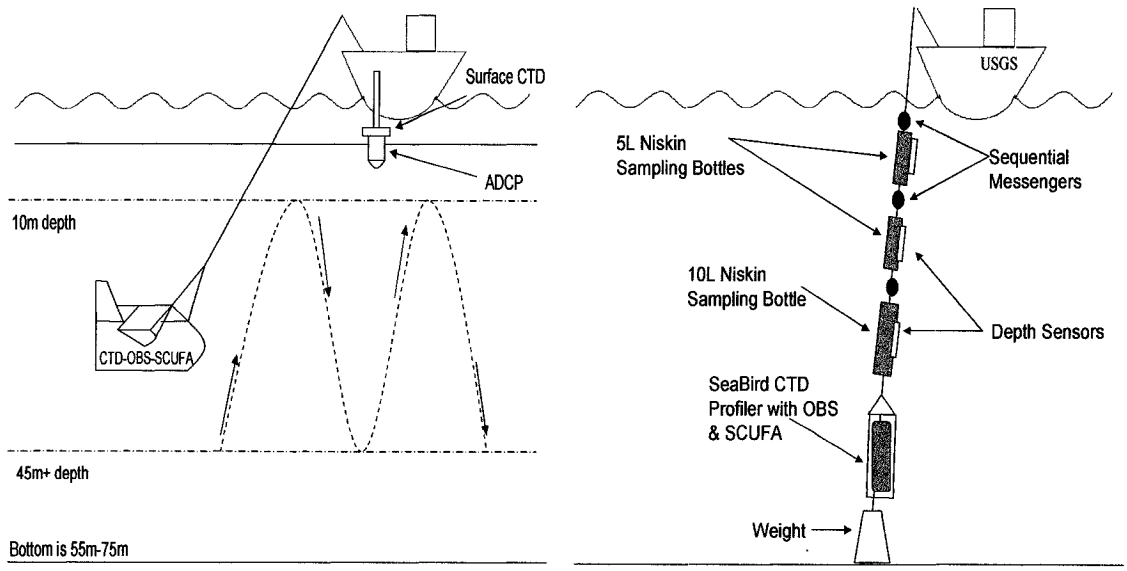


**Figure 2-2 Tow-yo schematic for sampling design on the left and the vertical profiling design on the right.**

## 2.2 Data Analysis

Current and scalar fields were mapped on to a 2-D arcing grid. The grid was arced instead of flat to follow the boat track and is roughly perpendicular to the primary tidal flow direction. The lateral resolution of the grid spanned 3300m from south to north, each cell approximately 50m wide, for a total of 66 cells. The vertical resolution of the grid was 1m, spanning 3 meters above mean lower low water (MLLW) to the bottom. The bottom differed between ebb and flood transects because the boat turned into the current at the end of each transect. The difference in bathymetry among transects occurs primarily at the southern and northern most points of the transect. The number of scalar data points gridded during each transect was on the order of 3000. The total number of raw data points per grid cell was on average 350 for each season. The center cells contained the majority of the scalar data. There were approximately 10-15 ADCP profiles per grid cell and almost every cell contained ADCP data for each transect.

Raw scalar data were interpolated within the area where the tow-yo body was able to fly (10-50m depth) using ordinary kriging (Fram et al. 2006) (Figure 2-3a). Kriged data from that area was then extrapolated to the surface and bottom boundaries using empirical equations fit to the vertical profiles collected during flood, ebb and slack tide during fall and summer (Figure 2-3b). For chlorophyll, the form of the vertical interpolation was

$$Chla(z) = a_1 + a_2 \exp(-a_3 z) \qquad \text{Eqn 2-1}$$

where $z$ is the depth below the surface. The unknown parameters ($a_1, a_2, a_3$) are fit for each column of the data grid. One of the features of the data that is reflected by this functional fit is a trend towards higher concentrations at depth than at the surface (Figure

2-4). This vertical distribution of chlorophyll was observed during fall and summer but because we did not have sufficient instruments during the spring it is unknown if this functional form accurately describes vertical distribution during spring.

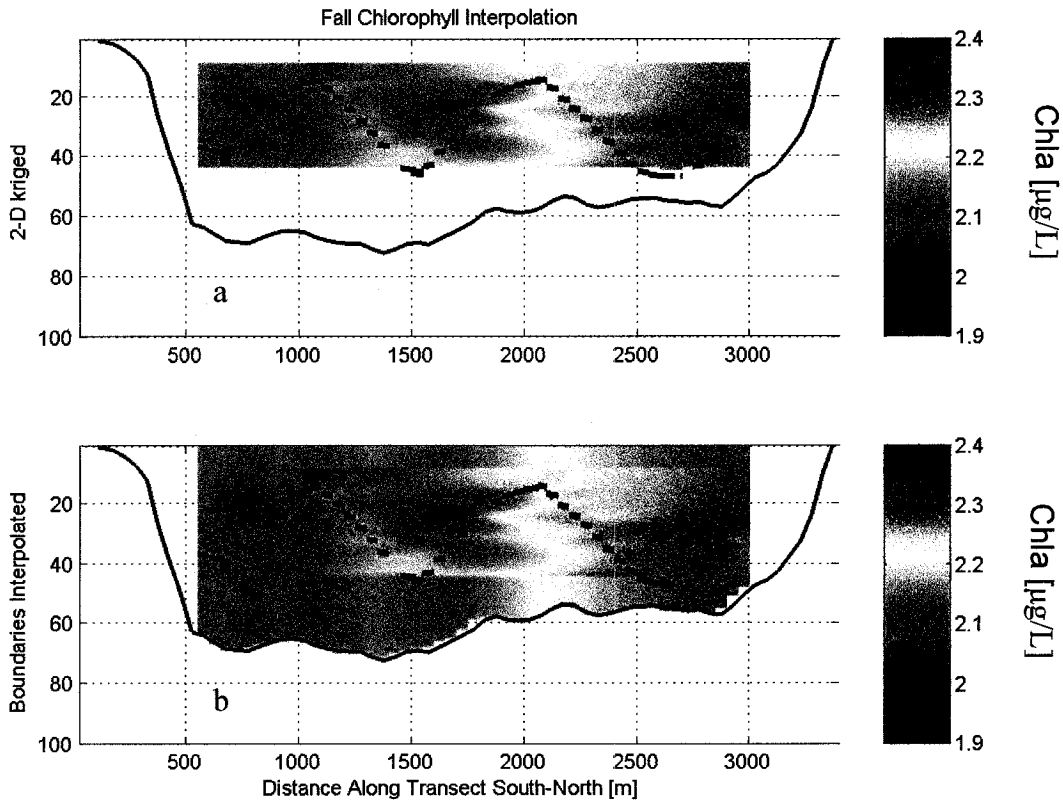


**Figure 2-3 Panel a) shows flight path of the tow-yo body, black line, and the data kriged, b) shows data interpolated from kriged values to the top and bottom of the water column using equation 2-1.**

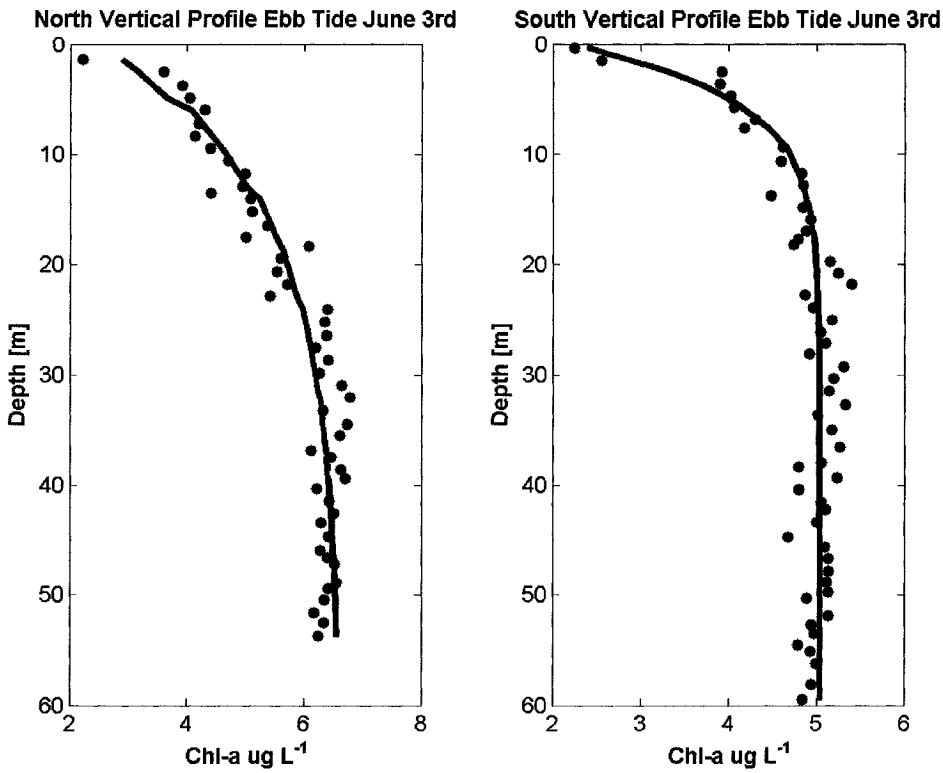


**Figure 2-4 Curve fit for summer chlorophyll profiles. The left panel was collected at the northern end of the transect and the right panel was collected on the southern side.**

To interpolate sediment concentrations near the bed we fit a Rouse-type profile

$$C(z) = a_1 * \left[ \frac{H - z}{z} * \frac{a_2}{H - a_2} \right]^{a_3} \qquad \text{Eqn 2-2}$$

where H is the total water column height, $z$ is the depth and $a_1$-$a_3$ are fit parameters (Figure 2-5). For the surface sediment concentration, we simply extended the concentration from the top of our data to the surface, creating vertically uniform concentrations above 10m depth.

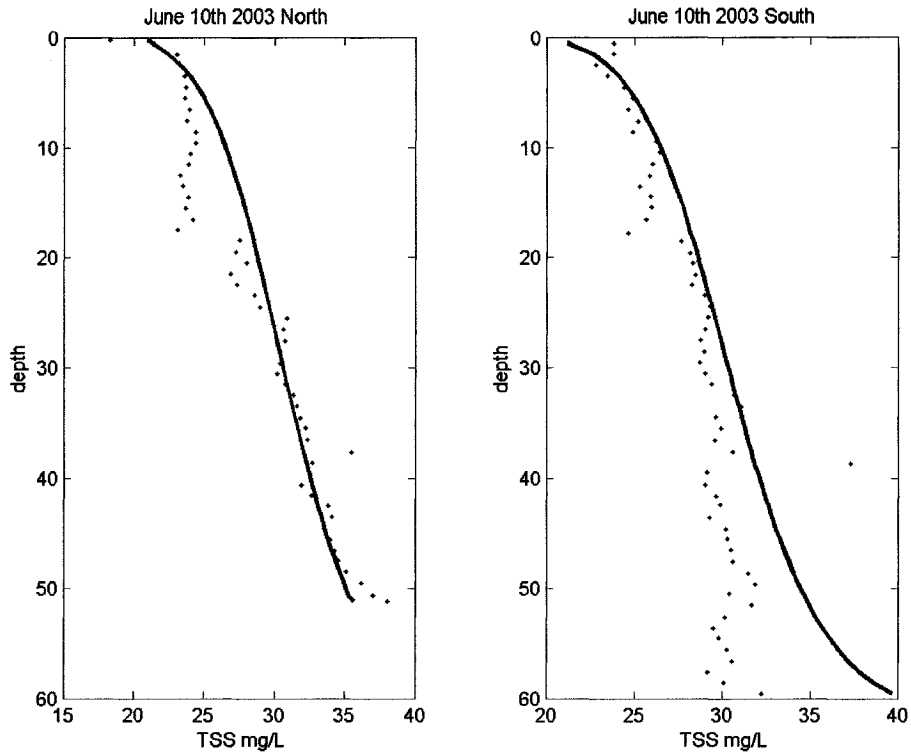


**Figure 2-5 Example of Rouse equation fit to profiles of suspended sediment June 10th 2003 on the north and south side of the transect.**

## 2.3 Optical Instrument Calibration

During each experiment vertical profiles were taken at the southern and northern end of the transect during flood, ebb and slack tide. Profiles measured salinity, temperature, fluorescence and turbidity (Figure 2-4, Figure 2-5). During each of these profiles water samples were collected at three different depths (approximately 10m, 30m, and 60m) using a series of Niskin sampling bottles. The closing mechanism for the bottles relied on a weight or messenger attached to the profiling line that releases the spring holding the two bottle ends open. To close the bottle closest to the surface, we sent the messenger down from the deck of the boat. Subsequent bottles were released by messengers attached to the bottle above it. These water samples were then used to

]calibrate the optical instruments. Through calibration, fluorescence and turbidity are converted to chlorophyll-a and sediment concentrations.

To calibrate the fluorometer, sample water was filtered and chlorophyll was extracted following Environmental Protection Agency Method 445.0. To calibrate the OBS, 1L of sample water was filtered onto a pre-washed and weighed Whatman micropore filter. The wet filters were then baked at 103 C° and weighed after baking. The difference between the initial and baked weights is the mass of sediment per liter. This method is slightly modified from the National Pollutant Discharge Elimination System method 160.2. These volumetric concentrations are then plotted against the instrument output to create a linear regression between concentration and instrument output (Figure 2-6).

### 2.3.1 Error Analysis of Calibration

The calibrations curves show that concentration of suspended sediment and chlorophyll have a weak dependence on the readings of the optical instruments, $R^2$ ~0.3. There are several explanations for this poor fit. The Niskin bottles were over 2ft long, therefore water collected averages over that distance. The SeaBird readings were selected by comparing depth the bottles with the depth of the instrument. The profiling Seabird was at the bottom of the line, followed by the sampling bottles (Figure 2-2), so samples and instrument data were not taken at the same place at the same time. Although every effort was made to stabilize the boat location during these profiles, the boat did in fact drift during the profiles so this could also lead to differences between waters seen by the optical instruments and waters collected in the bottles.

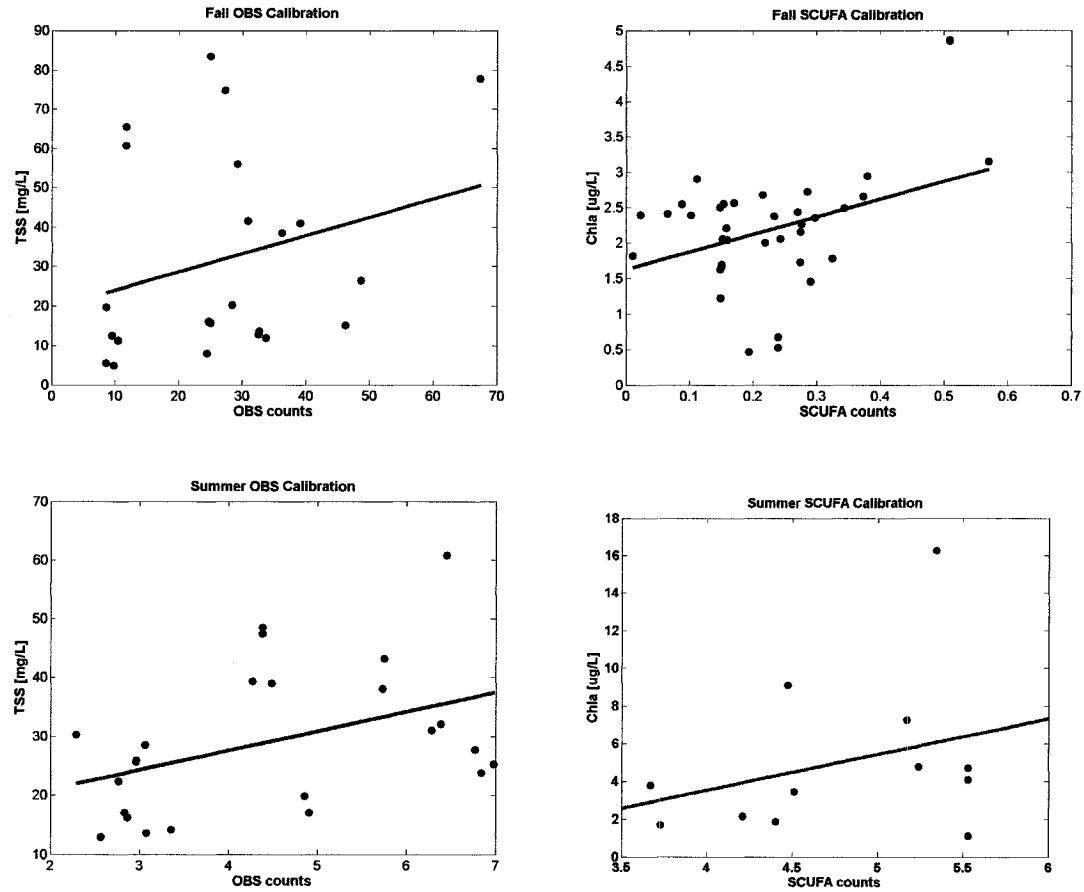


**Figure 2-6 Fall and summer optical instrument calibration. Note that summer scufa counts are an order of magnitude larger because we adjusted the sensitivity range of the sensor.**

We calculated the standard error, and the 95% confidence interval for each calibration (Table 2-1). The standard error is large for all the calibrations except the fall SCUFA-chlorophyll curve. Almost all of the minimum confidence levels extend into negative concentrations which is physically impossible. It should be emphasized that although these calibrations do form the basis for the subsequent chapters, the flux calculations themselves depend more on relative concentrations within each season. The flux quantities most likely affected by poor calibrations are the advective and tidal pumping fluxes because both are dependent on the average scalar concentration. Despite

the poor fit of calibration curves, these linear models predict concentrations of sediment and chlorophyll that are similar to measurements made routinely by the USGS (http://sfbay.wr.usgs.gov).

**Table 2-1 Standard deviation, standard error and the 95% confidence interval calculated for optical instrument calibrations.**

| | Number of samples | Standard Deviation | Standard Error | 95% CI |
|---|---|---|---|---|
| Fall OBS | 23 | 26 | 5 | +-11 |
| Fall SCUFA | 36 | 0.78 | 0.13 | +-0.3 |
| Sum OBS | 24 | 12 | 3 | +-5 |
| Sum SCUFA | 12 | 4.2 | 1.22 | +-2 |

## 2.4 Harmonic Analysis

To calculate net fluxes between the ocean and estuary an integration over time of the observed velocity (U) and chlorophyll (C) was required over the entire cross section (Eqn 2-3).

$$\text{Net Flux} = \frac{1}{T}\int_0^T \iint UCdydz \; dt \qquad \text{Eqn 2-3}$$

The y-direction here is north-south and the z-direction is top-bottom. We considered the net exchange of a scalar to be the mass exchange rate on timescales longer than the tidal and fortnightly (spring-neap) timescales. Due to subtle tidal asymmetries, a straight temporal average of the observations would not adequately resolve the sub-tidal fluxes. Instead, we relied on the integration of harmonics using the known tidal frequencies (K1 24 hrs period, M2 12.42 hrs, S2 12 hrs, N2 12.66 hrs, O1 25.8 hrs, and M4 6.21 hrs).

The observed velocity and scalar concentration for each grid cell are fit using a least squares approach, with a zero-frequency $A_0$, and an amplitude, $A_i$, and phase, $\varphi_i$, for each tidal frequency (or harmonic). The result is a timeseries of velocity and scalar concentration for each grid cell in the cross-section that can be directly integrated to define a net flux:

$$u(y,z,t) = A_0^{u(y,z)} + \sum A_i^{u(y,z)} * \sin(\omega_i + \phi_i^{u(y,z)}) \quad \text{Eqn 2-4}$$

$$c(y,z,t) = A_0^{c(y,z)} + \sum A_i^{c(y,z)} * \sin(\omega_i + \phi_i^{c(y,z)}) \quad \text{Eqn 2-5}$$

The zero-frequency harmonics for the scalar concentrations were the only components constrained; they could not be below the minimum or above the maximum concentration measured each season.

This analysis was applied to salinity with excellent fitting results ($R^2$ =~0 .98, Fram et al. 2006). The quality of fit for chlorophyll and sediment were reduced in comparison. Cross-sectional average chlorophyll fits for summer and spring were $R^2$ = 0.79 and fall was $R^2$ = 0.83. Fits for suspended sediment were poorer than chlorophyll, $R^2$ = 0.79 For illustrative purposes we show the harmonic fit for the cross-sectional average for summer (Figure 2-7), when calculating the fluxes, however, each grid cell has a harmonic fit.

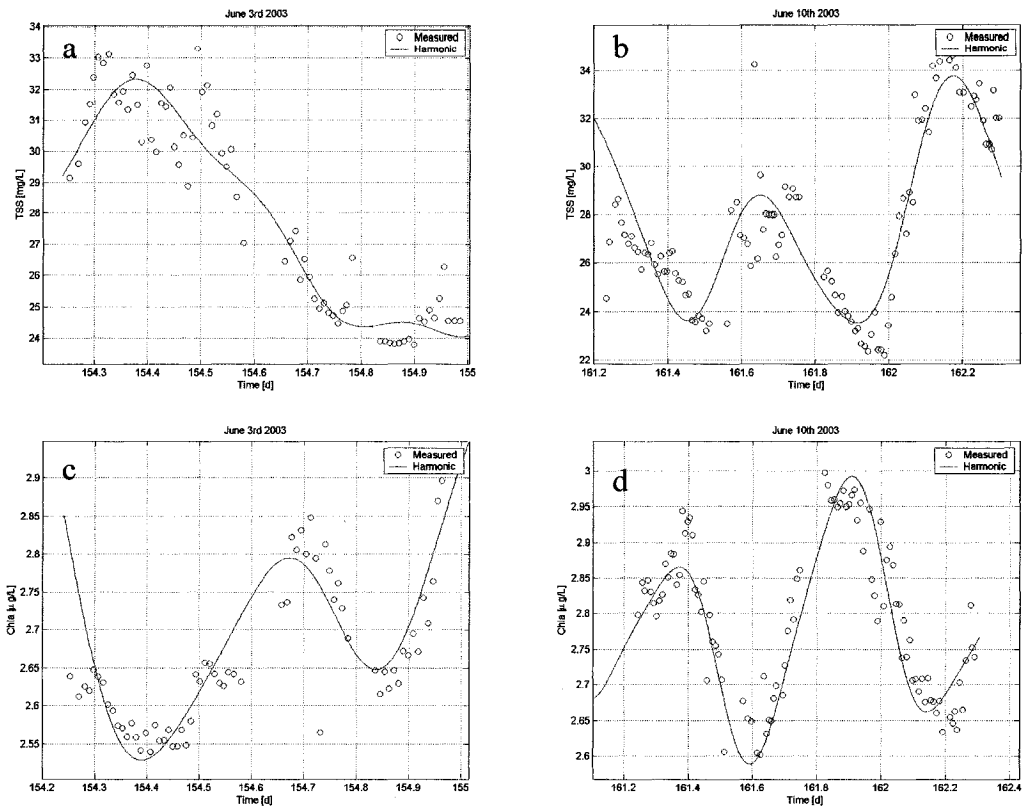


**Figure 2-7 Example of harmonic fit for cross sectionally average chlorophyll for summer data set. For flux calculations harmonics were fit for each grid cell. Open circles are actual data collected and solid line is the harmonic fit. The $R^2$ fit for June 3rd total suspended sediment (a) and June 10th (b) is 0.61. $R^2$ for June 3rd chlorophyll (c) and June 10th (d) is 0.79.**

## 2.5 Flux Decomposition

To discern which physical processes governed the net flux, we decomposed the velocity and scalar harmonic timeseries following Fischer 1972. The velocity and scalar timeseries were broken down into average and fluctuating components. The components of the velocity breakdown are: $u_0$, a temporal and spatial average, $u_1$, a cross sectional average with temporal variability, $u_2$, the tidal cycle average (steady), and $u_3$ a deviation (Figure 2-8) cross sectional deviation. The same decomposition was applied to chlorophyll and sediment concentrations.

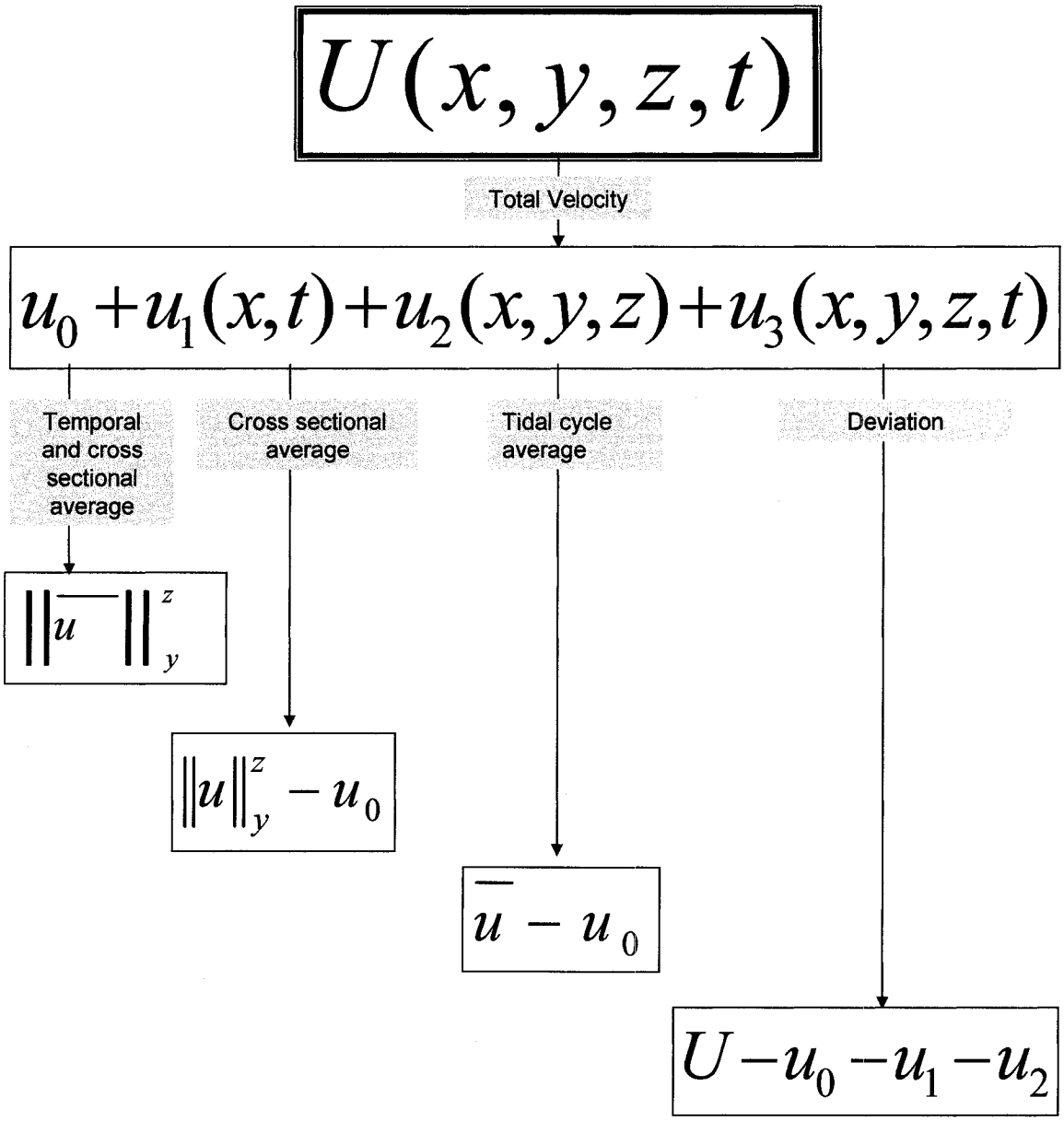


**Figure 2-8 Velocity field decomposed into average and fluctuating components. The x-direction is longitudinal or along the axis of the estuary. The z-direction is vertical and the y-direction is lateral. The first term $u_0$ is the cross-sectional (vertical bars) and temporal average over the tidal cycle (denoted by overbar). The second term $u_1$ is the cross sectional average, retaining variability in x and t. The third term $u_2$ is the temporal average minus the mean, retaining variability in all spatial dimensions. The fourth component $u_3$ is the remainder of the velocity once previous terms have been subtracted from original velocity. Although this is the most general form of the equation in all three spatial dimensions, it is important to note that we applied this decomposition at a fixed x-location, the Golden Gate.**

We applied this decomposition to each of the seasonal data sets to separate and quantify the physical processes responsible for the dispersive flux of chlorophyll. To define the cross-sectionally averaged mean outflow ($u_0$) or the advective component, we could not rely solely on the harmonic fitting, due to its small magnitude in comparison with instantaneous tidal velocity. Instead, we applied a bay-scale freshwater mass balance (Fram et al. 2006) (Eqn 2-6).

$$Q_f = u_0 * A_1 = Q_{delta} + Q_{LocalRivers} + Q_{MUD} - A_2(\frac{\partial Elevation}{\partial t} + Evaporation) \quad \text{Eqn 2-6}$$

$Q_f$ is the freshwater flow through the Golden Gate and is equal to the temporal and spatial average of velocity, $u_o$, multiplied by the cross sectional area over which fluxes were measured, $A_1$. Flow from Sacramento/San Joaquin delta is $Q_{delta}$,, flow from local rivers such as Coyote Creek are $Q_{localrivers}$, flow from municipal waste discharge is $Q_{MUD}$, and the last term is evaporation that is multiplied by the surface area of the Bay, $A_2$.

The flux of a scalar into or out of Central San Francisco Bay through the cross section of the Golden Gate is described by equation 2-7.

$$Flux = \dot{M} = Q_f C_0 + A_1[\overline{u_1 c_1} + \overline{\|u_2 c_2\|_y^z} + \overline{\|u_3 c_3\|_y^z}]$$

River Advection | Tidal Pumping & Trapping | Steady Circulation | Unsteady Shear Flow

Eqn 2-7

The first term on the right hand side of the equation represents the advective flux or the transport of the mean concentration by the river outflow, where $Q_f$ is freshwater flow as defined above [$m^3s^{-1}$] and $C_0$ is the mean concentration [mg $m^{-3}$]. The remaining terms represent dispersive processes where $A_1$ is cross sectional area of our study site [$m^2$]. The time average of $u_1c_1$ is the flux due to tidal cycle correlation of the cross

sectional averages, and for our study site is considered the net effect of both tidal pumping and trapping. The cross section average of $u_2c_2$ is the flux due to steady circulation, and is created by both baroclinic forcing and time-variable stratification events (Fram et al. 2006). The spatial and temporal average of $u_3c_3$ is the net flux due to oscillating shear flow, and includes mechanisms on smaller time scales.

There are two possible ways to apply Fischer's analysis to non-rectangular grids. The first involves averaging vertically initially and the second involves averaging laterally initially. While the two averaging techniques provide slightly different results, the difference between them is less than the uncertainties in our calculations so we present an average of the results from the two methods. There is less than a 2% difference between chlorophyll flux results and less than a 6% difference in the sediment flux results calculated using the two different methods.

## 2.6 Harmonic Sensitivity Analysis

To test how sensitive each of the flux mechanisms is to changes in the harmonics we re-calculated the fluxes using harmonic values that correspond to a fit 0.1 less than the optimum fit. In other words, if the optimized harmonics have an $R^2$ value of 0.90 we established the parameter range over which the $R^2$ remained above 0.80. The minimum and maximum values that were within the specified $R^2$ range were used to recalculate the fluxes. Error bars were constructed for each flux component based on the largest and smallest recalculated results.

# 3 Data Overview

The goal of this chapter is to provide a brief overview of the data we collected. This chapter will identify trends, both spatially and temporally each season. As outlined in the previous chapter, the scalar fluxes consist of components that vary both temporally and spatially. The physical processes described in the Chapter 1 will create a net scalar flux, as long as concentration gradients are established. In the case of tidal pumping, gradients must be established between the ocean and the estuary such that the timing of slack velocity is shifted from the timing of peak concentrations. In the case of steady exchange, gradients must be established in the lateral or vertical direction. These residual flow patterns combined with the spatial and temporal distribution of scalars determine the direction and quantity exchanged. Before considering the quantitative flux results it is useful to visualize some of the patterns of temporal and spatial correlation between velocity and scalars separately. This will provide a qualitative basis for understanding flux direction.

## 3.1 Temporal Patterns

First we can examine the temporal trends for each season, highlighting the fact that there is a difference in timing between peak scalar concentrations and slack tidal velocity. This phase difference is important to the tidal pumping component flux. In

order to create a tidal pumping flux, the phase difference between velocity and scalar must be greater or less than 90°. If the phase is less than 90° there will be a net flux of the scalar into the estuary, whereas the net flux will be out of the estuary if it is greater than 90°.

The spring data set is relatively incomplete because data could only be collected during daylight hours. Despite incomplete tidal cycle coverage, some trends can be discerned. Salinity is highest near the end of flood or beginning of high slack tide (72.5 &73.5), as would be expected (Figure 3-1b). There are fluctuations in the chlorophyll signal around slack tide, resulting in a slight increase in concentrations (Figure 3-1c). Although we didn't capture the low slack conditions, it appears chlorophyll is increasing on ebb. After high slack tide, sediment concentration drops until peak ebb velocities (72.6 & 73.6) and increases through the late part of ebb (Figure 3-1d). These temporal patterns indicate that tidal pumping flux of salt should be into the estuary and chlorophyll and sediment fluxes should be out of the estuary.

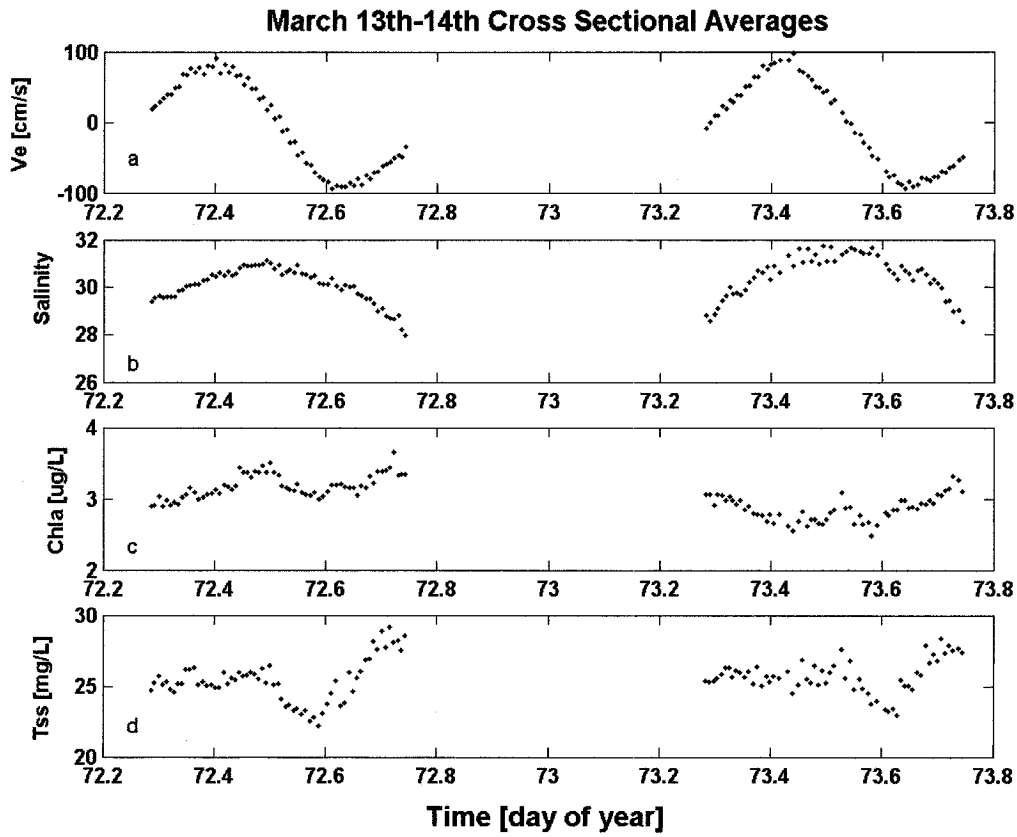


**Figure 3-1 Cross Sectional averages of velocity and scalar constituents March 13th-14th 2002. Panel a) is velocity east, b) is salinity, c) is chlorophyll and d) is suspended sediment.**

Fall cross section averages show that salinity is greatest after the end of flood tide (302.35, 302.78, 303.3) on October 29th (Figure 3-2b), and on November 6th (310.5, 311.15) (Figure 3-2f). Conversely, the minimum of salinity occurs at the end of ebb tide (303.1, 310.9) (Figure 3-2f). The salinity maxima are shifted slightly later in the tidal cycle during the fall compared to the spring. The chlorophyll minimum on October 29th occurs around maximum ebb tide (302.9) and the maximum for both days occurs at low slack (303.1, 310.8) (Figure 3-2c,g). This suggests the tidal pumping flux direction for chlorophyll will be opposite that of salinity. The sediment signal is slightly more difficult to interpret for the fall. During the first day, October 10th 2002, there is a large spike of suspended sediment (~80 mg/L) occurring close to the peak of flood velocity, 303.2

(Figure 3-2d). During the second day however, chlorophyll and sediment seem to be completely in phase so that maximum sediment concentrations occur at the end of ebb tide (310.8) (Figure 3-2h). Based on this signal it is not intuitive which direction the tidal pumping flux of sediment should be. Based on the first day alone, the flux of sediment would be into the estuary, and based on the second day alone, it seems as though the flux would be out of the estuary.

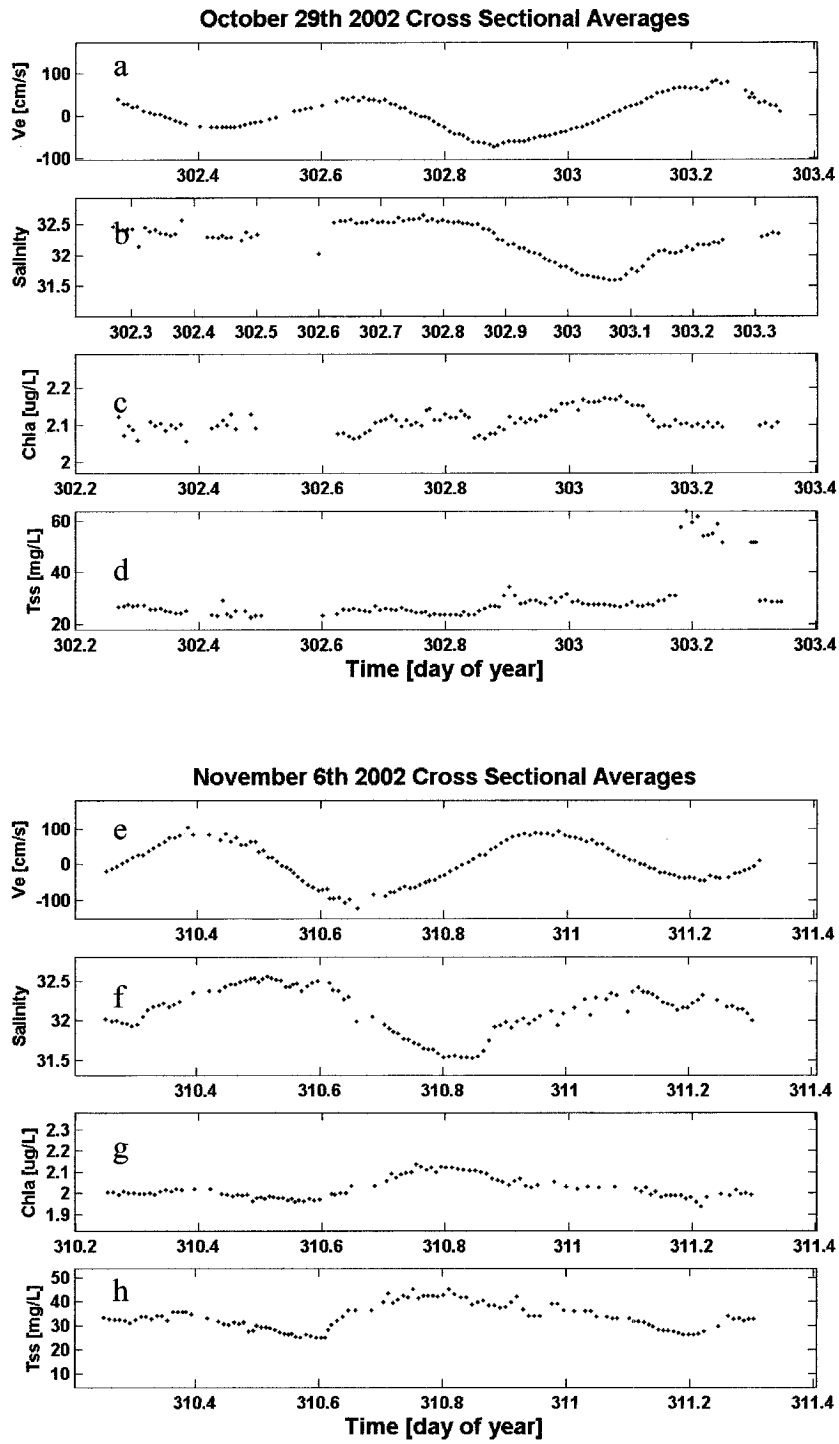


**Figure 3-2 Fall cross section averages of velocity and scalar constituents. Panels a-d are October 29th 2002, Panels e-h are November 6th 2002. Panels a&e) are velocity east, b&f) are salinity, c&g) chlorophyll and d&g) are suspended sediment.**

As in fall and spring, the maximum salinity occurs around the end of flood tide (154.7, 161.4, 161.93) and the minimum around the end of ebb tide (154.4, 154.88, 161.61, 162.2) (Figure 3-3b,f). The chlorophyll concentration maxima coincide with salinity maxima (154.7, 161.93) (Figure 3-3c,g). This means the tidal pumping flux for both chlorophyll and salinity should be into the estuary. Suspended sediment has a less well defined tidal signal and therefore it's more difficult to see a clear phase relationship. The highest suspended sediment concentrations on June 3$^{rd}$ occur near the end of ebb tide (154.4) (Figure 3-3d), and on June 10$^{th}$ around maximum ebb (162.19) (Figure 3-3h). While the timing of the suspended sediment concentration relative to tidal stage is not the same for June 3$^{rd}$ and 10$^{th}$, concentrations reach their maximum during ebb tide, suggesting a tidal pumping flux out of the estuary.

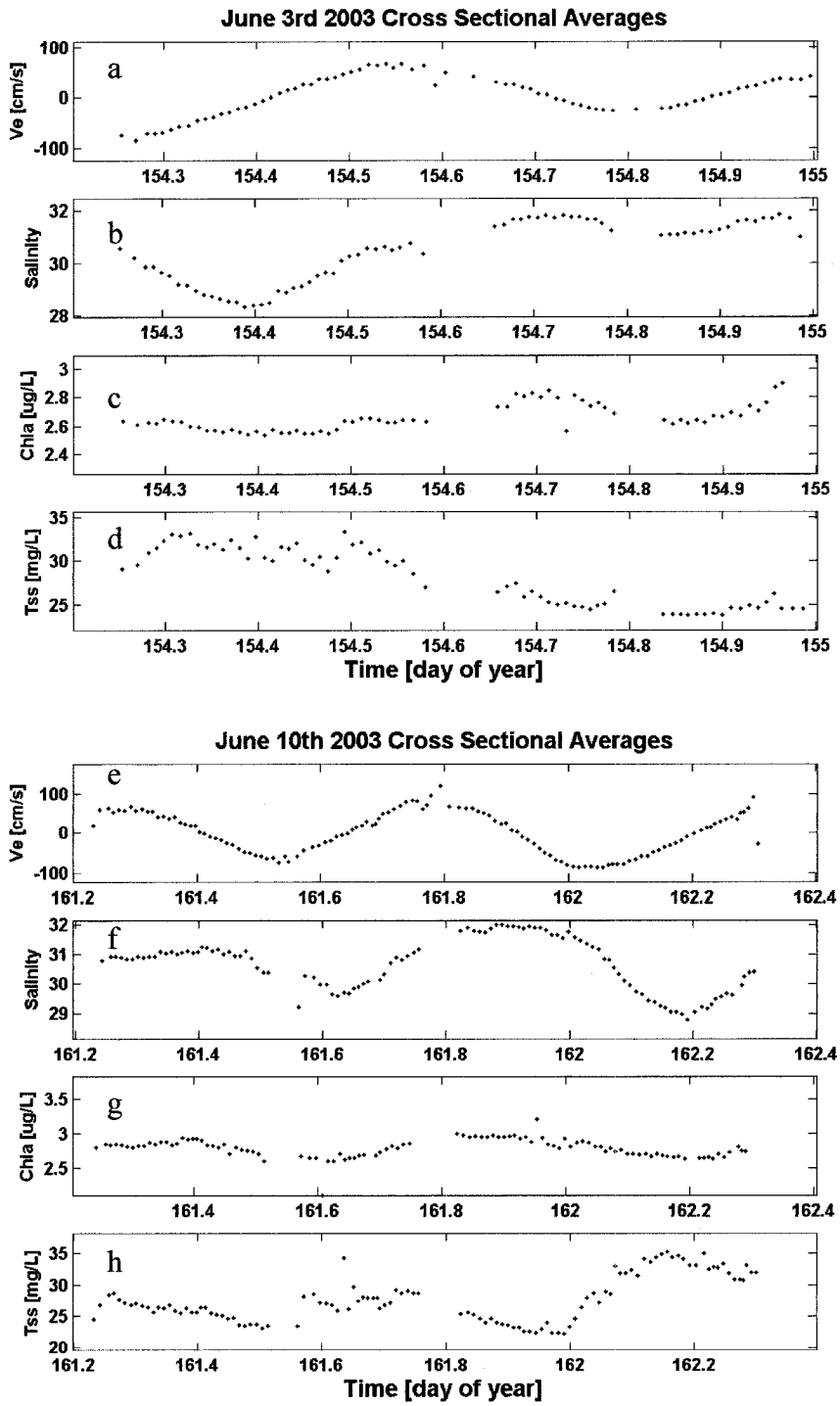


**Figure 3-3 Cross sectional averages of June 3rd and 10th. Panels a-d are June 3rd 2003, Panels e-h are June 10th 2003. Panels a&e) are velocity east, b&f) are salinity, c&g) chlorophyll and d&g) are suspended sediment..**

## 3.2 Spatial Patterns

We can also consider the temporal average of the cross section to visualize spatial patterns. The spatial distribution of scalars in conjunction with residual velocities determines the direction of the steady flux. The most well known and understood residual velocity structure in estuaries is estuarine circulation; driven by the longitudinal density difference between ocean and estuary. The residual flow is up estuary near the bed and seaward near the surface. A scalar flux due to this flow structure depends on the vertical distribution of that scalar. If the concentration is higher near the bed, the net flux will be up estuary and the opposite will be true if surface concentrations are relatively high. There is also a lateral circulation established by lateral density gradients at our location.

A simple way to visualize the lateral density gradients is using a salinity-temperature diagram (Figure 3-4). This type of diagram is used often in oceanography to distinguish different water masses. The South Bay waters are generally warmer and saltier than North Bay's cooler freshwater. The ocean water is much cooler and much saltier than estuary waters. This lateral density gradient creates flow in on the southern side of the transect and out on the northern side. This flow structure creates a scalar net flux based on the lateral distribution of scalar concentration. The lateral distribution of scalars such as sediment and chlorophyll is less intuitive than the vertical distribution.

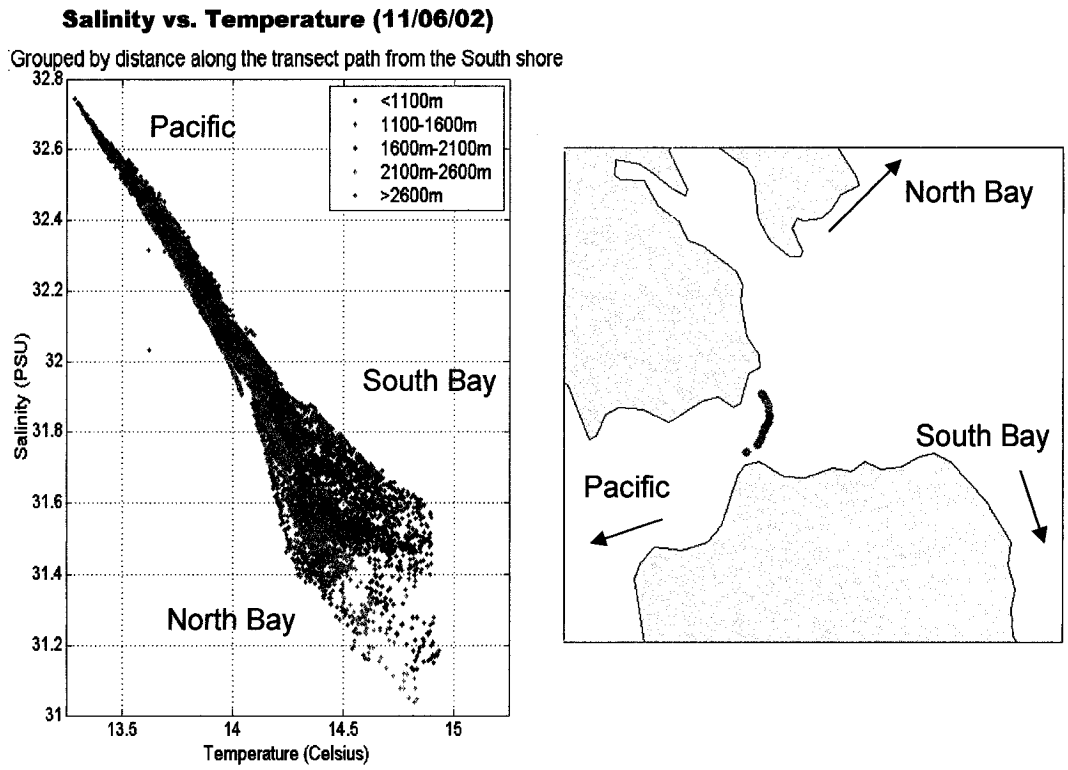


**Figure 3-4 using water masses distinguished by their temperature and salinity to show waters are not well mixed during ebb tide at our location**

Another steady lateral feature is introduced by the geometry of the estuary, shown in Figure 1-3. This structure consists of flood tide jet and an ebb tide drain. The residual flow created is into the estuary in the middle of the cross section, and out on the sides. This residual flow structure does not vary much seasonally compared to density driven flows because it is dependent on the geometry of the mouth of the estuary rather than seasonal freshwater inputs. First we will examine the velocity structure each season and then consider the distribution of chlorophyll and sediment.

The following graphs are interpolated data that have been averaged over time. The view is looking from the estuary out towards the Pacific, so the left hand side is the south end of the transect and the right hand side is the north end of the transect. The

black line represents the extent of the cross section over which we have consistent measurements. Velocities and scalar concentrations are represented by color in each of the graphs.

The dominant velocity structure year round is induced by the geometry of the basin; flow in at the middle and out on the sides (Figure 3-5). The magnitude and direction of this steady flow structure does not change much seasonally. Steady fluxes driven by this flow structure are determined by the spatial distribution of the scalar. If a scalar's concentration is higher in the middle of the channel compared to the sides, the flux will be into the estuary. Conversely, the flux will be out if the concentration is greatest at the sides.

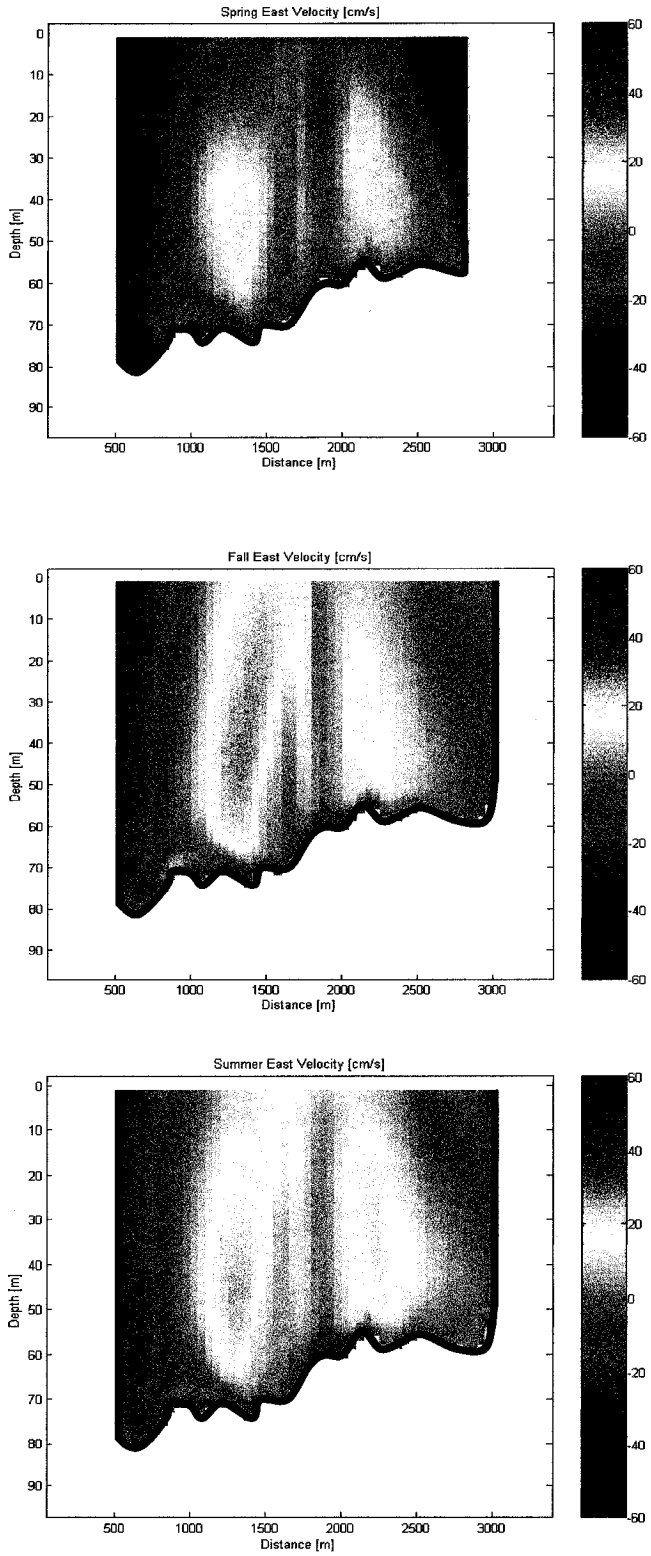


**Figure 3-5 Time average of the velocity east for all season. There is a persistent flow in at the center of the cross section and flow out at the northern and southern ends.**

Although the steady flow is dominated by the pattern shown in Figure 3-5, a smaller steady flow structure is induced by density gradients. In looking at the density distribution we can determine how baroclinic flows will affect the steady lateral and vertical fluxes of the other scalars. As expected, density increases with depth and is greatest on the southern end of the transect (Figure 3-6). The spatial density gradients are largest during the summer (Figure 3-6c), followed by spring (Figure 3-6a) and are weakest during fall (Figure 3-6b). Although freshwater flows were higher during the spring than the summer, the seasonal difference in density gradients observed is due to the difference in density near the bed rather than near the surface. This density structure suggests that coastal upwelling, combined with high freshwater flows, lead to the greatest spatial density gradients during the summer. The density distribution for all seasons will create a total steady baroclinic flux into the estuary if the scalar concentration increases with depth and towards the south. The converse would be true if the scalar distribution decreases with depth or increases towards the north.

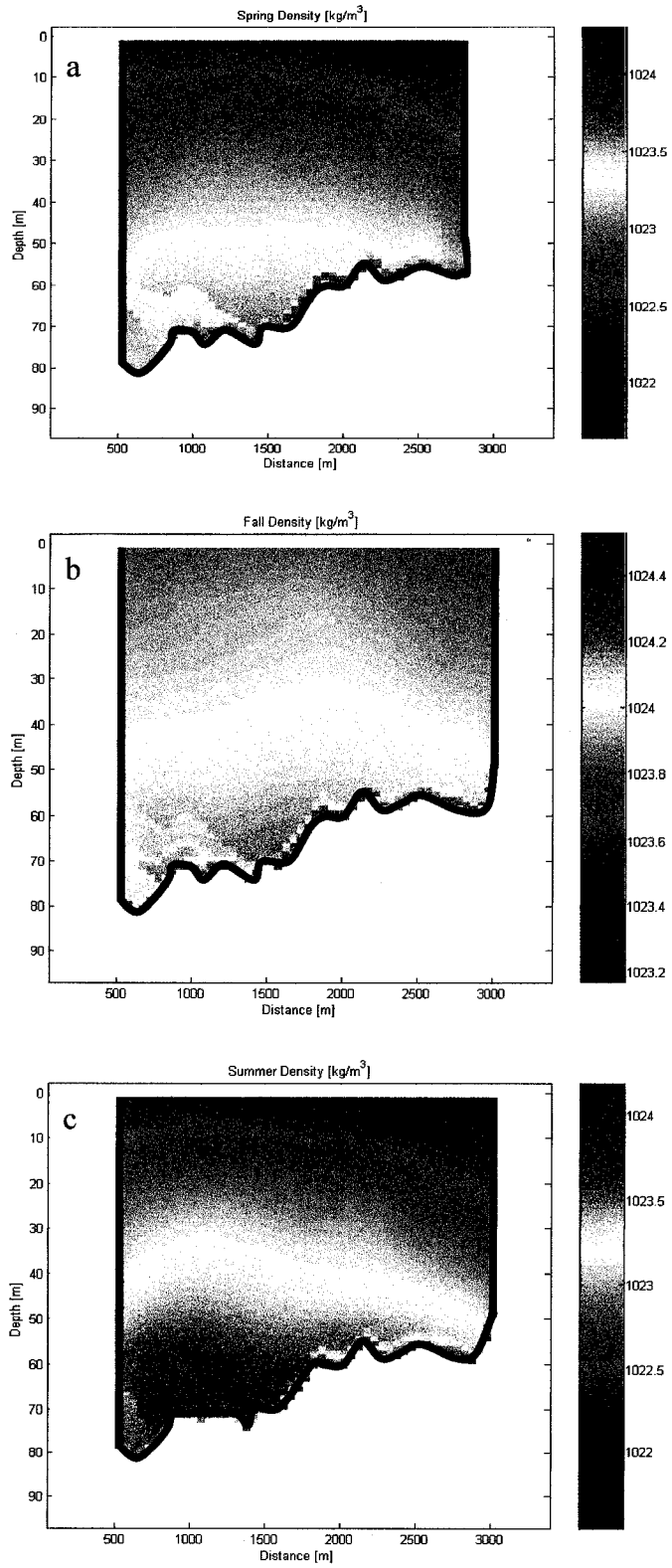


**Figure 3-6 Density distribution for spring 2002 (a), fall 2002(b) and summer 2003(c).**

We can now look at the seasonal the distribution of chlorophyll and sediment to determine the direction of the steady. The chlorophyll distribution changes significantly with season. During the spring, chlorophyll concentration is consistently higher on the south side of the transect (Figure 3-7 a). This distribution would create a lateral baroclinic flux into the estuary, but this could be counter acted by the steady flow induced by the mouth of the geometry. The direction of the steady vertical flux is not immediately obvious based on the vertical distribution of chlorophyll in spring. During the fall, the chlorophyll concentration is higher on the north side of the transect (Figure 3-7 b). This would lead to a steady lateral flux out of the estuary. The concentration is more uniform with depth than during the spring, but at some places it does increase with depth, likely creating a small steady vertical flux into the estuary. During the summer, the pattern is different. The concentration is more laterally uniform but the maximum concentration occurs mid water column, with the highest concentrations in the center (Figure 3-7c). The steady flow induced by the bay's geometry combined with this chlorophyll distribution will create a steady flux into the estuary. The spatial gradients chlorophyll are greatest during summer, followed by spring and fall. The spatial differences in concentration may seem very small, but these differences drive the steady flux. It is also important to note that even though the fluorometer calibration across seasons may not be accurate enough to compare the mass concentrations of chlorophyll, the flux directions would still be valid considering the relative fluorescence alone.

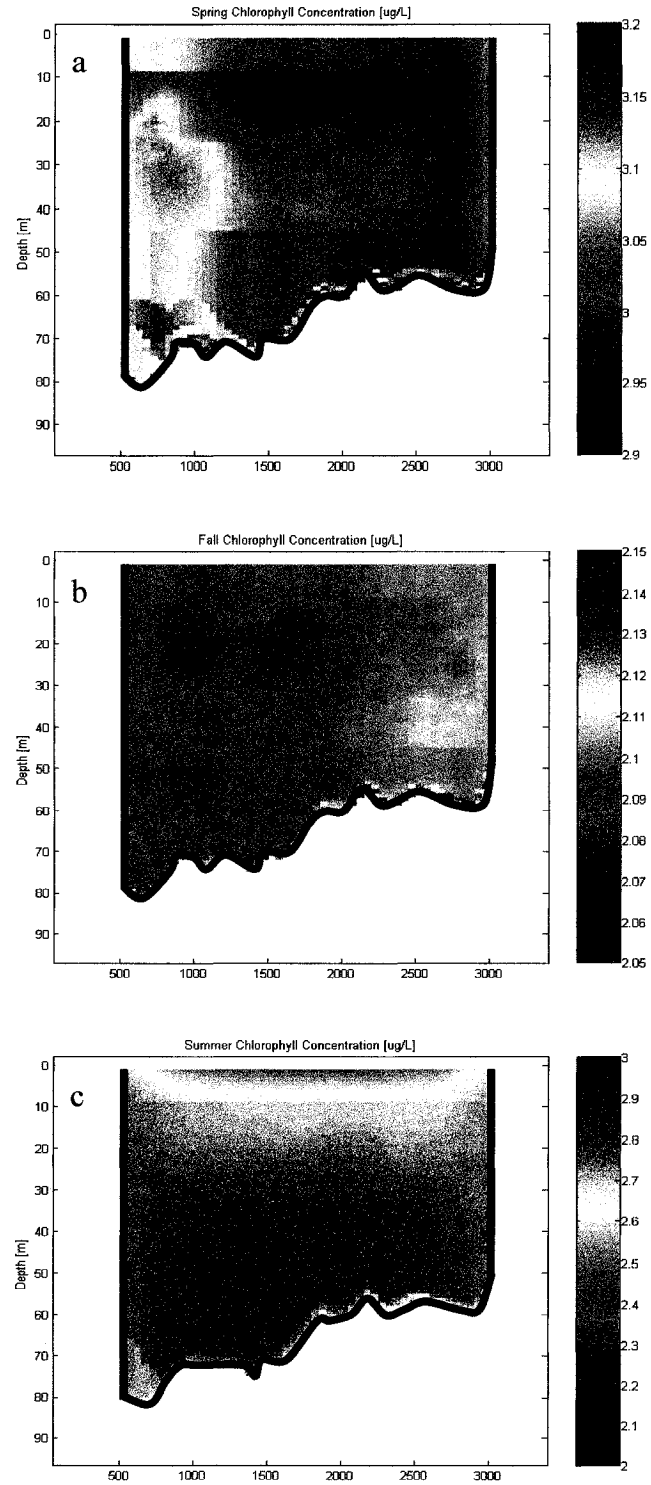


**Figure 3-6 Temporally averaged chlorophyll for all three seasons. Concentration ranges for each season do not overlap so the colormaps are different for each season.**

There is a difference in the vertical structure during spring and summer that is worth noting. The summer is smoothly interpolated but during the spring, the areas interpolated using the empirical equations stand out in contrast to the kriged data. This indicates there was most likely a different vertical profile of chlorophyll during the spring, possibly increasing near the surface rather than with depth.

The spatial distribution of sediment does not vary much with season (Figure 3-8). Sediment concentrations are consistently higher on the south side of channel closest to the bed. Both lateral and vertically driven baroclinic flux of suspended sediment will be into the estuary. Sediment concentration is greatest during the fall, presumably caused by the large pulse of sediment during flood tide. As noted for spring chlorophyll, the empirically interpolated boundaries form a sharp contrast to the kriged values (Figure 3-8b). This is most likely due to the nature of the empirical equations that fit the concentration to increase with depth. The large spike of sediment observed October 29$^{th}$ (Figure 3-2d) most likely created the high sediment concentrations observed on the south side during the fall. This suggests that the spatial averages are dominated by short term large spikes. These qualitative descriptions of the scalar and velocity structures will aide in understanding the quantitative flux measurements presented in the next several chapters.

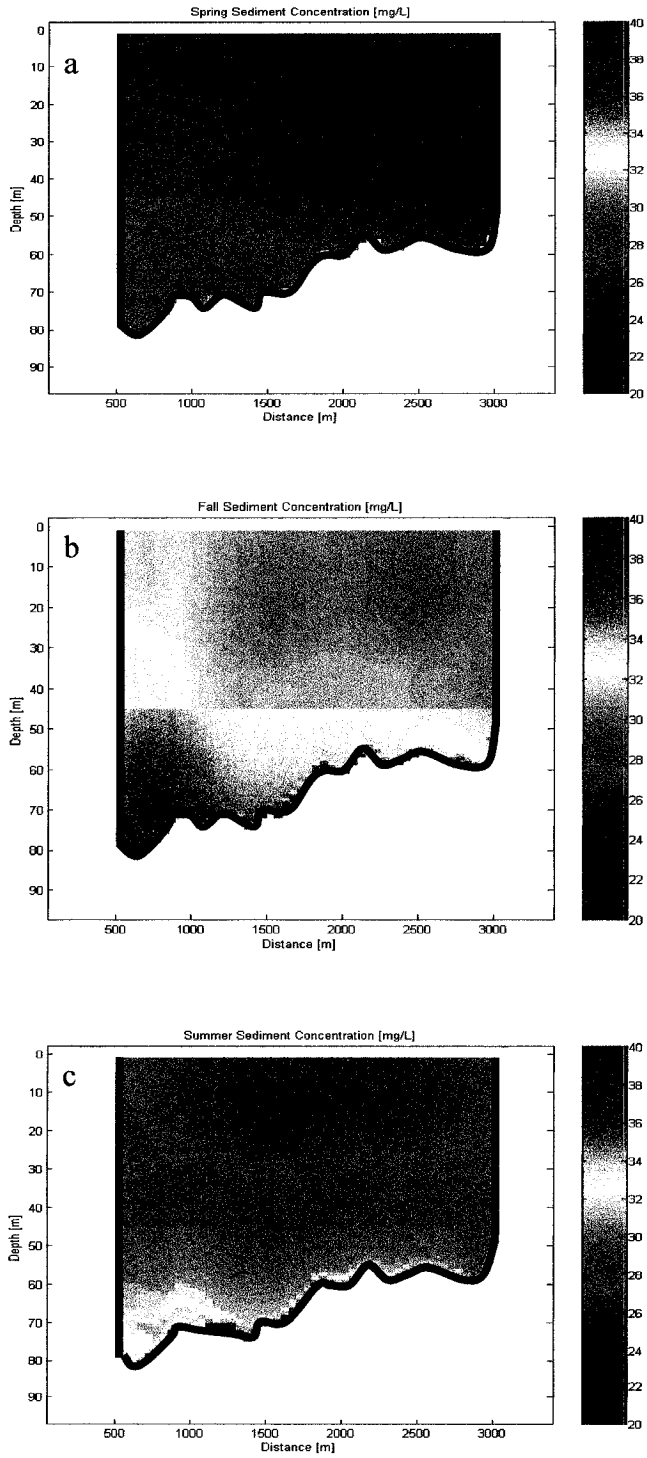


**Figure 3-8 Time averages of suspended sediments across seasons. Panel a) is spring, b) is fall and c) is summer.**

# 4 Chlorophyll Flux

The goal of this chapter is to quantify the net chlorophyll, and by proxy phytoplankton, exchange between San Francisco Bay and the coastal Pacific Ocean and distinguish which physical processes are responsible. Given the spatial and temporal patterns of chlorophyll and velocity reviewed in the last chapter, we can now consider how these patterns generate a net flux of phytoplankton.

The direction of the net flux of chlorophyll is determined by the magnitude and direction of both the dispersive and advective components. The advective flux is dependent on freshwater flows calculated using a bay-scale mass balance (Eqn 2-6) and the mean chlorophyll concentration calculated using the average of all the observed data. The dispersive flux was calculated using harmonic analysis. For each grid cell, harmonics were used to reconstruct a two week record of scalar concentration and velocity (Eqns 2-4, 2-5). These recreated timeseries were then decomposed using Fischer's method (eqn 2-7) and integrated over time to yield the flux for the various physical mechanisms described in Chapters 1 & 2.

The direction of the advective component is always out of the estuary (seaward) and the direction of the dispersive component changes seasonally. During the spring and fall the direction of the total dispersive flux is out of the estuary whereas during the summer it is into the estuary (Table 4-1). The net flux of chlorophyll is out of the estuary

during the spring and fall seasons, but the dispersive flux into the estuary is sufficiently large during summer to reverse the net flux into the estuary (Table 4-1).

**Table 4-1 Net chlorophyll-a flux results for spring, fall and summer. Negative sign means flux is out of the estuary.**

| Units [mg chl-a $s^{-1}$] | Spring (02) | Fall (02) | Summer (03) |
|---|---|---|---|
| Advection | -1900 | -290 | -1100 |
| Total Dispersion | -5900 | -470 | 2400 |
| Net Flux | -7700 | -750 | 1300 |

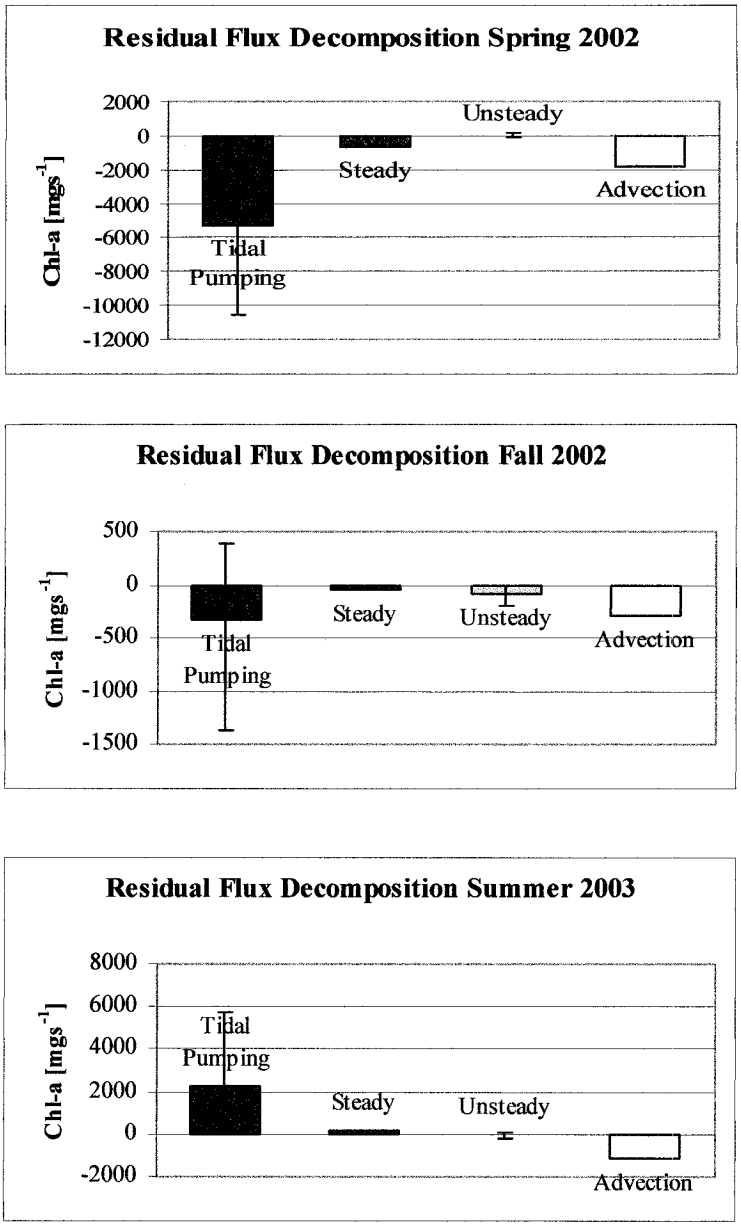


**Figure 4-1 Seasonal magnitude and direction of residual flux components. Negative values indicate a flux out of the estuary and positive indicates into the estuary. Error bars on dispersive components were calculated by testing the sensitivity of harmonics. Advective fluxes do not have error bars because they were not calculated using harmonic analysis.**

## 4.1 Advection

The advective flux is largest during the spring because freshwater flow and mean chlorophyll concentration are greatest (Table 4-2). Freshwater flows are lowest during the

fall and estuarine chlorophyll concentrations are also low, yielding the smallest advective flux. Freshwater flows were unusually high during this summer study leading to a relatively large advective flux. During a more typical summer freshwater input would probably be lower and the advective flux smaller.

**Table 4-2 Advective flow rates and mean chlorophyll concentration calculated in Central San Francisco Bay.**

| | Spring (02) | Fall (02) | Summer (03) |
|---|---|---|---|
| Freshwater flow $Q_f$ [$m^3 s^{-1}$] | -610 | -140 | -400 |
| Mean chlorophyll concentration $C_0$ [$mg\,m^{-3}$] | 3.0 | 2.1 | 2.8 |

### 4.2.0 Dispersion

The direction of the total dispersive flux is out of the estuary during spring and into the estuary during summer (Table 4-1). During the fall, the dispersive flux is relatively small, and dominated by tidal pumping; uncertainty in the tidal pumping harmonics suggests a net flux close to zero (Figure 4-1). In the remainder of this section, we discuss the mechanisms that cause this seasonal pattern; the separation of the fluxes into mechanisms is based on the processes identified in Chapter 2 (eqn 2-7 ).

### 4.2.1 Tidal Pumping

Tidal pumping is the dominant flux mechanism for all seasons and accounts for 79% of net dispersive flux during spring surveys, 64% during fall surveys and 93% during summer surveys. The spring and fall tidal pumping fluxes were 5300 mg $s^{-1}$ and

330 mg $s^{-1}$ respectively out of the estuary (Table 4-3). Summer tidal pumping flux was 2100 mg $s^{-1}$ into the estuary. These flux results indicate flood and ebb waters have different chlorophyll concentrations and there is a phase difference between the timing of slack water and the maximum chlorophyll concentration. At our site Fram et al. (2006b) found that the phase shift between velocity and salinity concentration varied seasonally due to baroclinic forcing of the headland eddy described in Chapter 2. This results in an increase in tidal pumping flux during winter/spring conditions relative to fall. Although the chlorophyll fluxes follow this pattern with the largest tidal pumping fluxes observed in spring and the smallest in the fall, this physical mechanism cannot account for the change in the direction of the tidal pumping flux. Therefore, we conclude that the seasonal trends in chlorophyll fluxes, particularly the reversal of the flux direction in the summer, must be driven by changes in the ambient chlorophyll gradient. This topic will be discussed in more detail in Section 4.4.

### 4.2.2 Steady Fluxes

Steady fluxes are about an order of magnitude smaller than tidal pumping fluxes during spring and are comprised of a vertical and lateral component. During spring and fall steady fluxes are 620 mg $s^{-1}$ and 44 mg $s^{-1}$ out of the estuary and during the summer they are 140 mg $s^{-1}$ into the estuary. Steady flux direction is determined by the chlorophyll distribution relative to the density induced circulation. As previously noted in Chapter 3, the distribution of chlorophyll changes seasonally (Figure 3-7). During the spring the concentration is highest on the southern side of the transect, this would lead to a steady lateral flux out of the estuary. The distribution of chlorophyll during the fall is practically uniform across the cross section, yielding a small flux out of the estuary, most

likely due to the higher concentrations on the northern side of the transect. During summer, the concentration increases with depth and is relatively uniform laterally. This suggests that the steady flux into the estuary during summer is driven by estuarine circulation, or the steady vertical shear in the water column.

### 4.2.3 Unsteady Shear Fluxes

Fluxes due to unsteady shear flow are an order of magnitude smaller than steady fluxes during spring and summer and are very sensitive to changes in harmonics. During fall unsteady flux is similar in magnitude as steady flux but is much more sensitive to changes in harmonics, and therefore, more uncertain. Given this we will not further emphasize the analysis of these fluxes.

**Table 4-3 Seasonal dispersive chlorophyll fluxes separated into physical processes**

| Units [mg $s^{-1}$] | Spring (02) | Fall (02) | Summer (03) |
|---|---|---|---|
| Tidal Pumping | -5300 | -330 | 2100 |
| Steady | -620 | -44 | 140 |
| Unsteady | 20 | -90 | -20 |

## 4.3 Harmonic Sensitivity Analysis

Although tidal pumping is the most sensitive of the flux mechanisms to changes in M2 amplitude and phase, the direction of the tidal pumping flux during spring and summer does not change. We note that the magnitude of the flux could be up to 100% larger in spring and 150% in summer than reported optimized values (Figure 4-1). The fall tidal pumping flux is very sensitive to small changes in the harmonics. Fall flux direction is unclear and the magnitude could be up to 4000% more or less than optimized value and we conclude that this result is not significantly different from zero.

Due to the incomplete tidal cycle coverage during the spring, harmonics with periods longer than 24 hours cannot be effectively constrained. The K1 phase harmonic is poorly constrained and a phase between 0 and $\pi$ yields an equally good fit ($R^2$) as a phase between 0 and $-\pi$. The K1 phase primarily affects mean chlorophyll concentration $C_0$ and the steady flux; the ambiguity between positive and negative phases lead us to conclude that the steady flux estimate during the spring season is not significantly different from zero. This fact does not, however, undermine the conclusion that the net dispersive flux is out of the estuary during the spring season because it is dominated by tidal pumping and is strongly dependent on the M2 harmonics.

## 4.4 Discussion

Although we only collected data for several days during each season for one year, the results are in agreement with previous studies descriptions of seasonal patterns of circulation and chlorophyll distribution (Cloern 1996; Pennington and Chavez 2000). The direction of the advective or river component is always out of the estuary or seaward. River inputs to the estuary are greatest during the spring when the snow pack begins to melt which corresponds with the largest advective velocities out of the estuary and largest advective flux (Conomos 1985). The direction of the dispersive component, which is comparable to or greater than the advective flux, changes seasonally. During the spring and fall the direction of the total dispersive flux is out of the estuary whereas during the summer it is into the estuary. The direction of dispersive transport changes seasonally because the distribution of chlorophyll changes seasonally.

Fick's dispersive flux is defined as: $Flux = -K_x \frac{\partial C}{\partial x}$ where $K_x$ is the dispersion coefficient and $\frac{\partial C}{\partial x}$ is the spatial gradient of chlorophyll along the direction of the major flow axis, primarily east-west at our field location. We calculated the dispersion coefficient using the salinity fluxes in conjunction with an assumed salinity gradient based on a constant oceanic salinity of 34 psu (Fram et al, 2006). This analysis yielded the following dispersion coefficients: 720 $m^2/s$ for summer, 380 $m^2/s$ for fall and 890 $m^2/s$ for spring. Using these dispersion coefficients, we calculated what the theoretical chlorophyll gradient was during each experiment. We compared these theoretical gradients to observations of chlorophyll concentration observed along the coast during our summer experiments. National Marine Fisheries Service (NMFS) collected chlorophyll and salinity data from June $5^{th}$-$10^{th}$, so we can estimate what the "actual" gradients were and compare them to our theoretical estimates of both chlorophyll and salinity.

Data from the NMFS study were mapped with our harmonic mean and a chlorophyll surface was created using a cubic interpolation (Figure 4-2). A gradient was calculated each day for both the east-west and north-south gradients using a finite difference method. The temporal and spatial average of the east-west gradient is the same order of magnitude for both salinity and chlorophyll as we estimated using the flux measurements but the NMFS chlorophyll gradient was larger and salinity gradient smaller than the gradients we estimated (Table 4-4).

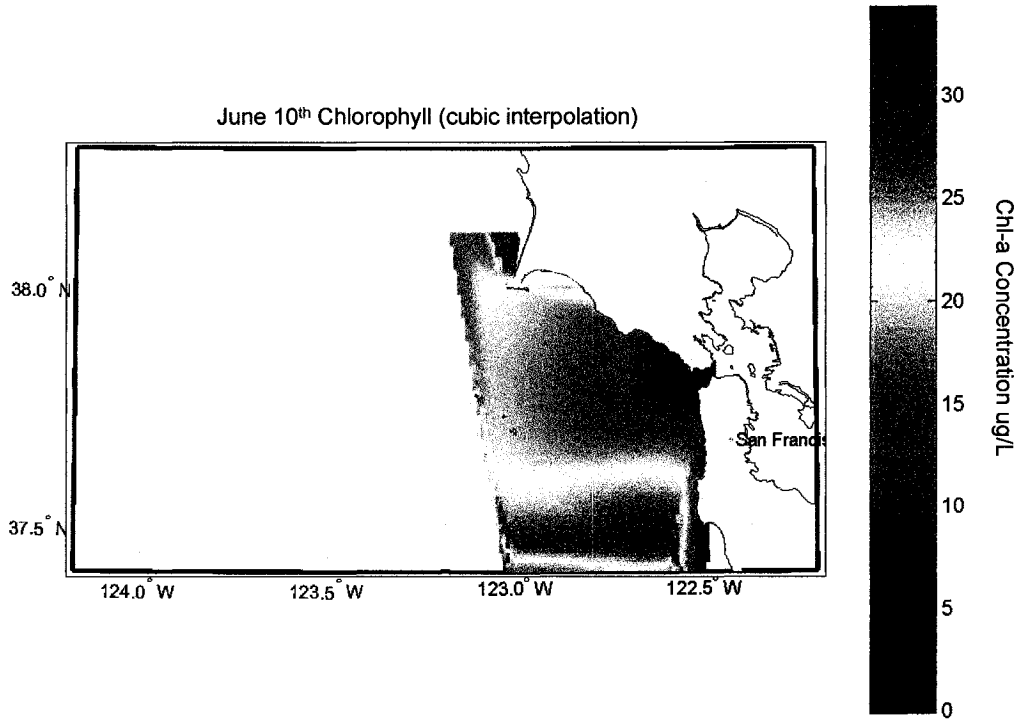


**Figure 4-2 Example of the cubic interpolation used to estimate chlorophyll gradients during the summer experiment day June 10th.**

The oceanic salinity observed by NMFS is slightly smaller, 33.3, than what we assumed using a constant oceanic salinity of 34 psu, therefore the gradient during this season is actually slightly smaller than we estimated. This implies that dispersion coefficient is even larger than we initially estimated. The location of the 34 psu isohaline may have been further offshore than was previously assumed by Fram et al (2006).

The discrepancy between the NMFS and estimated chlorophyll gradients may be due to a variety of factors. The most obvious source of error in this analysis is the use of a cubic spline to interpolate NMFS observations. Such an interpolation scheme creates a smooth surface between data points and as previously noted, phytoplankton blooms tend to be inherently patchy. This could lead to the overestimating of gradients in places

between high and low measured concentrations. Another possibility to explain the discrepancy is mixing in the Golden Gate channel. Flood waters during our experiment tended to be more homogenized in both lateral and vertical directions. Similar results have been found on the coastal side of the mouth of the estuary during ebb tide (Largier 1996). Measuring on the landward side of the estuary mouth combined with the intense mixing occurring in the channel may lead to an underestimation of the gradient. Another possibility is that phytoplankton in Central Bay or the adjacent coastal waters suffer a net loss or negative growth due to unfavorable conditions.

**Table 2-4 Comparing flux estimated chlorophyll gradients to observed chlorophyll gradients**

| | Dispersive Flux [ $m^{-2}s^{-1}$] | Kx [$m^2s^{-1}$] | Flux Derived Gradient [ $m^{-4}$] | NMFS Gradient [ $m^{-4}$] |
|---|---|---|---|---|
| Chl-a [mg] | 1.54E-02 | 720 | -2.12E-05 | -6.03E-05 |
| Salt [psu] | 1.49E-01 | 720 | -2.05E-04 | -1.42E-04 |

Because we cannot verify chlorophyll gradients for spring and fall, we consider our chlorophyll measurements in the context of the temperature and salinity of estuary and ocean water masses. In Figure 4-3, we present seasonal observations of cross sectionally averaged temperature and salinity, with measured chlorophyll, color-coded by concentration. In T-S space, the oceanic waters appear in the lower right corner (high salinity, low temperature), while estuarine waters are in the upper right (low salinity, high temperature). During the spring (Figure 4-3a), high concentrations of chlorophyll are associated with estuarine waters. During the summer (Figure 4-3c), this gradient is reversed, and the highest chlorophyll concentrations are associated with oceanic waters.

Combining these results with the relatively constant tidal dispersion coefficients, we conclude that the seaward dispersive flux of chlorophyll during the spring surveys is due to a positive concentration gradient, meaning higher in the estuary and lower in the coastal ocean; during the summer surveys, the gradient is reversed, with higher concentrations in the coastal ocean and lower in the estuary, creating a dispersive flux into the estuary. During the fall surveys there is essentially no chlorophyll gradient and the dispersive flux is close to zero. The variation in ocean-estuary chlorophyll gradient and hence exchange therefore depends on the seasonal variation of phytoplankton blooms and in turn, net growth conditions in both the estuary and coastal environments.

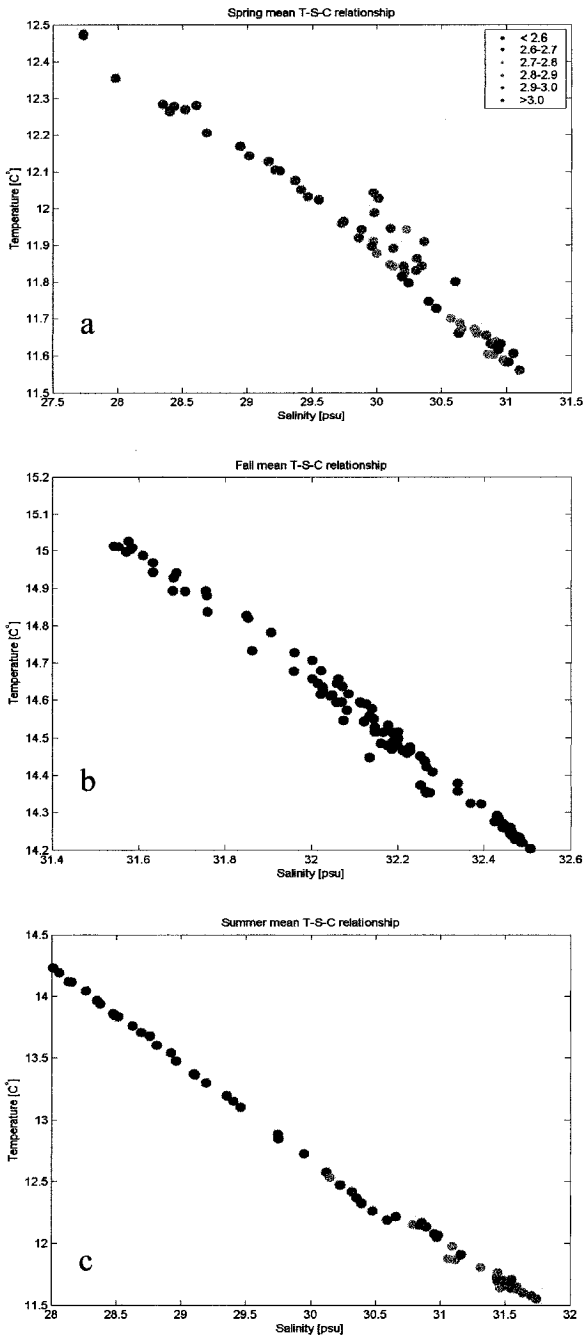


**Figure 4-3 The estuary water signature is low salinity-high temperature and the coastal water is high salinity-low temperature. Colors indicate concentrations of chlorophyll in mg $m^{-3}$. Chlorophyll concentration is higher in the estuary during spring (a), uniform during fall (b) and higher in coastal waters during summer (c), illustrating that the chlorophyll source and gradient changes seasonally.**

Although it is common practice to model dispersive fluxes following a Fickian approach, it should be emphasized that we can only model the dispersive flux in this

particular case following a Fickian approach, using the east-west gradient, $\frac{\partial C}{\partial x}$, because tidal pumping dominates. If baroclinic, or steady vertical exchange dominated, the dispersive flux would scale very differently from a Fickian approach. For a baroclinic flux the velocity would scale as:

$$U_{bc} = \frac{\frac{g}{\rho_0}\frac{\partial \rho}{\partial x} H^3}{\upsilon}$$

where $\frac{g}{\rho_0}\frac{\partial \rho}{\partial x}$ is the pressure due to the river-ocean density gradient, $H$ is the total water column depth, and ν, is the viscosity. The concentration determining the baroclinic flux, or steady vertical flux, would be dependent on, vertical diffusion, $K_z(z)$, the water column depth, $H$, the phytoplankton settling velocity, $w_s$, and the net growth rate, μ (z), such that: $C_{bc} = f(K_z(z), H, w_s, \mu(z))$

And so, the baroclinic flux, $\int U_{bc} C_{bc} dt$, is not a function of the east-west chlorophyll gradient, $\frac{\partial C}{\partial x}$ and cannot be modeled using the Fickian approach previously described.

### 4.4.1 Seasonal Variability in Estuarine Phytoplankton Blooms

There are distinct seasonal phytoplankton cycles within San Francisco Bay. North San Francisco Bay historically had blooms during the summer but they have declined since 1989 when an invasive clam was introduced to the ecosystem (Cloern 1996). Currently the largest annual production of phytoplankton occurs during spring after the annual freshwater pulse reaches South San Francisco Bay. Freshwater flows are usually greatest between January and March. During neap tides, when mixing energy is

low, this freshwater pulse stratifies the water column in parts of the estuary. When the water column is stratified phytoplankton in the photic zone are decoupled from the benthos, thereby reducing benthic grazing and light limitations due to tidally re-suspended sediments. Release from light and grazing-induced limitations leads to a bloom (Cloern 1982; Cloern 1991). The result is high concentrations of chlorophyll within the estuary, especially in South San Francisco Bay every spring.

Based on an analysis of temperature and salinity, we found the water at the southern end of our transect was largely made up of South Bay waters (Figure 3-4). Although we do not have simultaneous measurements of conditions in South Bay a bloom was likely occurring due to the coincidence of peak freshwater pulse and neap tides during our spring surveys. During spring of 2002, Sacramento/San Joaquin River peak flow was January 6$^{th}$ and assuming the travel time of the freshwater pulse from the Delta to South Bay is between 35- 50 days (Uncles and Peterson 1996) we would expect the pulse to arrive between February 10$^{th}$ and 26$^{th}$. Spring to neap tide transition occurred between February 27$^{th}$ and March 6$^{th}$ and it is reasonable to assume this was the window when the onset of a bloom occurred. Our measurements in Central Bay were made on March 6$^{th}$-7$^{th}$ and 13$^{th}$-14$^{th}$, therefore, if the high concentration of estuarine chlorophyll measured during our spring surveys was derived from a South Bay bloom, the travel time between Central and South Bay would be approximately 1-2 weeks.

Although we cannot refine this description further with the data available at this point, we conclude that the direction of ocean-estuary exchange is gradient driven and will be consistently be out of the estuary while there are estuarine blooms within the

realm of Central exchange. The magnitude of phytoplankton exchange will depend on the intensity and duration of the bloom.

### 4.4.2 Seasonal Variability in Coastal Phytoplankton Blooms

The normal pattern of coastal upwelling (typical in years without El Nino or La Nina conditions) on the west coast of the U.S.A. is driven by southerly winds and the Ekman transport of surface waters offshore (Hickey 1979). This upwelling brings nutrients into the photic zone, releasing coastal phytoplankton from nutrient limitation in the photic zone (Hutchings et al. 1995). The result is a period of intense growth in the coastal ocean. In Monterey Bay, increases in surface nitrate are observed initially after upwelling and high surface chlorophyll concentration generally lag behind surface nitrate concentration by weeks (Pennington and Chavez 2000; Collins et al. 2003). During El Nino years temperatures are warmer, the thermocline is deeper and waters in the photic zone tend to be low in nutrients. The opposite is true during La Nina when surface waters are cool, the thermocline is elevated and surface nutrients from upwelled waters is greater than normal. These conditions lead to unseasonably low phytoplankton growth during El Nino and high growth during La Nina (Chavez et al. 2002). January 2003 until spring of 2004 was a 'normal' oceanic year so our summer observations characterize normal conditions (Goericke et al. 2004).

During our summer observations, coastal chlorophyll concentrations were elevated compared to estuarine concentrations (http://sfbay.wr.usgs.gov/access/wqdata). National Marine Fisheries Service (NMFS) collected hydrographic and biological data (including chlorophyll concentration) from June 3$^{rd}$ -10$^{th}$ in the coastal region offshore from San Francisco. Their data indicate high surface chlorophyll concentrations (~25

μg/L) throughout their study, especially June 10th to the north and south of San Francisco Bay (Keith Sakuma NMFS, personal communication) (Figure 4-2).

These blooms were most likely initiated by upwelling. Large (daily average >100 tons/s-100m of coastline) offshore Ekman transport began May 5th 2003 and with the exception of June 3rd -6th continued until June 26th (http://www.pfeg.noaa.gov/products/PFEL). The break in the winds between June 3rd and 6th may have initiated the very high chlorophyll concentrations measured by NMFS. Pennington & Chavez (2000) and Hutchings (1995) have found that diatoms, the dominant type of coastal phytoplankton (Chavez et al. 1991; Venrick 2002; Collins et al. 2003), bloom after large upwelling events during times of relatively low mixing. These data confirm that wind driven upwelling initiated blooms in the coastal ocean offshore of San Francisco Bay during our study.

Coastal blooms during the summer result in a gradient driven dispersive flux into the estuary. Our flux measurements from summer of 2003 are representative of summer conditions in most years, with the possible exception of El Nino years when the coastal bloom may be weakened or absent.

### 4.4.3 Implications for Ocean-Estuary Exchange

The difference in timing of peak growth periods in the estuary and coastal ocean establishes the annual cycle in net chlorophyll fluxes presented in Table 4-1. As growth conditions improve in the estuary during winter/spring neap tides, the net flux of chlorophyll is out of the estuary due to both advection and dispersive mechanisms. During the summer months, as estuarine (net) growth decreases and coastal upwelling begins, the ocean-estuary gradient of chlorophyll reverses, and the flux of chlorophyll is

into the estuary. It is important to note that the shifting in the direction of chlorophyll flux is not a function of different physical flux mechanisms, but is rather purely a result of a changing gradient in chlorophyll. Instead, the physical mechanism that dominates ocean-estuary exchange, tidal pumping, is relatively constant throughout the year, and will always create a down-gradient flux.

We note seasonal variability could look different if the analysis focused on a single species, as opposed to total chlorophyll. Diatoms have been found to perennially dominate both the coastal region offshore of San Francisco Bay and within the estuary (Cloern & Dufford 2005, Chavez et al. 1991). While it has been shown that the relationship between fluorescence and chlorophyll-a is variable as is the relationship between chlorophyll and biomass (Laws 1980); Chavez et al. (1991) found that coastal diatoms offshore of San Francisco Bay had the highest correlation between number of cells (total biomass) and amount of chlorophyll. Assuming populations during our study period were mostly diatoms, chlorophyll fluxes measured are reasonable estimates of phytoplankton biomass exchanged between San Francisco Bay and the coastal Pacific Ocean.

Chlorophyll gradients can change on timescales ranging from days to weeks. Although the gradient may be very large between the ocean and estuary, especially during a bloom event, the net flux is ultimately limited by the balance between transport and growth timescales. The longer the bloom is and the closer it is to the mouth of the estuary, the greater the amount of phytoplankton transported between coastal and estuarine ecosystems.

Several other estuaries along the western U.S. have reported qualitatively similar results. Roegner and Shanks (2001) found that chlorophyll was transported from the coastal Pacific into South Slough, Oregon during upwelling events. While there were no quantitative measurements made of the net flux, there was a relatively strong ocean-estuary gradient, suggesting that similar physical mechanisms (tidal pumping) may be controlled ocean-estuary exchange. In Willapa Bay, Washington, Newton and Horner (2003) found that the highest primary productivity in the bay was associated with the transport of coastally derived phytoplankton species into the bay. This seasonal reversal of the ocean-estuary chlorophyll gradient may hold true for other estuaries and embayments along eastern boundary currents where upwelling occurs, such as in Saldanha Bay in South Africa, and embayments along the Northwest Iberian coast.

# 5 The Role of Phytoplankton Growth in the Central Bay Chlorophyll Balance

Based on the chlorophyll flux measurements we concluded that seasonal change in the dispersive flux direction was due to the reversal in the sign of the chlorophyll gradient. These gradients are established by differences in the timing and magnitudes of blooms in the estuary and ocean. Typically, blooms are isolated patches of high chlorophyll or phytoplankton concentrations that are triggered by changes in the physical environment (Martin 2003). Local processes that control phytoplankton populations include: the production of new biomass (which is controlled by the availability of visible light and nutrient resources); mortality, grazing losses to pelagic and benthic consumer animals, turbulent mixing by the tides and wind, sinking and deposition of phytoplankton on the bottom sediments, and resuspension of bottom-deposited microalgae by tidal currents and wind waves (Cloern 1996).

Several different effective or net growth models have been developed for San Francisco Bay (Cloern et al. 1995, Lucas et al. 1999, Alpine and Cloern 1988). These models attempt to take into consideration the relevant biological processes into a single variable often symbolized as $\mu_{net}$, net growth. Net growth rates in San Francisco Bay

most often incorporate light dependent growth, respiration and benthic grazing. In San Francisco Bay, when conditions are optimal, sufficient nutrients, low turbidity, low predation and small transport rates, blooms occur. The methods we used to calculate the chlorophyll flux did not explicitly account for any biological processes, yet we determined that the flux direction and magnitude was largely due to the differences in growth conditions between ocean and estuary. To discern the relative importance of biological (net growth) and physical processes affecting the phytoplankton in Central Bay, we constructed a simple box model that includes advection, dispersion, and growth.

### 5.1.0 Model Description

The simplest way to model phytoplankton within Central Bay is with a box model where the only direction considered is east-west exchange (Figure 5-1). Assuming the chlorophyll concentration is uniform and well mixed throughout the Central Bay box, we can use the following equation to describe the phytoplankton balance:

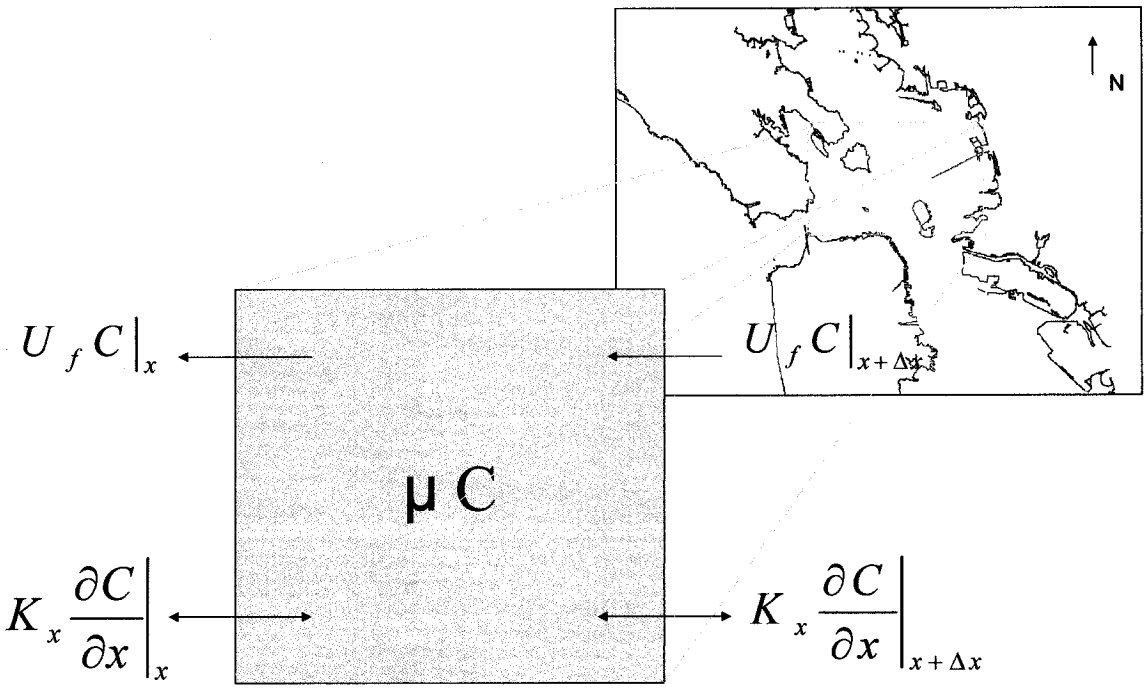


**Figure 5-1 Schematic of chlorophyll box model for Central Bay. The model includes advection, growth and dispersion.**

$$\frac{\partial C}{\partial t} = \mu_{net} C + U_f \frac{\partial C}{\partial x} + \frac{\partial}{\partial x}\left( K_x \frac{\partial C}{\partial x} \right) \quad \text{Eqn 5-1}$$

The rate of change of chlorophyll in our box is dependent on net growth, advection and dispersion. The first term on the right hand side of equation 5-1, $\mu_{net}$, is the net growth rate occurring in Central Bay [$s^{-1}$], the next term, $U_f$, is the river advection and the final term, $d/dx(K_x\, dc/dx)$, is the net flux due to dispersion.

An analytical solution can be found if the following approximation is made:

$$\frac{\partial C}{\partial t} \approx \underbrace{\frac{U_f(C_{est}-C)}{L}}_{U\frac{\partial C}{\partial x}} + \underbrace{\frac{K_{est}(C_{est}-C)}{L^2} + \frac{K_{oc}(C_{oc}-C)}{L^2}}_{\frac{\partial}{\partial x}\left(K_x \frac{\partial C}{\partial x}\right)} + \mu_{net} C \quad \text{Eqn 5-2}$$

Then substituting,

$$X = \frac{U_f C_{est}}{L} + \frac{K_{est} C_{est}}{L^2} + \frac{K_{oc} C_{oc}}{L^2} \qquad \text{Eqn 5-3}$$

and

$$Y = -\frac{U_f}{L} - \frac{K_{est}}{L^2} - \frac{K_{oc}}{L^2} + \mu_{net} \qquad \text{Eqn 5-4}$$

The subscript *est* indicates conditions on the east or estuary side of the box, and the subscript *oc* indicates conditions of the west or ocean side of the box. $L$ is the east-west length of box. Assuming X and Y are constant in space and time we can integrate the following equation from t=0 to T:

$$\int \frac{dC}{X + Y C} = \int dt \qquad \text{Eqn 5-5}$$

and arrive at the solution

$$C(t) = \frac{X}{Y}\left[e^{YT} - 1\right] + C_0 e^{YT} \qquad \text{Eqn 5-6}$$

where $C_o$ is the initial condition.

### 5.1.1 Model Coefficient Calibration

The model coefficients $U_f$, and $K_{oc}$ were calculated using data gathered during our summer field experiments (Chapter 4). The length, $L$, was estimated using two methods: the first is a physical scaling based on the size of the Central Bay box, the second is a lengthscale based on the salinity exchange. Chlorophyll concentrations were estimated using data collected by the USGS ($C_{est}$) (http://sfbay.wr.usgs.gov) and NMFS ($C_{oc}$) (Keith Sakuma, personal communication). The net growth, $\mu_{net}$, was calculated

using our seasonal light (PAR) measurements collected. The estuary dispersion coefficient was estimated by averaging the South Bay and North Bay dispersion coefficients reported by Uncles and Peterson (1996) where $K_{sb}$ = 190 $m^2/s$, and $K_{nb}$ = 130 $m^2/s$ (Table 5-1); the average is $K_{est}$ = 160 $m^2/s$.

### 5.1.2 Net Growth Rate

To calculate the net growth rate, we used our photosynthetic active radiation (PAR) measurements (Figure 5-2) to calibrate a light-limited growth model that has been previously used in San Francisco Bay.

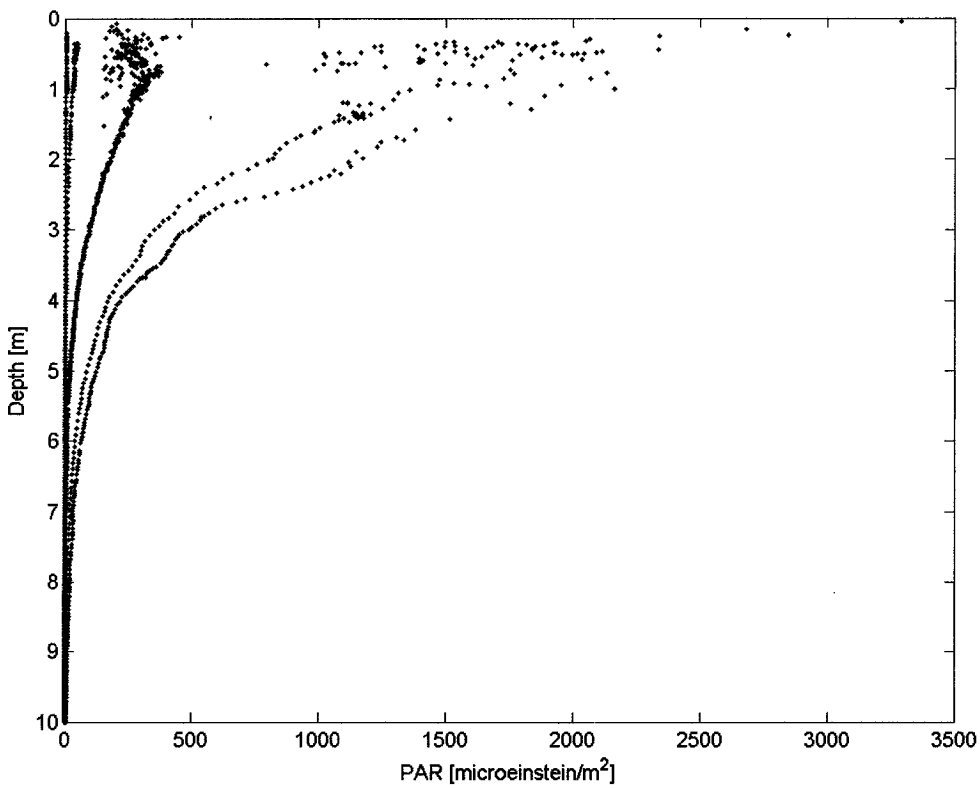


**Figure 5-2 PAR vs depth for June 3rd and June 10th 2003. These data were collected on the yow-yo package. One should note that our measurements include both day and night measurements, so during the night, there is no PAR at the surface.**

The model we used was developed by Jassby and Platt 1976 and we followed a similar application of this formulation as Lucas et al. 1998:

$$\mu_{net} = \frac{1}{T}\frac{1}{H}\int_0^T \int_0^H \left( \frac{P(z,t)}{\theta} - \zeta \right) dzdt \qquad \text{Eqn 5-7}$$

where $\mu_{net}$ is the effective growth rate, $P(z,t)$ is the biomass-specific rate of photosynthesis at depth $z$; $\theta$ is the ratio of phytoplankton cellular carbon to chlorophyll a, which is assumed constant and equal to 50 (Cloern 1991); and $\zeta$ is the loss due to zooplankton grazing and assumed constant with depth and time (Table 5-1). The water column height, $H$, is assumed to be constant throughout the study.

The rate of photosynthesis per unit biomass is

$$P(z,t) = P_{\max}\{\tanh[I(z,t) * a] - r\} \qquad \text{Eqn 5-8}$$

where $P_{max}$ is the maximum (light saturated) rate of photosynthesis per unit biomass; $a$ is the photosynthetic efficiency at low irradiance; $I(z,t)$ is the irradiance at depth z; $r$ is the respiration rate, expressed as a percentage of $P_{max}$.

The PAR, or light available for photosynthesis, can be described by:

$$I(z,t) = I_0(t)\exp(-kz) \qquad \text{Eqn 5-9}$$

where $Io$ is the surface irradiance, and $k$ is the extinction coefficient.

**Table 5-1 Net Growth Model Parameters**

| Parameter | Units | Value | Description |
|---|---|---|---|
| a | $m^2$-d/einstein | 0.1 | Photosyntehtic efficiency |
| H | m | 50 | Water column height |
| Io | Einstein $m^{-2}$ $d^{-1}$ | 20-40 | Mean daily surface irradiance |
| I(z,t) | Einstein $m^{-2}$ $d^{-1}$ | | Photosynethtically active radiation |
| k | $m^{-1}$ | 0.5 | Abiotic light attenuation |
| P(z,t) | mg C mg chl-$a^{-1}$ $d^{-1}$ | | Phytoplanklton carbon assimilation rate per biomass |
| Pmax | mg C mg chl-$a^{-1}$ $d^{-1}$ | 50 | Maximum carbon assimilation per biomass |
| r | | 0.05 | Resipiration percentage of Pmax 1998 model |
| $\zeta$ | $d^{-1}$ | 0.1 | Zooplantkon grazing rate |
| $\theta$ | mgC mg chl-$a^{-1}$ | 50 | Ratio of cellular carbon to chlorophyll |

The net growth $\mu_{net}$ is constant 1.8 $d^{-1}$ in the upper four meters of the water column, becomes negative after 12m depth and is constant -0.2 $d^{-1}$ below 20m depth. The depth integrated summer values for $\mu_{net}$ is 0.18 (Figure 5-3).

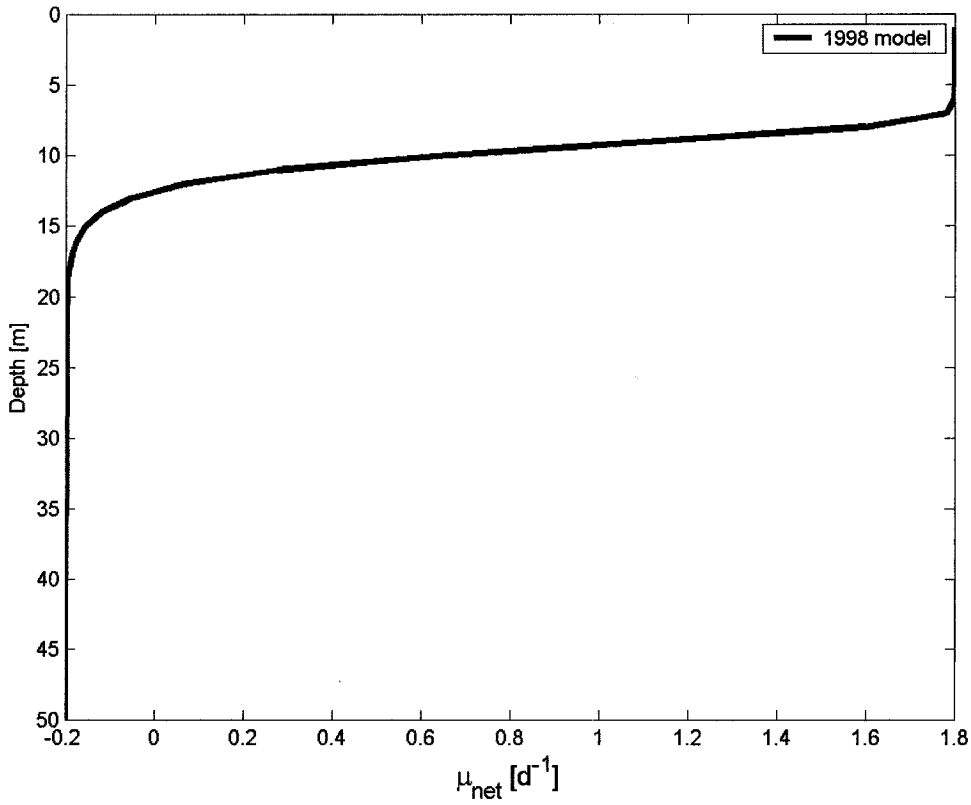


**Figure 5-3 Net growth rate calculated using summer data to calibrate the growth model. The net growth rate integrated over the depth is 0.18 $d^{-1}$.**

### 5.1.3 Lengthscale

One of the most sensitive parameters in equation 5-1 is the east-west lengthscale, L. We can determine the length by using the geometry of Central Bay, or the length of our box ~ 10 km. We can also find a lengthscale that is determined by salinity gradient. We estimated the lengthscale using the following equation:

$$L \propto \Delta X = \frac{\Delta S}{\frac{\partial S}{\partial x}} \qquad \text{Eqn 5-10}$$

$\Delta S$ is the difference between oceanic and estuary salinities calculated using NMFS data. The salinity gradient, $\frac{\partial S}{\partial x}$, was the observed salinity gradient during our summer study. The length scale calculated with equation 5-13 yields a lengthscale of 15 km (Table 5-2). This lengthscale is equal to the transport lengthscale previously found in San Francisco Bay by estimating the length of the flood tide jet (Wilkinson 1978, Largier 1996).

**Table 5-2 Lengthscale derivation using salinity gradient**

| | Measured Gradient [$m^{-4}$] | Mean Central Bay Salinity [psu] | Mean Ocean Salinity [psu] | $\Delta S$ [psu] | $\Delta X \sim L$ [km] |
|---|---|---|---|---|---|
| Salt | 2.05E-04 | 30 | 33 | 3 | 15 |

### 5.1.4 Boundary Concentrations

The estuary concentrations were estimated using the average of the last 10 years of monthly profiles the USGS collected in Central Bay. The USGS Station 18 is due east of our experiment site. Data were available at that station during fall and summer. We used station 21, located at the Bay Bridge, for spring because station 18 is often not surveyed during the spring (http://sfbay.wr.usgs.gov). Ocean concentrations for the winter/spring scenario were based on observations made by Wilkerson et al. 2002). From 1997-1999, they surveyed chlorophyll concentration from Central Bay out to the Gulf of the Farallones, and found concentrations generally ranging from 1- 1.5 μg/L. For summer ocean concentrations, we used the average surface concentration, 13 μg/L, of NMFS surveys conducted from Half Moon Bay to Point Reyes during our summer experiments. We could find no historical ocean concentrations during fall but assumed a value consistent with spring (Table 5-3).

**Table 5-3 Chlorophyll box model parameter values**

| | Spring | Fall | Summer |
|---|---|---|---|
| L [m] | 15000 | 15000 | 15000 |
| Co [μg/L] | 2 | 2 | 2 |
| $K_{est}$ [$m^2/s$] | 160 | 160 | 160 |
| $K_{oc}$ [$m^2/s$] | 888 | 382 | 724 |
| Cest [μg/L] | 12 | 4 | 4 |
| Coc [μg/L] | 1 | 1 | 13 |
| $U_f$ [m/s] | .0035 | .0008 | .0023 |
| $\mu_{net}[d^{-1}]$ | 0.1 | 0.1 | 0.1 |
| X | 1.7E-05 | 4.8E-06 | 4.5E-05 |
| Y | -3.7E-06 | -1.3E-06 | -3.0E-06 |

### 5.2.0 Model Results

There are two basic features of the solution, the steady concentration, $C_{ss}$, and the time it takes to reach that concentration, $\tau_{ss}$. The solution converges on the steady concentration value, -X/Y, as exp(Y*t) approaches zero. The time it takes to converge to -X/Y is proportional to $Y^{-1}$. We initially solved equation 5-6 with the conditions measured for each season (Figure 5-4) (Table 5-3). For summer conditions, the modeled chlorophyll concentrations increased from the initial conditions ($C_o$ = 2 μg/L) to much higher concentration (15 μg/L), than our measured mean (2.7 μg/L). The time to reach steady state for the summer run was 14 days. For spring conditions, the modeled concentration increased to 4.0 μg/L, higher than our observed mean spring concentration (3.0 μg/L). The time to reach steady state during the spring is shortest, 9 days. For fall conditions, the modeled concentration increased from initial conditions, reaching a steady

concentration (2.2 μg/L) greater than the fall mean observed (2.0 μg/L). The time to reach steady state for the fall run was the longest, 23 days.

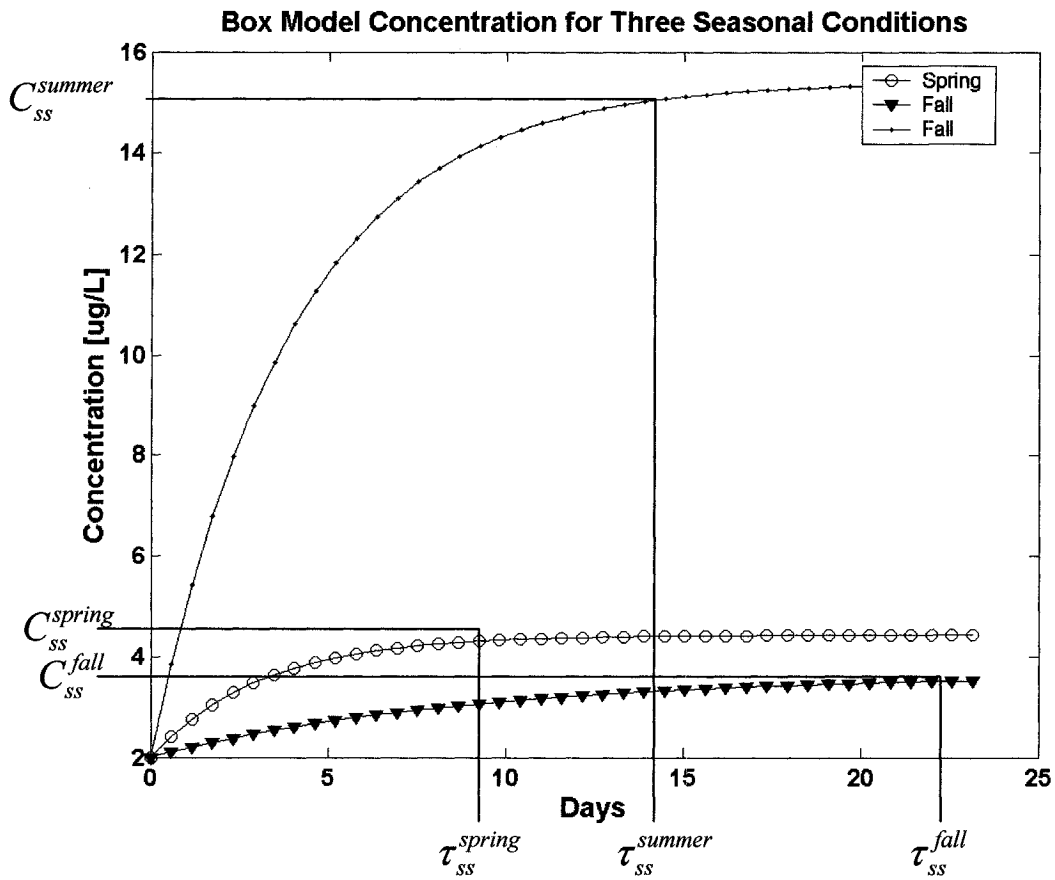


**Figure 5-4 Central Bay box model chlorophyll concentrations. Three seasonal conditions examined using data from flux experiments. There are two important values for each solution, the steady state concentration, Css, and the time to reach steady state, τss.**

The most obvious discrepancy between the modeled concentrations and observed concentrations occurs during the summer. Our measured mean concentration, 2.7 μg/L, is considerably lower than the model output of 15 μg/L. Based on a review of historical USGS profiles collected in Central Bay, chlorophyll concentration has rarely exceeded 7 μg/L. The discrepancy between summer model outputs and observations will be discussed further in subsequent section. Because several parameters vary during each season run, it is not immediately obvious which of those factors contributes to the

differences in the observed and modeled concentrations. To understand how each of the model parameters controls the steady concentration and the time to reach it, we ran the model for each season varying one parameter but keeping the rest at the values constant equal to those values listed in Table 5-3.

### 5.2.1 General Model Behavior

The following graphs are illustrating just two values for each model run, the steady state concentration, $C_{ss}$, and the time it takes to reach that concentration $\tau_{ss}$. For each new model run, the solution appears similar to those shown in Figure 5-4.

### 5.2.2 Dispersion

Changing the dispersion coefficient on either side (ocean or estuary) of the box has different effects that depend on the concentration at each of those boundaries (Figure 5-5). During the spring, the estuary concentration is relatively high, so increasing the $K_{est}$ leads to an increase in steady state concentration in Central Bay. During the summer when the ocean concentration is relatively high, increasing the $K_{oc}$, also leads to an increase in the steady state concentration. When $K_{est}$ is increased during the summer, steady concentrations decrease, similarly to when $K_{oc}$ is increased during spring. Increasing either dispersion coefficient leads to a decrease in the time it takes to reach steady state. The time to reach steady state is larger for fall than for spring and summer. The decrease in the time to reach steady state as dispersion increases suggests that the timescale is determined by dispersion, or the time scale is proportional to $\frac{L^2}{K_x}$.

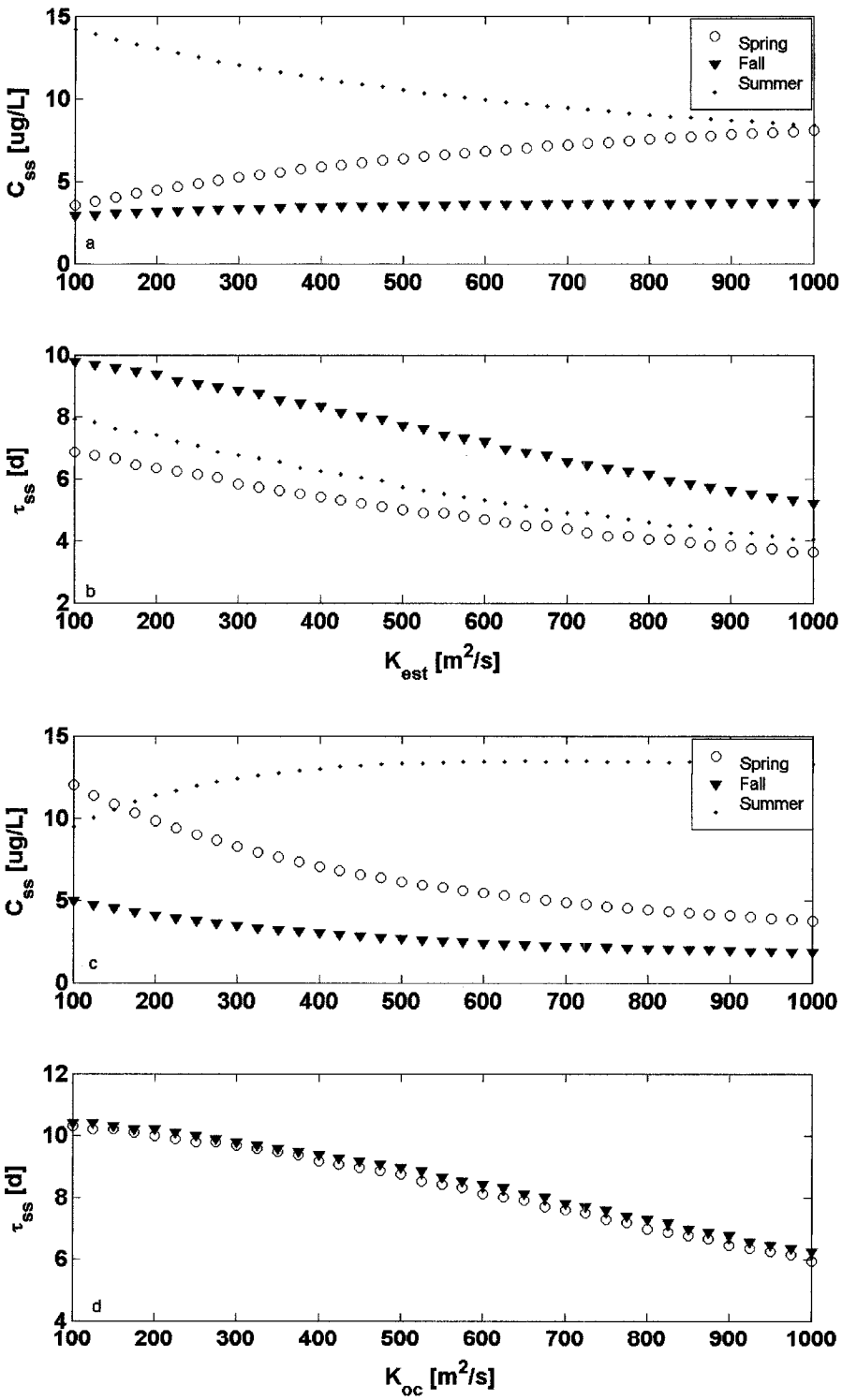


**Figure 5-5 The effects of changing the dispersion coefficients from 100-1000 m2/s on steady state concentration (Css) and time to reach steady state ($\tau_{ss}$). Panels a and b are show changes in the estuary dispersion coefficient and panels c and d show changes in the oceanic dispersion coefficient.**

### 5.2.3 Boundary Concentrations

Increasing the boundary concentrations leads to a linear increase in modeled steady state concentration (Figure 5-6). This result may seem fairly obvious; however, it is interesting to note the slope is different for the oceanic and estuary conditions. Changing the oceanic boundary condition leads to a nearly uniform increase in the modeled steady concentration for all seasons. Increasing the oceanic boundary condition corresponded to higher modeled steady state concentration than increasing the estuary boundary condition by the same amount. Changing the estuary boundary condition has a more variable effect across seasons than changing oceanic boundary condition, but the effect is small. Although the summer model runs have greater modeled steady concentration for any given estuary boundary concentration, the spring conditions are the most sensitive to changes in the estuary boundary concentration, as estimated by the slope of the line. The fall model runs were the least sensitive, smallest slope, to changes in the estuary boundary condition. These results imply that the modeled Central Bay chlorophyll concentration is largely dependent on the boundary conditions, particularly the oceanic concentrations, because dispersion is greatest at that boundary.

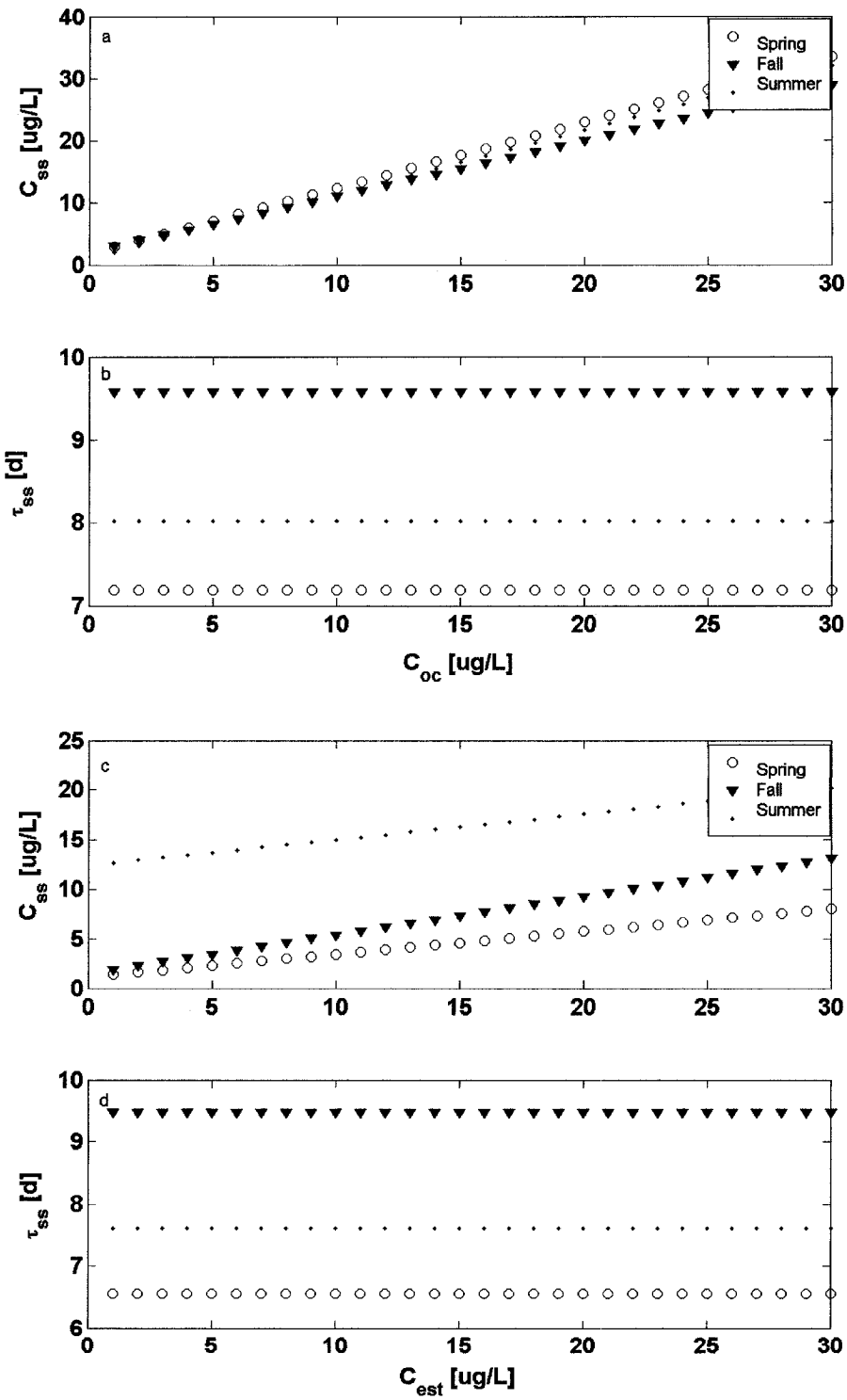


**Figure 5-6 Changing ocean and estuary boundary concentrations from 1 to 30 mg/L. Panels a and b show changes in the oceanic chlorophyll concentration, panels c and d show changes in the estuarine concentration.**

### 5.2.4 Lengthscale

The east-west lengthscale has a stronger effect on the time to reach modeled steady state than the other parameters discussed above. As the lengthscale increases, $\tau_{ss}$ also increases until L is greater than 20 km where it asymptotically approaches a value of approximately 10 days (Figure 5-7). If the timescale is determined by $\frac{L^2}{K_x}$ then this asymptotic behavior suggests that once L becomes too large, the timescale is determined by other processes such as growth or advection.

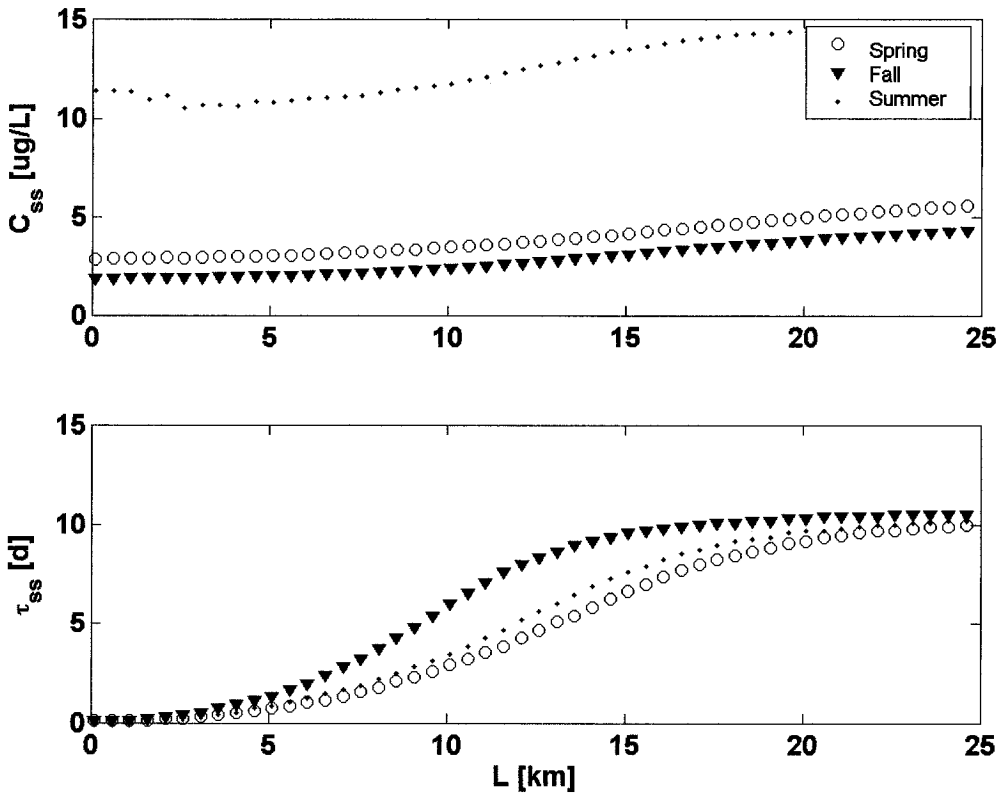


**Figure 5-7 The effects of changing the lengthscale from 100 to 20,000 m on steady state concentration ($C_{SS}$) and time to reach steady state ($\tau_{ss}$).**

### 5.2.5 Freshwater Flow

Changing the freshwater flow, modeled as changes in $U_f$, had relatively little effect on concentration or time to reach steady state compared to other parameters (Figure 5-8). This indicates that freshwater flows are small in Central Bay in terms of the effects on chlorophyll concentration. This also reinforces the notion that transport of scalars in Central Bay are dominated by dispersion.

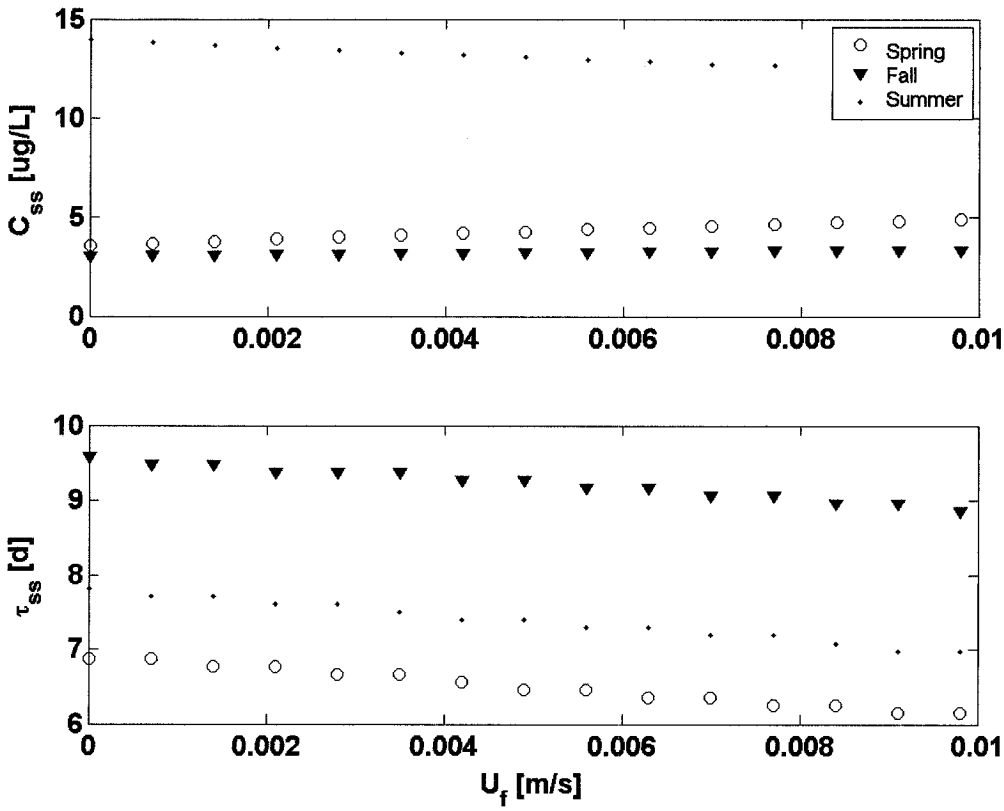


**Figure 5-8 Effects of freshwater flow on steady state concentration ($C_{SS}$) and time to reach steady state ($\tau_{ss}$) are small compared to other parameters.**

### 5.2.6 Net Growth

As the growth rate, $\mu_{net}$, increases so does the steady concentration and the time to reach steady state. However, once the net growth rate becomes large enough, the final

concentration does not reach steady state but rather increases exponentially. This transition from decay to growth occurs when Y (eqn 5-4) changes signs. We can define this critical value as

$$\mu_{crit} = \frac{U_f}{L} + \frac{K_{est}}{L^2} + \frac{K_{oc}}{L^2} \qquad \text{Eqn 5 -11}$$

The critical value for spring is 0.43 $d^{-1}$, fall, 0.21 $d^{-1}$, and summer, 0.36 $d^{-1}$. These results indicate that in order for exponential growth to occur in Central Bay during the spring, growth rates would have to be double what they must be in the fall to achieve the same conditions. Fall has the smallest $\mu_{crit}$, suggesting that exponential growth, or a bloom is most likely to occur during the fall.

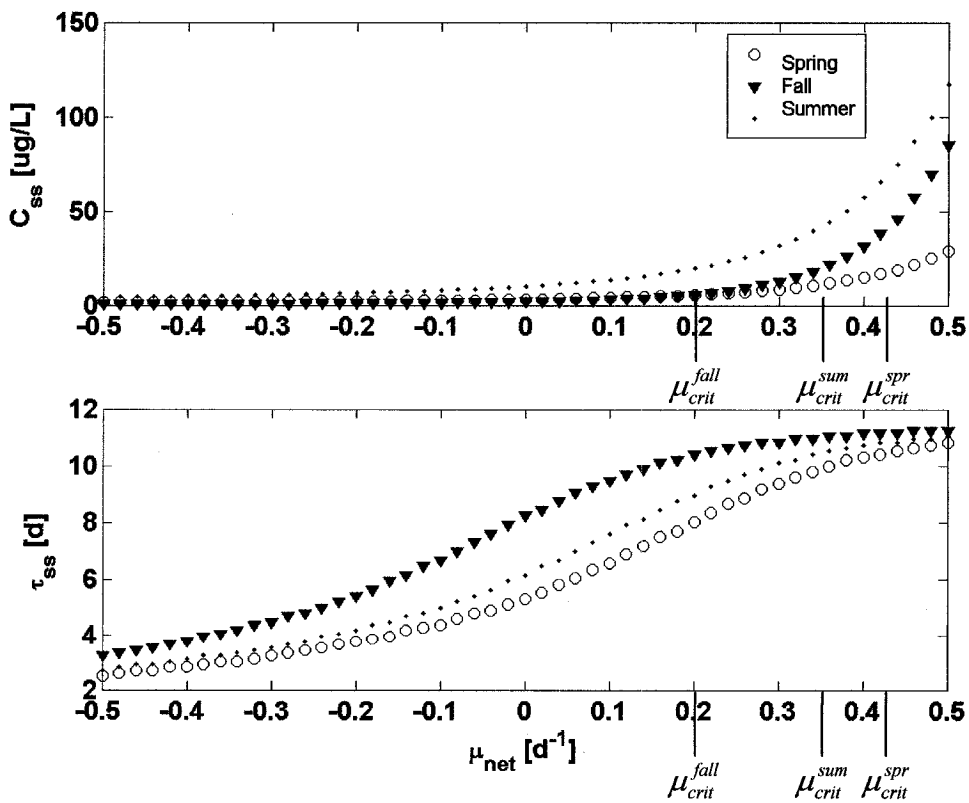


**Figure 5-9 Concentrations in Central Bay increase exponential for values larger than $\mu_{crit}$.**

### 5.3.0 Discussion

The summer model behavior shows that a steady concentration close to our observations can be achieved if the dispersion coefficient decreases, the growth rate decreases, the lengthscale increases and the oceanic concentration decreases. All these factors indicate that there is less exchange than would be expected given the difference between the observed mean ocean and estuary concentrations. This discrepancy could suggest that the model is too simple to capture the dynamics of the system. However, the mean concentrations during our fall and spring runs were adequately resolved. The most likely source of error in the summer model lies in the assumptions used to estimate the coastal concentration. Using the mean of the entire NMFS coastal data set effectively removes spatial variability and assumes that the waters along the coast are well mixed. In order for phytoplankton to be transported into the estuary from the coast, they must be within the region that exchanges with the bay. A reasonable estimate how far west the region of exchange extends from the mouth of the estuary is 15km. However, we have no information on how far to the north or south this region of exchange extends. The highest concentrations of chlorophyll were observed to the north and south of the estuary mouth so it is difficult to estimate how likely those patches will be transported into the estuary. If the north-south transport rate of phytoplankton is small relative to how long the bloom exists, the transport of these phytoplankton into the estuary would be diminished.

In order to better understand the relative importance of the growth and transport timescales, we re-examine the governing equation in a non-dimensional context. If we

assume that the timescale of Central Bay is governed by the dispersion, we can non-dimensionalize the governing equation by making the following substitutions:

$$C^* = \frac{C}{C_0} \qquad x^* = \frac{x}{L} \qquad t^* = \frac{L^2}{K_x}$$

We get the following dimensionless governing equation:

$$\frac{\partial C^*}{\partial t^*} = \left(\frac{\mu L^2}{K_x}\right)C^* - \left(\frac{UL}{K_x}\right)\frac{\partial C^*}{\partial x^*} + \frac{\partial^2 C^*}{\partial x^{*2}} \qquad \text{Eqn 5-12}$$

The two dimensionless numbers that emerge are the Damkohler number, comparing the growth rate to the dispersive rate, and the Peclet number, comparing advection to dispersion. If we compare these numbers across seasons, using the $\mu_{net}$ formulation of the growth rate each season, we see that the relative importance of growth varies seasonally (Table 5-4).

**Table 5-4 Dimensionless numbers across seasons**

| | Spring | Fall | Summer |
|---|---|---|---|
| $\frac{\mu L^2}{K_x}$ | 0.35 | 0.75 | 0.55 |
| $\frac{UL}{K_x}$ | 0.06 | 0.03 | 0.05 |

From these numbers and the analytical solution, it is clear that freshwater advection is negligible in the chlorophyll balance in Central San Francisco Bay. During the spring, dispersion dominates the chlorophyll balance; during the summer, dispersion is about twice as important as growth; and during fall, growth is more important in determining

the concentration of chlorophyll in Central Bay. If the fall growth rate is increased from the calculated 0.1 $d^{-1}$ to 0.15 $d^{-1}$, the Damkohler number is greater than 1, indicating that growth and dispersion make equal contributions to the chlorophyll concentration.

While phytoplankton populations are often considered limited by processes such as light or nutrient availability, it is also possible that blooms are "transport limited". Cloern et al. 1983 found that blooms occur in San Francisco Bay if the residence time of that basin is greater than the doubling time of the population. If the transport rates are much larger than the growth rates, there is not enough time for the phytoplankton to accumulate within the basin. Using the timescale, $L^2/K_{oc}$, as the residence time of Central Bay, we can see the residence time is much shorter than the population doubling time year-round (Table 5-5). This implies that most of Central Bay phytoplankton is derived from allochthonous rather than autochthonous sources.

**Table 5-5 Residence time based on dispersive transport vs the population doubling time by season**

| | Spring | Fall | Summer |
|---|---|---|---|
| Population Doubling Time [d] | 17 | 18 | 11 |
| Residence Time [d] | 3 | 7 | 4 |

There are three sources for allochthonous phytoplankton entering Central Bay, the coastal ocean, South Bay and North Bay. The balance of phytoplankton in Central Bay is dominated by tidal dispersion and the dispersive flux is dependent on the spatial gradient of chlorophyll. We can consider the balance of phytoplankton for each basin that feeds into Central Bay to understand how regional differences in sources and sinks affect the Central Bay. In the South Bay, phytoplankton are almost entirely autochthonous,

assuming there is relatively little input from local tributaries and the Central-South Bay gradient does no promote dispersive transport into South Bay (Jassby et al. 1993). The South Bay is characterized by low freshwater inputs, slow circulation determined by relatively weak dispersion, with an estimated residence time ($\frac{L^2}{K^{sb}_x}$) on the order of 170 days (Uncles and Peterson 1996). This implies that the Damkohler number would be large compared to Central Bay and the Peclet number would be small in the South Bay. The opposite is true in the North Bay which is characterized by highly variable freshwater flow rates, and small net growth rates due to benthic grazing (Jassby et al. 2002). The majority of organic carbon in the North Bay, mostly in the form of phytoplankton and phytoplankton derived detritus, is advected there from the Delta (Jassby et al. 1993, Jassby et al. 2002). This indicates that the Damkohler number in the North Bay would be small and the Peclet number would be large. In terms of the coastal ocean, we have shown during coastal upwelling, coastal phytoplankton are autochthonous and during spring there is an allochthonous source from the estuary. However, we do not have much information about the coastal ocean and the region of exchange west of the Golden Gate. It is likely that additional processes should be considered in determining the balance of chlorophyll in the coastal ocean such as wind, ocean swell, large scale currents, and Coriolis force. Regional differences in the dominant phytoplankton sources and sinks suggest that the magnitude of the dispersive flux in Central Bay is determined by the net growth rate or bloom timescale in the South Bay and the timing and magnitude of freshwater advection of Delta derived phytoplankton in the North Bay.

We can compare the transport of chlorophyll in Central Bay to historical estimates of organic carbon sources and sinks in the North and South Bays. Taking the average of

net chlorophyll fluxes reported in Chapter 4, we estimate the annual rate of transport in Central Bay is approximately 7 g/s of chlorophyll transported out of the estuary. Assuming the carbon to chlorophyll ratio is 50 (Cloern 1995), we estimate that there is about 30 Gg/yr of carbon leaving Central Bay. Our estimates do not include other terms such as benthic microalgae or dissolved organic carbon (DOC), which are important in North and South Bay carbon budgets. Compared to other estuary carbon sinks, tidal dispersion of phytoplankton in Central Bay is about one third the rate of the largest carbon sink previously estimated for the rest of the estuary, planktonic respiration, -120 Gg/yr (Jassby et al. 1993). This implies that the seaward transport of carbon is an important sink and should be incorporated into future carbon budgets.

We used a simple box model to investigate if local growth is important in determining the chlorophyll concentration in Central Bay. Although the summer modeled and measured mean concentrations were not well reconciled, we can glean some insight using this simple model. In general, the accumulation of phytoplankton in Central Bay is limited by large dispersive transport rates rather than small growth rates. However, when the dispersive transport rate is small, growth is more important. Measured dispersion coefficients were smallest during fall and largest during spring. This means that exponential growth is possible during the fall and phytoplankton observed in Central Bay during this time of year may be due to local growth conditions. However, phytoplankton observed there during spring are most likely derived elsewhere and dispersed into Central Bay. This conclusion is supported by the relatively rare blooms that have occurred in Central Bay. Most of the recorded blooms in that area have

happened during the fall, especially during times of weak physical transport (Cloern et al. 2005).

Future work should focus on quantifying the timescale of the ocean-estuary chlorophyll gradient to the transport timescale because the total transport into and out of a dispersion dominated estuary depends on how long the specific chlorophyll gradient persists. The timescale of the ocean-estuary gradient will be determined in part by South Bay blooms and freshwater flow. Considering such phenomenon in a seasonal and inter-annual context may provide more insight into how climate or anthropogenic changes will affect the primary productivity of similar coastal bays and estuaries.

# 6 Suspended Sediment Flux

The goal of this chapter is to quantify the suspended sediment flux and distinguish which flux processes are most important. The net flux was into the estuary during the fall, and out of the estuary spring and summer. The magnitude of the fall fluxes was an order of magnitude larger than spring and summer. Year round, the dispersive fluxes were larger than advective fluxes and tidal pumping was the dominant mechanism. We did not perform a sensitivity test on the sediment harmonics because even the optimized fit was relatively poor.

We compare our sediment flux results to estimates of historical fluxes based on a time series of suspended sediment concentrations collected from 1996-1997 at the Golden Gate. One feature common to both data sets is the occasional large spike of suspended sediment. We investigate if these spikes can be explained by vertical dynamics such as vertical mixing or differences in sub-tidal vertical distribution of sediment.

**6.1 Advection**

The advective fluxes are proportional to freshwater flow so the largest advective flux was in spring, -16 kg/s, followed by summer, 11kg/s, and fall, 4 kg/s. The advection component was the same order of magnitude as the dispersive fluxes during spring and summer (Table 6-1). During the fall, the dispersive flux was two orders of magnitude larger than the advective flux and in the opposite direction.

**Table 6-1 Advective and Dispersive Suspended Sediment Fluxes.**

| Units [kg/s] | Spring (02) | Fall (02) | Summer (03) |
|---|---|---|---|
| Advection | -16 | -5 | -11 |
| Dispersion | -32 | 250 | -30 |
| Net total | -48 | 245 | -41 |

## 6.2 Dispersion

The dispersive flux was dominated by tidal pumping year-round. In contrast to chlorophyll, both steady and unsteady fluxes were important as well. Tidal pumping was large and inward during fall, 240 kg/s, but comparatively small and outward during spring, -32 kg/s, and summer, -27 kg/s. The steady fluxes due to vertical gradients were into the estuary year round, the largest during the spring, 3 kg/s, followed by summer, 2 kg/s and fall, 0.9 kg/s. The steady flux due to lateral gradients was inward during fall, 7 kg/s, and spring, 6 kg/s, but outward during summer, -1 kg/s. The unsteady flux was inward during the fall and outward during spring and summer. The unsteady fluxes were the same order of magnitude as the steady fluxes, meaning both steady and unsteady exchange is important. This is in contrast to salt and chlorophyll whose steady fluxes were an order of magnitude larger than the unsteady component. This implies that although the dispersive flux is dominated by the tidal pumping, it is equally affected by processes taking place on longer timescales, such as baroclinic exchange, and process that occur on shorter timescales such as unsteady shear (Table 6-2). Collectively these

results suggest that all of the processes are important to the direction and magnitude of the net sediment flux.

**Table 6-2 Dispersive flux of suspended sediment by mechanism.**

| Units [kg/s] | Spring (02) | Fall (02) | Summer (03) |
|---|---|---|---|
| Tidal pumping | -34 | 238 | -27 |
| Steady Lateral | 6 | 7 | -1 |
| Steady Vertical | 3 | 0.9 | 2 |
| Unsteady Lateral | -6 | 2 | -2 |
| Unsteady Vertical | -2 | -2 | -1 |

## 6.3 USGS Timeseries Analysis

The USGS maintained a suspended sediment station at the Golden Gate Bridge from October 1996- August 1997 (Figure 6-1). Salinity, temperature, and suspended sediment were recorded every 15 minutes during the study. Throughout the course of the year the station was maintained, there were large data gaps due to instrument malfunctions. The suspended-solids sensor was deployed at 14 m above the bottom. Mean lower low water depth at this site is about 23 m and increases to a maximum depth of 150 m in the main channel. The instruments were housed in a 6- by 6- by 8-foot fiberglass shelter on the south pier footing of the bridge. Sensors were suspended in place using PVC carriages and 3/8-inch stainless-steel line attached to a 600-pound railroad wheel. A data logger and modem were used to control sensor timing, data storage, and retrieval (http://sfbay.wr.usgs.gov/sediment/cont_monitoring/site_info.html).

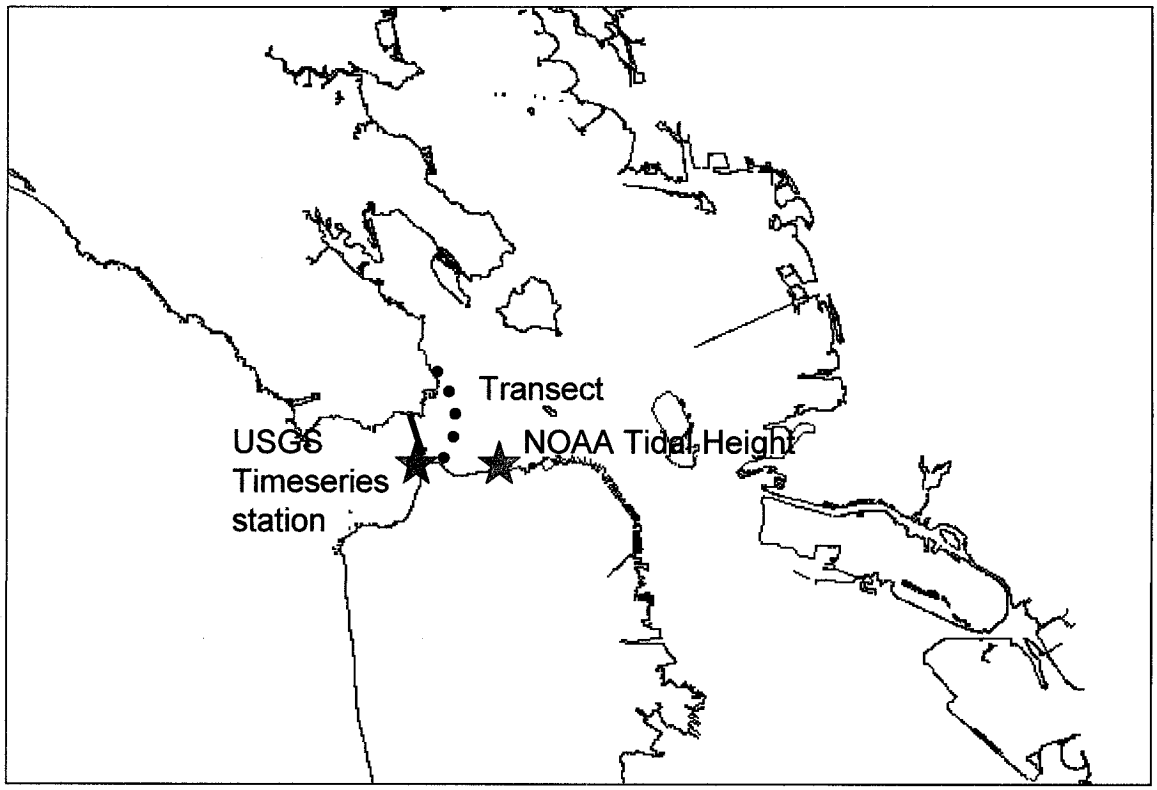


**Figure 6-1 Site map showing locations of USGS tss timeseries and NOAA tidal height stations compared to our transect in Central Bay.**

Tidal height is also recorded by NOAA between Fort Point and Crissy Field (Figure 6-1) (http://tidesandcurrents.noaa.gov/data_menu.shtml?type=Tide+Data&mstn=9414290 ). Based on our measurements and previous studies done by Walters et al. 1985, we were able to determine a relationship between the rate of change in tidal height [m/s], $\frac{\partial \eta}{\partial t}$ using mean sea level (MSL) as a datum, and cross sectionally averaged velocity, $U_{CA}$, at our location east of the Golden Gate Bridge such that:

$$U_{CA}[m/s] = \frac{\partial \eta}{\partial t}\frac{1}{12} \qquad \text{Eqn 6-1}$$

Velocity lags the tidal height by about 75 minutes, so slack velocity is 1.25 hours after low/high tide. We can recreate the fall tidal pumping fluxes within 10% of our original estimates using velocity estimated by equation 6-1 (Figure 6-2).

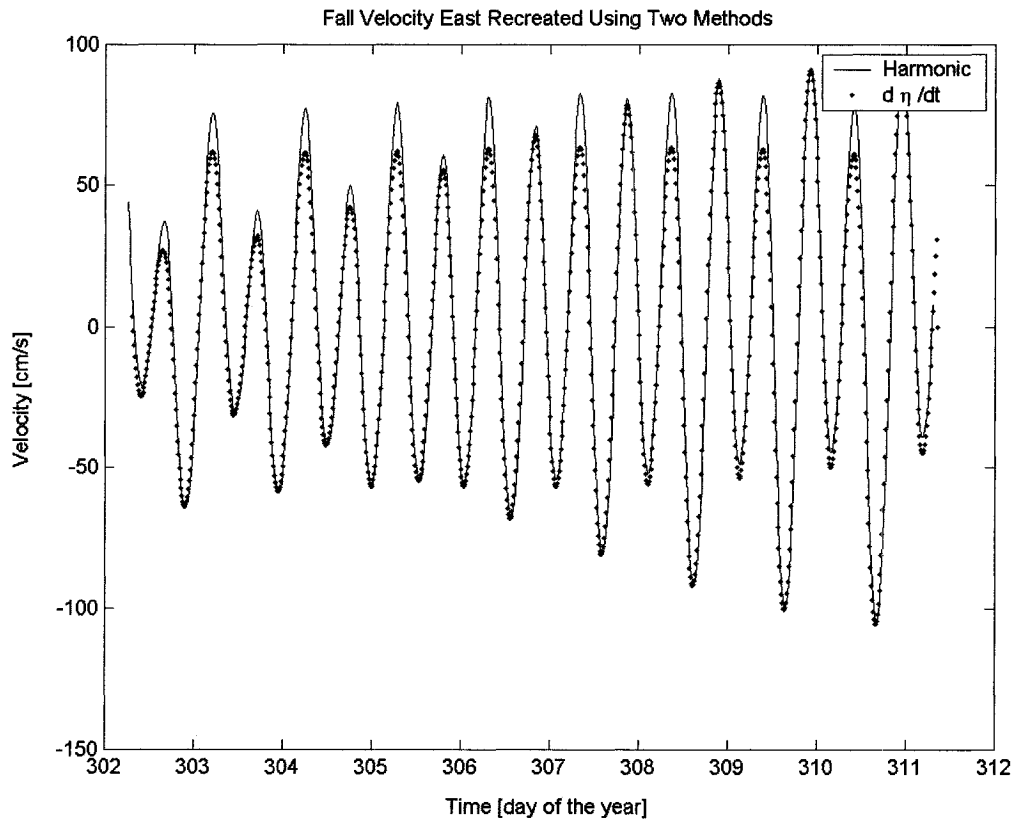


**Figure 6-2 Cross sectional averaged velocity. Harmonic recreated velocity east is shown in the solid line and recreated velocity using equation 6-1 is dotted. Note the tidal height method does not always capture the flood tide maximums as well as the ebb tide.**

If we assume that tidal pumping was the dominant forcing mechanism during the USGS timeseries we can estimate the dispersive flux during that period by assuming the point measurements are representative of the entire cross sectional average. We can then transform the tidal height into the cross section average velocity and calculate the tidal

pumping flux directly rather than using harmonics. The data have been broken down into month and the flux is calculated for October 1996, April 1997, and June 1997 (Figure 6-3). We chose these months because they had the most complete suspended sediment records and most closely matched the seasonal variability we hoped to capture during our experiment.

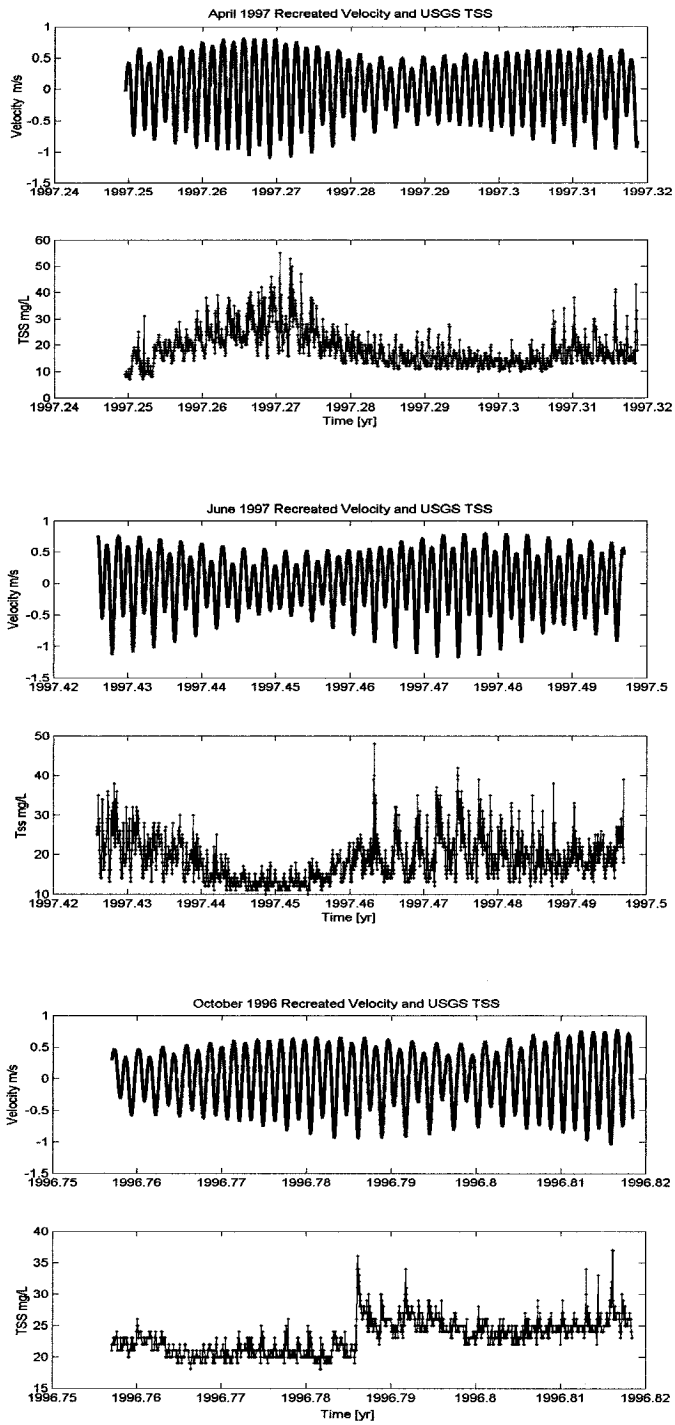


**Figure 6-3 USGS suspended sediment concentrations 1996-1997 for spring, summer and fall. There is a clear spring-neap cycle to velocity and suspended sediment concentration. There are many large spikes in suspended sediment that do not appear related to velocity.**

The flux calculated for October, over 21.2 days, was -30 kg/s, out of the estuary (Table 6-3). The flux in April 1997 was -84 kg/s out of the estuary, calculated over 27.4 days. The June flux was similar to our original calculated tidal pumping flux, -64 g/s out of the estuary, calculated over 25.4 days. Our original flux measurements calculated the flux over 15 days so if we constrain our direct USGS flux calculations to 15 days after the start time, we obtain very similar results for all seasons using the USGS information. The seasonal pattern inferred by these fluxes is different than the one we derived using harmonics. USGS tidal pumping fluxes are all out of the estuary. The order of magnitude is similar to our harmonic derived spring and summer fluxes but is substantially smaller than our fall flux estimate. Moreover, the ranking of the USGS fluxes were different than ours: the largest USGS flux was during spring and smallest during fall.

**Table 6-3. Historical dispersive sediment flux estimates at the Golden Gate**

| USGS Month | Estimate Tidal Pumping Flux [kg/s] |
|---|---|
| October 1996 | -30 |
| April 1997 | -84 |
| June 1997 | -64 |

One feature common to the USGS dataset and our measurements is the occasional large spikes occurring on sub-tidal timescales. In the October 1996 timeseries there is a large spike in TSS occurring around 1996.786 during max ebb (Figure 6-4).

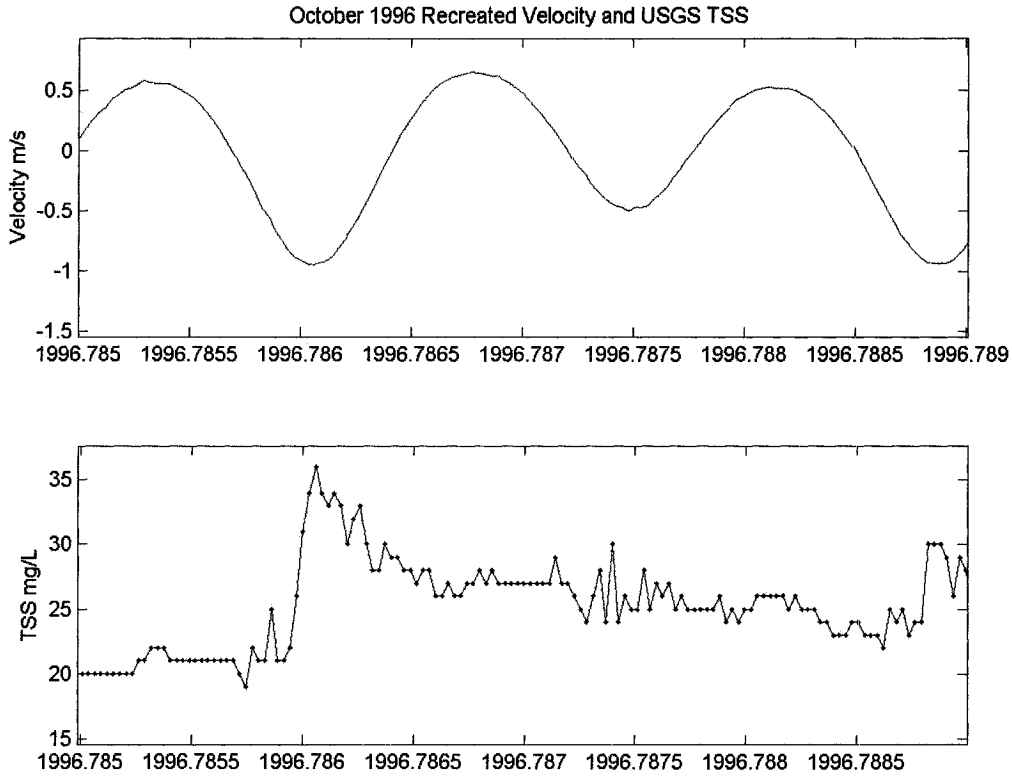


**Figure 6-4 Expanded view of large spike that occurs in the middle of the October 1996 suspended sediment record. This jump occurs at maximum ebb velocity, suggesting a large instantaneous flux out of the estuary.**

Our fall data show a large spike occurring at max flood tide (figure 6-5). This spike has a large influence over the net flux results, but does not drive them entirely. If that spike is removed, the tidal pumping flux during fall remains into the estuary and is still relatively large, ~60 kg/s (Figure 6-5).

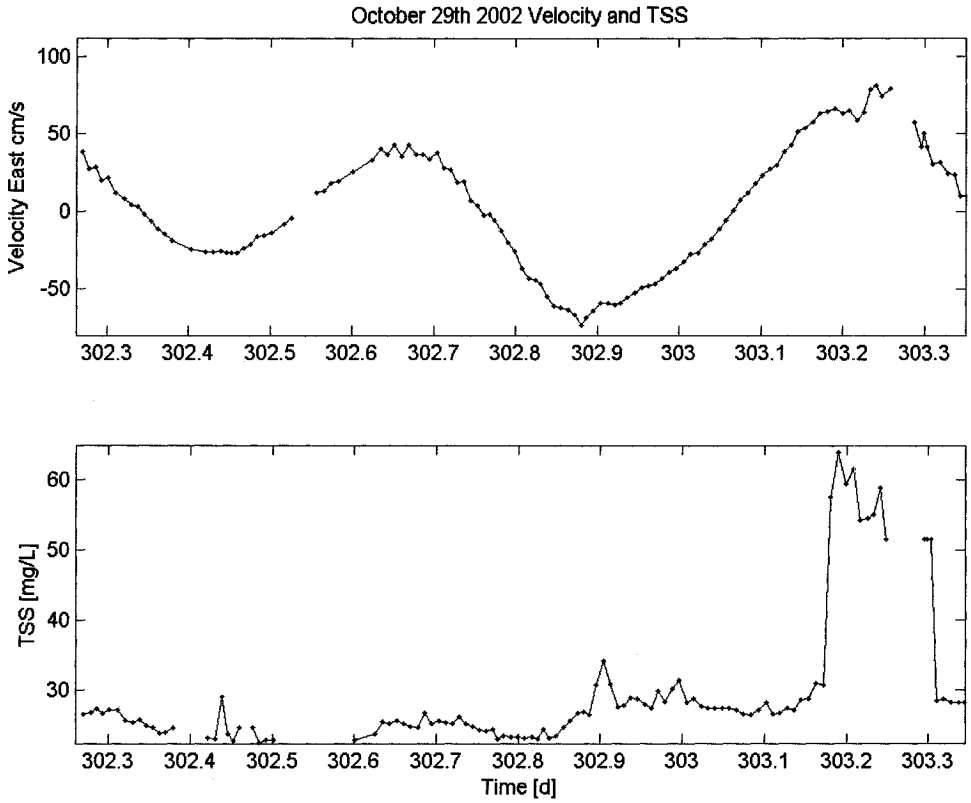


**Figure 6-5 Our flux measurements show a large spike of suspended sediment that occurs at maximum flood tide, creating a large instantaneous flux into the estuary and ultimately influencing the harmonic flux for the entire neap-spring cycle.**

It is a possibility that these spikes are created by something other than sediment, such as a piece of seaweed temporarily blocking the instrument. However, since both data sets collected during the fall exhibit this behavior, we can assume that this is not a systematic measurement error, and that there is a more mechanistic reason.

One possible explanation invokes tidal asymmetries in vertical mixing. In estuaries, strain induced periodic stratification (SIPS) creates asymmetries in stratification such that on flood tides stratification is decreased and the converse is true during the ebb tide (Simpson 1990). This asymmetry in stratification can affect the vertical distance sediments suspended from the bed can travel up through the water column. During flood tide, the decrease in stratification promotes sediment transport

higher into the water column, or enhances the vertical diffusivity of sediment. The converse would be true during ebb tide, effectively damping the vertical diffusivity of sediment. This potential tidal asymmetry in the vertical distribution of sediment combined with a sheared velocity profile, i.e., larger velocities away from the bed, can create a larger flux into the estuary on flood tide than the flux out of the estuary on ebb tide, resulting in a net flux of sediment into the estuary. Pringle and Franks (2001) developed a quasi-analytical solution for coastal boundary layers with this type of asymmetric tidal mixing and found that sinking particles were transported towards land (Pringle and Franks 2001).

We developed two ways to investigate the effects of mixing and stratification on the vertical diffusivity of sediment, and in turn, on sediment fluxes. The first is to develop a way to distinguish how high sediment concentrations travel. The second is to develop a simple mixing model based on the vertical density differences observed during our experiments.

## 6.4 Vertical Sediment Diffusivity

If the vertical diffusivity of sediment is dependent on vertical stratification then we would expect sediment to travel further up the water column during flood tide. During spring and summer, which had comparable levels of stratification, sediment spikes may be confined closer to the bed and therefore below the domain of our observations. We can estimate the vertical extent to which sediments are diffused by creating a timeseries of the vertical location at which center of mass, $Z_{cm,}$ occurs:

$$Z_{cm}(t) = \frac{1}{Tss_{tot}} \int_{H}^{0} zTss\ (z,t)\,dz \qquad \text{Eqn 6-2}$$

$Tss_{tot}$ is the sum of concentrations over the whole water column, $z$ is the depth, and $Tss\ (z,t)$ is laterally averaged sediment concentrations. We confine our analysis to summer and fall because the spring does not have complete tidal coverage. During the summer $Z_{cm}$ increases linearly from max ebb to max flood (Figure 6-6). Max ebb and flood velocities are very similar during the summer, so any differences in $Z_{cm}$ are not due to differences in velocity or bed shear. Summer $Z_{cm}$ is about 3.5 meters further from the bed during the flood tide than on ebb. During the fall there is a non-linear increase in $Z_{cm}$ from ebb to flood. Moreover, there is a sharp increase in $Z_{cm}$ during max flood tide. Fall $Z_{cm}$ during max flood is about 7 meters higher than during max ebb. Max flood velocity is also faster than max ebb velocity, so it is possible that differences in $Z_{cm}$ is due to differences in velocity or bed shear.

Although the data suggest there maybe enhanced sediment diffusivity on the flood tide during both summer and fall, that enhancement does not necessarily lead to a larger flux into the estuary. If we consider the $Tss_{tot}$ and $Z_{cm}$, we see a more complete picture. The total sediment in the water column during summer is slightly greater on max ebb than max flood and is fairly constant around slack tide. Despite the center of mass of the vertical profile of sediments being higher during the flood, potentially creating a flux into the estuary, this is offset by the lower flood tide concentration. During fall, the concentrations are highest during max flood. The larger tidal velocities combined with higher concentrations and higher center of mass, all collectively enhance the flux into the estuary during the fall (Figure 6-6).

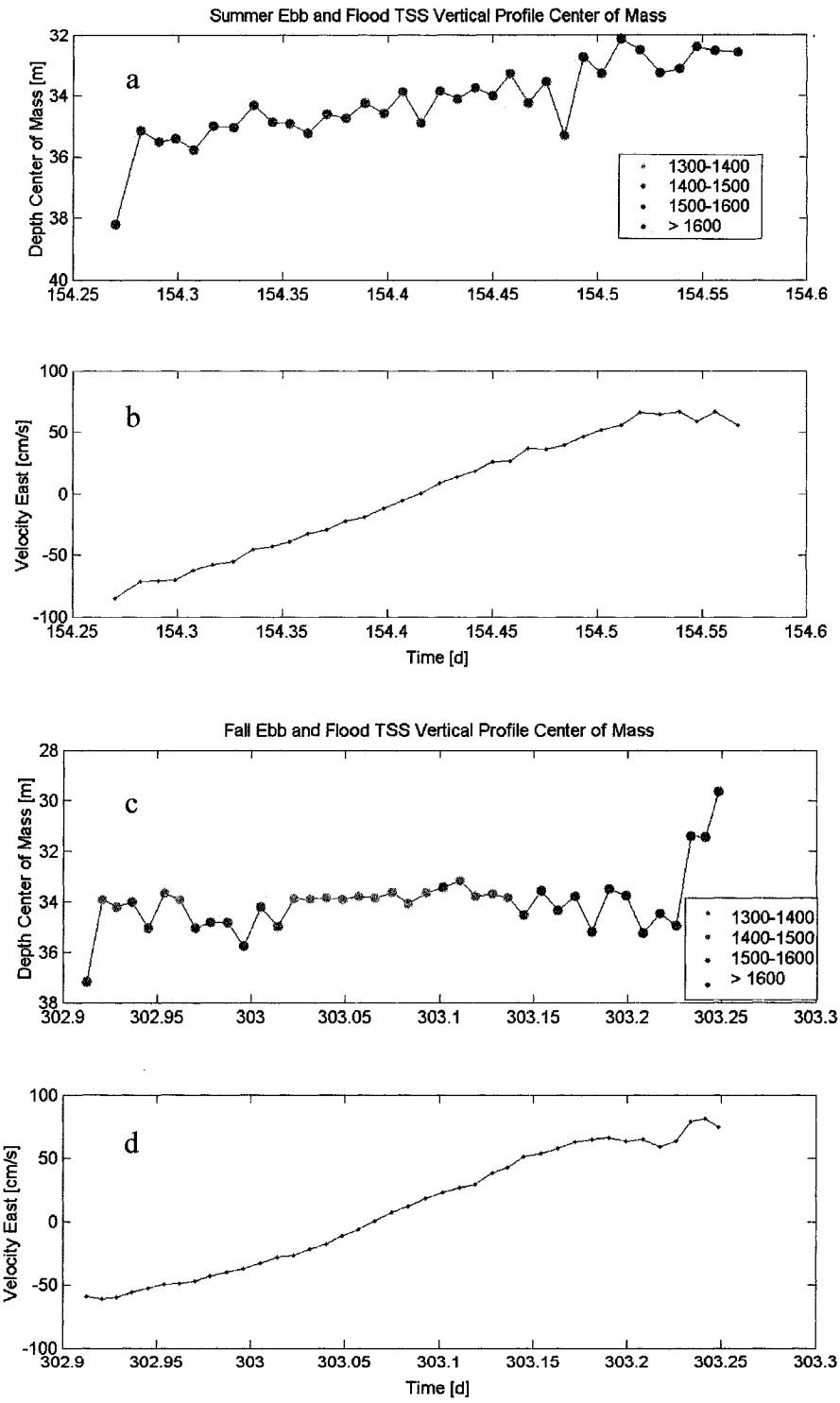


**Figure 6-6 Tidal asymmetries in vertical sediment distribution over a single tidal cycle. Panel a) is summer Zcm, and b) is the summer velocity east. The lower panel c) is fall Zcm and d) is fall velocity east. The color represents the total sediment concentration (mg/L) in the water column.**

Using $Z_{cm}$ as a proxy for the vertical diffusivity of sediment, it seems that SIPS may enhance diffusivity during flood tides. This asymmetric diffusivity occurs during both fall and summer, and presumably, year round, yet we only observed a flux into the bay during fall. While SIPS may enhance vertical sediment diffusivity during flood tides, this does not explain the difference in concentrations observed during max ebb and flood. The timing and magnitude of the peak concentration determines the flux direction. To investigate additional vertical processes that contribute to the timing and quantity of suspended sediment, we construct a simple vertical mixing model.

## 6.5 Mixing Model Description

Using our data, we calibrated an idealized water column model to investigate the combined effects of sub-tidal stratification, sinking, and bed availability. We created a 2-layer box model that assumes the water column is permanently stratified, the depth of the water column is constant, and that the vertical diffusivity for sediment is the same as the eddy viscosity (Figure 6-7). The sediment concentration in the top box, $C_1$, is a function of mixing, $K_z$, and settling, $W_s$, while the concentration in the lower box, $C_2$, is a function of settling, mixing and a positive erosive source term, $S$. Note that the vertical mixing coefficient, $K_z$, has units of $s^{-1}$ and is not a traditional vertical diffusivity.

$$\frac{dc_1}{dt} = K_z(c_2 - c_1) - \frac{W_s c_1}{h_1} \qquad \text{Eqn 6-3}$$

$$\frac{dc_2}{dt} = K_z(c_1 - c_2) - \frac{W_s c_2}{h_2} + \frac{W_s c_1}{h_1} + S \qquad \text{Eqn 6-4}$$

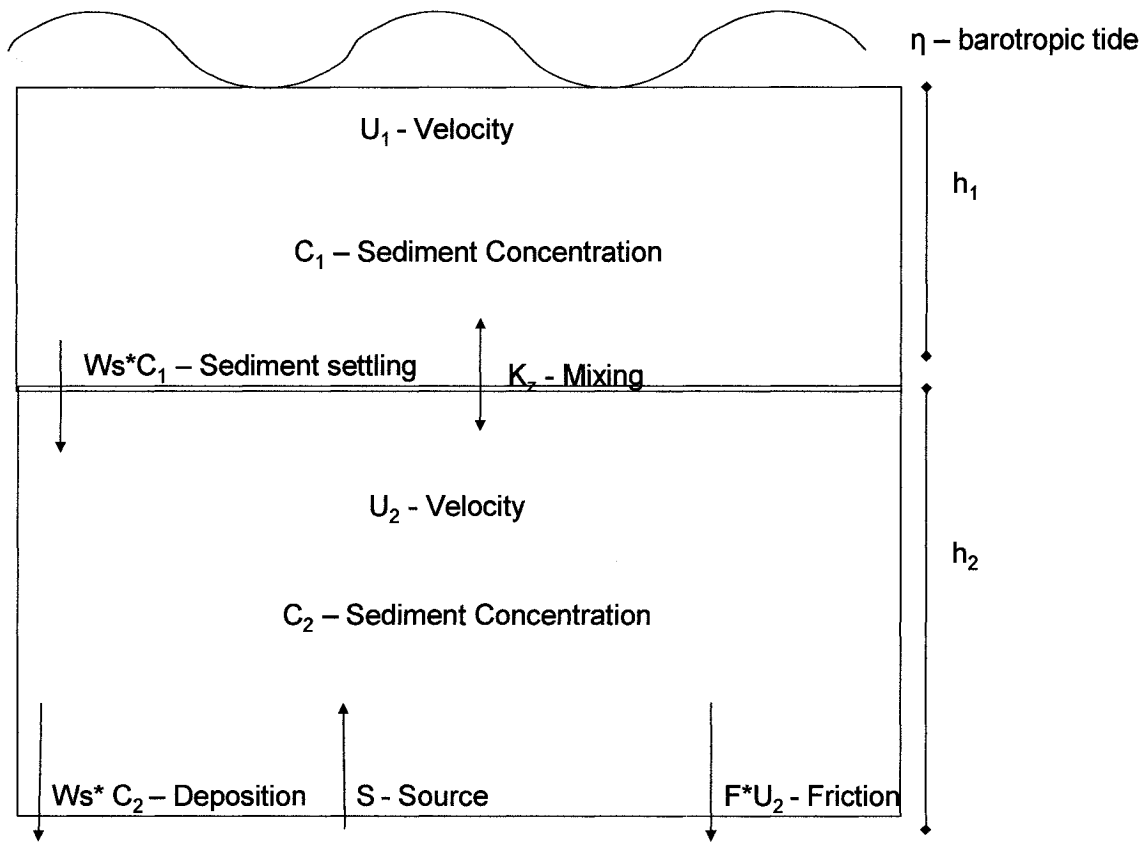


**Figure 6-7 Two-layer water column model for sediment and velocity. The relevant processes are, sinking, resuspension, tidal velocity, bed friction and vertical mixing.**

The velocity in the top box is dependent on mixing, $K_z$, and the barotropic pressure gradient per unit mass, $g\, d\eta/dx$, while the lower layer is also affected by friction, $F$. The momentum equations for upper (U1) and lower layers (U2) become:

$$\frac{du_1}{dt} = K_z(u_2 - u_1) - g\frac{d\eta}{dx} \qquad \text{Eqn 6-5}$$

$$\frac{du_2}{dt} = K_z(u_1 - u_2) - g\frac{d\eta}{dx} - Fu_2 \qquad \text{Eqn 6-6}$$

The density difference between the two boxes is used to determine the mixing between them. The density in each box is dependent on vertical mixing, $K_z$, and advection, $u$, of the longitudinal salinity gradient, $\frac{\partial \rho}{\partial x}$. The mass conservation implies:

$$\frac{\partial \rho_1}{\partial t} = K_z(\rho_2 - \rho_1) - u_1 \frac{\partial \rho}{\partial x} \qquad \text{Eqn 6-7}$$

$$\frac{\partial \rho_2}{\partial t} = K_z(\rho_1 - \rho_2) - u_2 \frac{\partial \rho}{\partial x} \qquad \text{Eqn 6-8}$$

To calculate the density based mixing coefficient, $K_z$, we assume a constant longitudinal density gradient that is not a function of depth. We then use the measured rate of change in our two boxes with the measured velocity of the two layers to rearrange the density equations to give:

$$Kz = \frac{\frac{\partial(\rho_1 - \rho_2)}{\partial t} - \frac{\partial \rho}{\partial x}(u_2 - u_1)}{2(\rho_2 - \rho_1)} \qquad \text{Eqn 6-9}$$

Once the mixing coefficient is calculated we are able to incorporate it into the sediment balance of the lower layer to find the source term $S$ in equation 6-4.

$$S = \frac{dc_2}{dt} - K_z(c_1 - c_2) + \frac{W_s c_2}{h_2} - \frac{W_s c_1}{h_1} \qquad \text{Eqn 6-10}$$

### 6.5.1 Model Results

Looking at the fall sediment concentration in both layers, we see that they are in phase and are nearly equal in concentration at all times (Figure 6-8). The lower layer concentrations are slightly greater than those of the upper layer. Using the density to estimate the mixing, we see that mixing does not have a clear pattern from ebb to flood tide. Mixing does not necessarily increase during flood tide as we might expect based on

the SIPS theory. A sediment source is required to create the large spike we observed during flood tide. The source spike coincides with the spike in our bottom sediments. Once the large source spike has delivered sediments to the water column, the largest positive mixing event coincides with the maximum suspended sediment concentration observed in the lower layer.

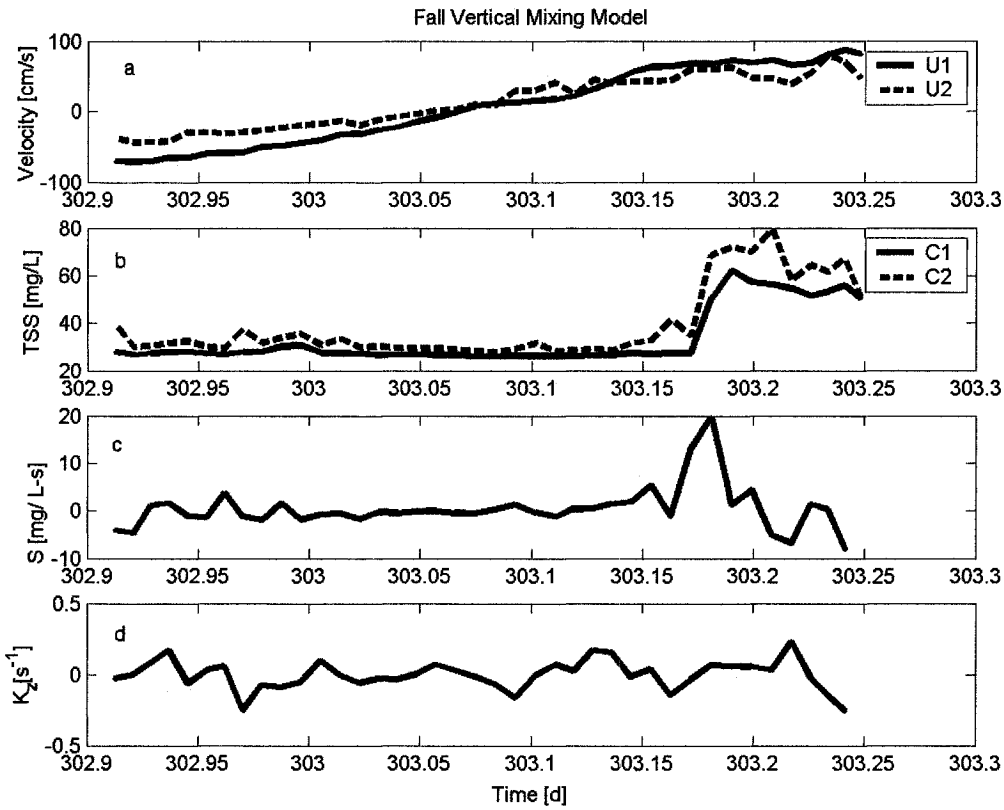


**Figure 6-8 Fall mixing model results over one tidal cycle. Panel a) is velocity east for the top(U1) and bottom layers (U2), b) is suspended sediment concentration for the top(C1) and bottom layer(C2), c) is the source term in the lower layer, and d) is vertical mixing inferred from density in upper and lower layers. There is no tidal pattern to the vertical mixing.**

Summer experiments reveal a different pattern (Figure 6-9). Sediment concentrations in the two boxes are distinct in terms of their temporal patterns and concentrations until maximum flood tide when the concentrations are equal. This

suggests there is enhanced mixing occurring during the flood tide that leads to greater homogenization of sediments throughout the water column. However, there is no pattern in the density derived mixing $K_z$. The largest positive mixing does occur during flood tide and coincides with the initial increase in the upper layer sediment concentration, $C_1$. The pattern in the lower layer sediment concentration is largely dependent on the source term.

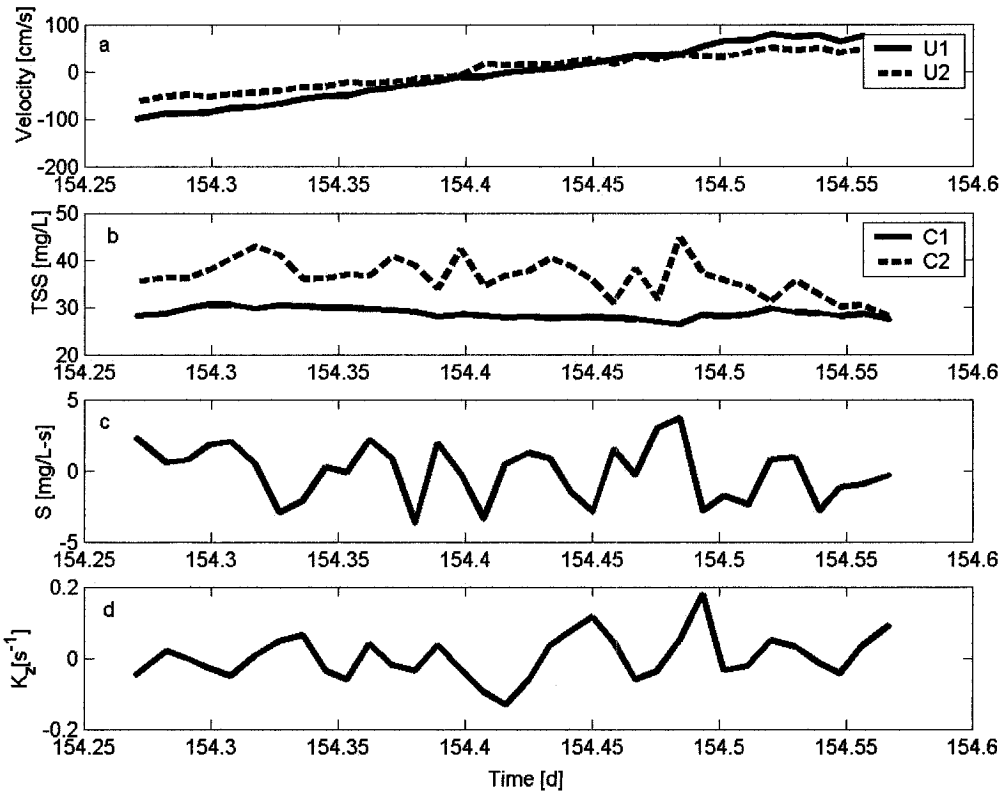


**Figure 6-9 Summer mixing model results. Panel a) is velocity east for the top(U1) and bottom layers (U2), b) is suspended sediment concentration for the top(C1) and bottom layer(C2), c) is the source term in the lower layer, and d) is vertical mixing inferred from density in upper and lower layers. There is no tidal pattern to the vertical mixing. At max ebb the sediment concentrations are distinct and by max flood tide the concentrations in the upper and lower layer are the same.**

Despite trends in the sediment concentrations of the upper and lower boxes and in $Z_{cm}$, there is no appreciable tidal trend in mixing based on the density. The increase in $Z_{cm}$ over the transition from ebb to flood was assumed to be caused by a decrease in

stratification, but the density differences in the upper and lower water column do not appear related to sediment concentration. Within this conceptual framework, tidal asymmetry in stratification, SIPS, is not sufficient to create large spikes of sediment. Spikes of high TSS measured in the upper water column must be generated by an increase in bed availability or horizontal advection of a sharp sediment feature. Enhanced vertical mixing can sustain high concentrations in the upper water column and contribute to a flux into the estuary, but it is not the sole process creating a net flux into the estuary.

## 6.6 Discussion

The direction of the net suspended sediment flux is determined by the timing and magnitude of peak velocities and sediment concentrations. Sediment concentrations and tidal velocities vary over a wide range of timescales. A previous spectral analysis of suspended sediment variability in San Francisco Bay reveals that the majority of explainable variance (65%) is due to processes occurring on timescales longer than the tidal (24 hrs) timescale. These longer scale processes include, spring-neap tidal variability (21%), monthly tides (19%), semi-annual (12%) and annual freshwater inputs (13%) (Schoellhamer 2002). Based on the USGS timeseries, we see that in general the velocity and sediment signals examined over a month show a strong spring-neap cycle. If we low pass filter the root-mean-squared velocities, $U_{rms}$, and sediment concentration, by inspection, we observe a strong coherence between the signals during spring and summer (Figure 6-10a,b). However, during the fall this pattern breaks down when there are large peaks in sediment concentration on one phase of the tide alone, suggesting important

variability on timescales shorter than 24 hours (Figure 6-10c). Although we do not know what physical mechanisms cause these asymmetric large spikes, we may be able to estimate the net direction of the flux over the annual cycle based on asymmetries in flood and ebb tide velocities.

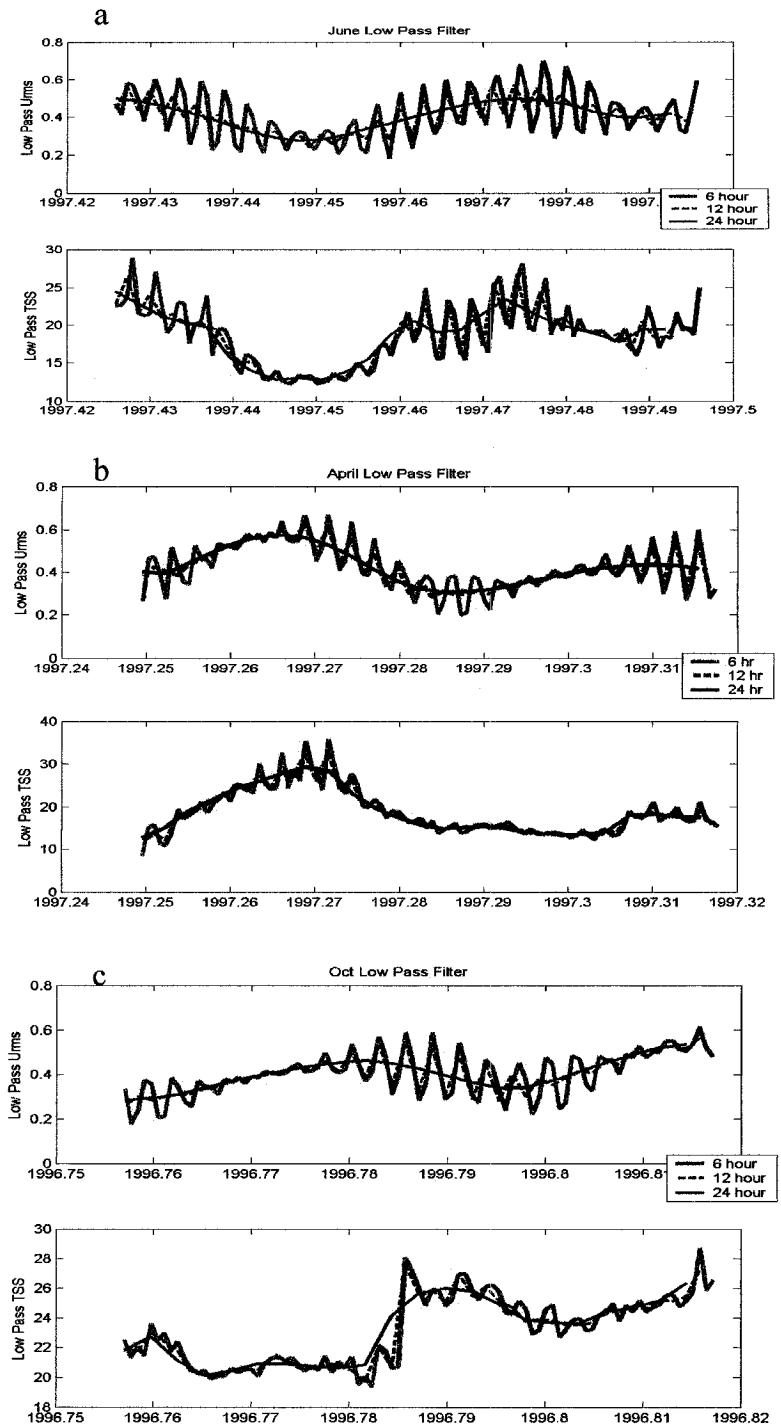


**Figure 6-10 USGS low pass filtered velocity and suspended sediment signals. The coherence between signals appears strong during spring and summer but weak during October.**

If suspended sediment concentration is proportional to speed, we can examine the annual variation in velocity to predict the direction of the annual net flux of sediment. To investigate if suspended sediment concentration is proportional to current speed, we constructed a general linear model utilizing the statistical software package, JMP 5.1. We used a least squares approach to test for significance in several relationships: 1) the absolute value of tidal velocity and suspended sediment concentration for all seasons; 2) large flood tide velocity and suspended sediment concentration by season; 3) and large ebb tide velocity and concentration by season. The condition for large velocity was 0.5 m/s based on visual inspection of the sediment and velocity relationship

For both the USGS data and our measurements, there is a positive slope between absolute velocity and concentration. The equation of the line for all seasons comparing the absolute velocity and TSS was

$$Tss_{as}(mg/L) = 7.7 * |U_{CA}| + 16 \qquad \text{Eqn 6-11}$$

This line had a poor fit in terms of $R^2$, 10%, but nonetheless was statistically significant, with a p-value <.0001. If we re-examine this linear relationship, considering just the large velocities (for both ebb and flood), there is a better fit in terms of $R^2$, 20%, and the empirical equation for max velocity and suspended sediment concentration becomes:

$$Tss_{,\arg e}(mg/L) = 19 * |U|_{l\arg e} + 9 \qquad \text{Eqn 6-12}$$

We extended the analysis to separate large ebb or flood velocities across seasons to see if there were tidal asymmetries in this relationship. For April and June, both ebb and flood large velocities were positively, and significantly, correlated with sediment concentration (Table 6-3). The slope varies across seasons but within June and April,

there is no statistical difference between suspended sediment concentration and large ebb or large flood velocities (Table 6-3).

**Table 6-3 Relationship between USGS velocities and suspended sediment concentrations. The units of the slope are (s-mg/m-L) and the intercept are (mg/L).**

| | Oct-96 | | | Apr-97 | | | Jun-97 | | |
|---|---|---|---|---|---|---|---|---|---|
| | Slope | Intercept | $R^2$ | Slope | Intercept | $R^2$ | Slope | Intercept | $R^2$ |
| All Large Velocity | 14 | 14 | 0.24 | 29 | 2.4 | 0.25 | 15 | 10 | 0.23 |
| Large Ebb Velocity | 17 | 12 | 0.38 | 27 | 1.4 | 0.25 | 15 | 11 | 0.23 |
| Large Flood Velocity | 24 | -3 | 0.00 | 30 | 1.4 | 0.25 | 14 | 11 | 0.23 |

The pattern changes for the October 1996 data set. During this period, large ebb tide velocities have a significantly positive correlation with suspended sediment concentrations, but large flood tide velocities are not related to sediment concentrations (Table 6-3). These findings further emphasize the unknown mechanisms governing the suspended sediment concentration during the fall season, especially on sub-tidal timescales.

Despite the unknown mechanisms governing the fall sediment variability, we our studies show a statistically significant relationship between TSS and velocity magnitude. Examining a histogram of the last five years tidal height converted to tidal velocities through equation 6-1, we can see that the largest magnitude velocities occur more often on ebb tide (Figure 6-11). Because ebb tide velocities are likely to be greater than flood velocities, and there is a positive correlation between ebb velocity and concentration for

all seasons, we conclude that the suspended sediment flux over long time scales will be out of the estuary.

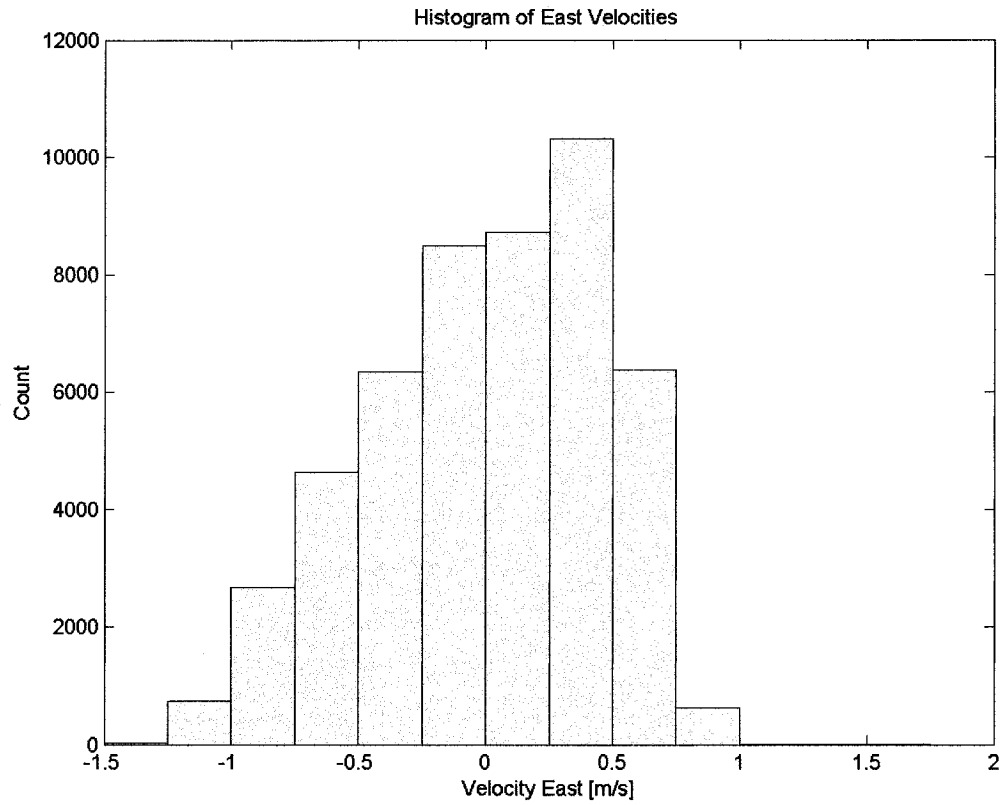


**Figure 6-11 Histogram of 2000-2005 6 minute tidal data converted to tidal velocity using eqn 6-1.**

Taking the average of the tidal pumping fluxes calculated (excluding our fall 2002 measurements) we estimate the annual flux of sediment leaving the estuary is about -53 kg/s or -1.8 Mtons/yr. Historical estimates of long term average for sediment load entering the San Francisco Bay from local tributaries is 0.83 million short tonnes suspended-sediment (Krone 1979) equivalent to 0.75 Mt/y. A recent study has calculated the long term load of suspended sediments from the Central Valley is 1.0 Mt/y (McKee et

al. 2006). Together there is approximately 1.75Mt/yr of sediment entering the estuary and the same amount leaving the estuary.

It should be noted that the balance between sediment loading and exports would be very different if our fall 2002 flux measurements were included. Although it cannot be ruled out that our fall data were bad, examination of both data sets suggests that sediment transport into and out of the estuary is dependent on average trends as wells as short timescale fluctuations in concentration. It could be that on average, sediment transport is out of the estuary, but sediment transport is dominated by large events whose physical origins remain unknown. Future studies should consider the possibility that sediment transport is not always out of the estuary. The underlying physical mechanisms could potentially be elucidated if additional work was done closer to the bed. Separating events due to resuspension and advection of sediment fronts remains a difficult and important challenge in this area.

The majority of suspended sediment transport in San Francisco Bay is due to tidal resuspension as opposed to river inputs of suspended sediment (Shoellhammer et al 2002). Changes in the amount of sediment delivered from the upper watershed, or in the amount trapped in tidal wetlands will first affect the local sediment balance but eventually those changes will propagate through the system. Given that the system seems to be in balance, the average particle residence time would be a useful management tool in understanding how changes in sediment loading would propagate throughout the estuary. Clearly sediment deposition and resuspension are highly variable throughout the bay; however, if on average a typical particle path starts at the watershed boundary and ends leaving the estuary through the Golden Gate, export rates would lag

behind import rates. Developing an estimate of this particle residence time would increase our understanding of how quickly the system as a whole would respond to the anticipated decrease in sediment loading due to dams and restoration projects.

# 7 CONCLUSION

Through field experiments and harmonic analysis, we have quantified the seasonal net flux of suspended sediment and chlorophyll between San Francisco Bay and the coastal Pacific. The seasonal conditions studied were: spring, when there are large freshwater flows; summer, when wind patterns bring cool nutrient rich water to the surface along the coast; and fall, the transition from upwelling conditions to winter storm conditions.

Through mathematical decomposition and simple models, we distinguished some of the important physical processes driving the net flux. The net flux consists of an advective and dispersive component. Advection is due to freshwater flow; therefore, the magnitude of the advective flux is proportional to flow rate and the direction is always out of the estuary. Dispersive fluxes were broken down into several different physical mechanisms, tidal pumping, steady circulation and unsteady shear flow. Tidal pumping dominated the dispersive flux for all scalar concentrations year-round.

The tidal pumping flux is dependent on the timing asymmetries between maximum velocity and the average scalar concentrations. Asymmetries in the velocity structure are caused by the geometry of Central Bay. Flood waters enter Central Bay through the narrow constriction at the Golden Gate as a jet, waters leaving the estuary

exit as a radial drain. Asymmetries in flood and ebb tide concentrations depend on the spatial gradients and mixing that occurs throughout the tidal cycle. Mixing over the tidal cycle is primarily due to a tidally trapped eddy that forms near Angel Island (Fram et al. 2006).

Because tidal pumping is only dependent on the cross sectionally averaged concentrations we can model it with a classic Fickian flux with a dispersion coefficient $K_x$ and the east-west scalar gradient. The gradients for chlorophyll and sediment are governed by different processes. The chlorophyll gradient is determined by differences in growth conditions within the coastal ocean and estuary. The sediment gradient is determined by a wide range of processes, occurring on timescales anywhere from an hour to a year.

The chlorophyll gradient changes direction seasonally based on the timing and magnitude of blooms in the coastal ocean and estuary. During the summer while coastal upwelling occurs, chlorophyll concentration is higher in the ocean than in the estuary creating a gradient driven dispersive flux of coastal phytoplankton into the estuary. The opposite is true during spring, when freshwater flows promote blooms in South San Francisco Bay, and the dispersive is out of the estuary. While the magnitude and timing of these fluxes may change annually or inter-annually depending on the specific physical and biological conditions, the seasonal direction of chlorophyll fluxes measured in this study are consistent with physical and biological process of a typical year.

Although the dispersive transport depends on the distribution and timing of blooms, blooms due to local growth are relatively rare in Central Bay. The accumulation of phytoplankton within Central Bay is limited by large dispersive transport rates. When

the dispersive transport rate is small, local growth is more important. Measured dispersion coefficients were smallest during fall and largest during spring. This means that blooms driven by local growth conditions can occur in Central Bay during the fall, but not during spring. During our study, the highest concentration of chlorophyll was observed during the spring, indicating that spring phytoplankton were derived elsewhere, most likely in South Bay, and transported into Central Bay.

Future work should focus on relating the timescale of the ocean-estuary chlorophyll gradient to the transport timescale because the total transport into and out of a dispersion dominated estuary depends on how long the specific chlorophyll gradient persists. Specifically in San Francisco Bay, future work would greatly benefit from the routine measurement of water quality parameters in the adjacent coastal waters. Incorporating satellite imagery with shipboard observations would be a useful tool in getting adequate spatial coverage to estimate the gradient. Considering such phenomenon in a seasonal and inter-annual context may provide more insight into how climate or anthropogenic changes will affect the primary productivity of similar coastal bays and estuaries.

Although the net sediment flux was dominated by tidal pumping, processes occurring at both longer and shorter timescales are important as well. The net sediment flux was outward during spring and summer, but was inward during the fall. This flux into the estuary was largely due to a big pulse of sediment that occurred during max flood tide. We compared our fall flux results to a suspended sediment time series collected from 1996-1997. Both data sets have very large spikes of suspended sediment, occurring at maximum velocity. During October 1996, the sediment spike observed occurred

during maximum ebb tide, creating a flux out of the estuary, whereas our fall 2002 spike occurred during maximum flood. To investigate if vertical stratification and mixing could explain this spike during flood tide, we constructed three simple metrics, a sediment mixing coefficient, $K_z$, a source term, $S$, and height above the bed to which the majority of mass is diffused, $Z_{cm}$. These metrics showed that although sediments may be able to travel higher up in the water column during flood tide, the concentration difference between flood and ebb tide ultimately determine the direction of the flux. Differences in vertical mixing could not generate a large spike in sediment without a large spike in the source term as well.

Sediment concentrations are proportional the root-mean squared velocity and currents are ebb dominated. So over time, despite occasions when there are large spikes during flood tide, the tidal pumping flux should be out of the estuary. Estimates of annual sediment loading from the watershed are in balance with our estimated flux of sediment out of the estuary. Future sediment studies in the area should investigate if there is a mechanistic reason for the contrast in fall sediment dynamics compared to other seasons. Additionally, future studies would benefit from focusing more explicitly on the bed interaction with the water column. All of the observations used in this analysis were at least 10m off the bed. This may have been too far away to adequately capture vertical dynamics such as sinking and resuspension.

Although some processes are still not understood, such as the processes driving sediment dynamics in the fall, or transport and mixing of phytoplankton in the adjacent coastal ocean, the basic pattern and mechanisms of residual fluxes are clear. Advection is seasonally proportional to freshwater flows and always creates a flux out of the estuary.

Advection is generally less important than the dispersive component in determining the magnitude and direction of the total flux. The dispersive component is dominated by tidal pumping and is the most important process driving net ocean-estuary exchange. Collectively these investigations characterize the residual fluxes of scalar constituents between San Francisco Bay and the coastal ocean and will hopefully help guide future studies and management decisions in San Francisco Bay and other urbanized estuaries where similar processes create ocean-estuary exchange.

# References


Baines, S. B. and N. S. Fisher (2001) Interspecific differences in the bioconcentration of selenite by phytoplankton and their ecological implications. Marine Ecology-Progress Series **213**: 1-12.

Chavez, F. P., R. T. Barber, P. M. Kosro, A. Huyer, S. R. Ramp, T. P. Stanton and B. R. d. Mendiola (1991) Horizontal Transport and the distribution of nutrients in teh coastal transition zone off Northern California: effects on primary production, phytoplankton biomass and species composition. Journal of Geophysical Research-Oceans **96**(C8): 14833-14848.

Chavez, F. P., J. T. Pennington, C. G. Castro, J. P. Ryan, R. P. Michisaki, B. Schlining, P. Walz, K. R. Buck, A. McFadyen and C. A. Collins (2002) Biological and chemical consequences of the 1997-1998 El Nino in central California waters. Progress in Oceanography **54**(1-4): 205-232.

Cheng, R. T. and J. W. Gartner (1985) Harmonic-Analysis of Tides and Tidal Currents in South San-Francisco Bay, California. Estuarine Coastal and Shelf Science **21**(1): 57-74.

Cloern, J. E. (1982) Does the Benthos Control Phytoplankton Biomass in South-San-Francisco Bay. Marine Ecology-Progress Series **9**(2): 191-202.

Cloern, J. E. (1991) Tidal stirring and phytoplankton bloom dynamics in an estuary. Journal of Marine Research **49**: 203-221.

Cloern, J. E. (1996) Phytoplankton bloom dynamics in coastal ecosystems: a review with some general lessons from sustained investigation of San Francisco Bay, California. Reviews of Geophysics **34**(2): 127-168.

Cloern, J. E., A. E. Alpine, B. E. Cole, R. L. J. Wong, J. F. Arthur and M. D. Ball (1983) River Discharge Controls Phytoplankton Dynamics in the Northern San-Francisco Bay Estuary. Estuarine Coastal and Shelf Science **16**(4): 415-&.

Cloern, J. E. and R. Dufford (2005) Phytoplankton community ecology: principles applied in San Francisco Bay. Marine Ecology-Progress Series **285**: 11-28.

Cloern, J. E., C. Grenz and L. VidergarLucas (1995) An empirical model of the phytoplankton chlorophyll:carbon ratio - The conversion factor between productivity and growth rate. Limnology and Oceanography **40**(7): 1313-1321.

Cloern, J. E. and F. H. Nichols (1985) Time Scales and Mechanisms of Estuarine Variability, a Synthesis from Studies of San-Francisco Bay. Hydrobiologia **129**(OCT): 229-237.

Cloern, J. E., T. S. Schraga and C. B. Lopez (2005) Heat wave brings a red tide to San Francisco Bay. Eos Transactions of the American Geophysical Union **86**(7): 66.

Collins, C. A., J. T. Pennington, C. G. Castro, T. A. Rago and F. P. Chavez (2003) The California Current system off Monterey, California: physical and biological coupling. Deep-Sea Research Part Ii-Topical Studies in Oceanography **50**(14-16): 2389-2404.

Conomos, T. J., R. E. Smith and J. W. Gartner (1985) Environmental Setting of San-Francisco Bay. Hydrobiologia **129**(OCT): 1-12.

Dyer, K. R. (1986). Coastal and Estuarine Sediment Dynamics, John Wiley & Sons.

Falkowski, P. G., R. T. Barber and V. Smetacek (1998) Biogeochemical controls and feedbacks on ocean primary production. Science **281**(5374): 200-206.

Fischer, H. B. (1972) Mass transport mechanisms in partially stratified estuaries. Journal of Fluid Mechanics **53**: 671-687.

Fischer, H. B., N. H. Brooks, J. Imberger, R. C. Y. Koh and E. J. List (1979). Mixing in inland and coastal waters. New York, Academic Press.

Fram, J., M. Martin and M. Stacey (2006) Residual Flow Creation: Dispersive Fluxes. Journal of Physical Oceanography **Accepted for publication**.

Ganju, N. K., D. H. Schoellhamer, M. C. Murrell, J. W. Gartner and S. A. Wright (2003). Constancy of the relation between floc size and density in San Francisco Bay. Proceedings of the 7th International Conference on Estuarine Nearshore Cohesive Sediment Transport processes, Glouster Point, Virginia.

Geyer, W. R., J. H. Trowbridge and M. M. Bowen (2000) The dynamics of a partially mixed estuary. Journal of Physical Oceanography **30**: 2035-2047.

Goericke, R., E. Venrick, A. Mantyla, S. J. Bograd, F. B. Schwing, A. Huyer, R. L. Smith, P. A. Wheeler, R. Hooff, W. T. Peterson, G. Gaxiola-Castro, J. Gomez-Valdes, B. E. Lavaniegos, K. D. Hyrenbach and W. J. Sydeman (2004) The state of the California Current, 2003-2004: A rare "normal" year. California Cooperative Oceanic Fisheries Investigations Reports **45**: 27-59.

Hanes, D. H. (2006) Giant sand waves at the mouth of San Francisco Bay. Eos Transactions of the American Geophysical Union **87**(29).

Hansen, D. V. and M. Rattray (1965) Gravitational circulation in straits and estuaries. Journal of Marine Research **5**: 485-496.

Hutchings, L., G. C. Pitcher, T. A. Probyn and G. W. Bailey (1995). The chemical and biological consequences of coastal upwelling. New York, Wiley.

Jassby, A. D., J. E. Cloern and B. E. Cole (2002) Annual primary production: Patterns and mechansims of change in a nutrient-rich tidal ecosystem. Limnology and Oceanography **47**(3): 698-712.

Jassby, A. D., J. E. Cloern and T. M. Powell (1993) Organic-Carbon Sources and Sinks in San-Francisco Bay - Variability Induced by River Flow. Marine Ecology-Progress Series **95**(1-2): 39-54.

Jassby, A. D. and T. Platt (1976) Mathematical Formulation of Relationship between Photosynthesis and Light for Phytoplankton. Limnology and Oceanography **21**(4): 540-547.

Jay, D. A. and J. D. Musiak (1994) Particle Trapping in Estuarine Tidal Flows. Journal of Geophysical Research-Oceans **99**(C10): 20445-20461.

K.H. Mann, J. R. N. L. (1996). Dynamics of Marine Ecosystems, Blackwell Science.

Knowles, N. and D. R. Cayan (2002) Potential effects of global warming on the Sacramento/San Joaquin watershed and the San Francisco estuary. Geophysical Research Letters **29**(18).

Krone, R. B. (1979). Sedimentation in the San Francisco Bay system. San Francisco BayThe Urbanized Estuary. T. J. Conomos. San Francisco, Pacific Division of the American Association for the Advancement of Science: 347-385.

Largier, J. L. (1996). Hydrodynamic exchange between San Francisco Bay and the ocean: the role of oceanic circulation and stratification. San Francisco Bay: the Ecosystem. J. T. Hollibaugh, AAAS: 69-104.

Laws, E. A., T. T. Bannister (1980) Nutrient and light-limited growth of Thalassiosira fluviatilis in continuous culture, with implications for phytoplankton growth in the oceans. Limnology and Oceanography **25**: 457-473.

Leatherbarrow, J. E., L. J. McKee, D. H. Schoellhamer, N. K. Ganju and A. R. Flegal (2005). Concentrations and Loads of Organic Contaminants and Mercury associated with Suspended Sediment Discharged to San Francisco Bay from the Sacramento-San Joaquin River Delta, California. RMP Technical Report San Francisco Estuary Regional Monitoring Program for Trace Substances. Oakland, CA, San Francisco Estuary Institute.

Lucas, L. V., J. E. Cloern, J. R. Koseff, S. G. Monismith and J. K. Thompson (1998) Does the Sverdrup critical depth model explain bloom dynamics in estuaries? Journal of Marine Research **56**(2): 375-415.

Lucas, L. V., J. R. Koseff, J. E. Cloern, S. G. Monismith and J. K. Thompson (1999) Processes governing phytoplankton blooms in estuaries. I: The local production-loss balance. Marine Ecology-Progress Series **187**: 1-15.

Lucas, L. V., J. R. Koseff, S. G. Monismith, J. E. Cloern and J. K. Thompson (1999) Processes governing phytoplankton blooms in estuaries. II: The role of horizontal transport. Marine Ecology-Progress Series **187**: 17-30.

Malone, T. C., W. M. Kemp, H. W. Ducklow, W. R. Boynton, J. H. Tuttle and R. B. Jonas (1986) Lateral Variation in the Production and Fate of Phytoplankton in a Partially Stratified Estuary. Marine Ecology-Progress Series **32**(2-3): 149-160.

Martin, A. P. (2003) Phytoplankton patchiness: the role of lateral stirring and mixing. Progress in Oceanography **57**(2): 125-174.

McKee, L. J., N. K. Ganju and D. H. Schoellhamer (2006) Estimates of suspended sediment entering San Francisco Bay from the Sacramento and San Joaquin Delta, San Francisco Bay, California. Journal of Hydrology **323**(1-4): 335-352.

Newton, J. A. and R. A. Horner (2003) Use of phytoplankton species indicators to track the origin of phytoplankton blooms in Willapa Bay, Washington. Estuaries **26**(4B): 1071-1078.

Okubo, A. (1973) Effect of shoreline irregularities on streamwise dispersion in estuaries and other emabyments. Netherlands Journal of Sea Research **6**(2): 213-224.

Pennington, J. T. and F. P. Chavez (2000) Seasonal fluctuations of temperature, salinity, nitrate, chlorophyll and primary production at station H3/M1 over 1989-1996 in Monterey Bay, California. Deep-Sea Research II **47**: 947-973.

Pringle, J. M. and P. J. S. Franks (2001) Asymmetric mixing transport: A horizontal transport mechanism for sinking plankton and sediment in tidal flows. Limnology and Oceanography **46**(2): 381-391.

Ribeiro, C. H. A., J.J Waniek, J. Sharples (2004) Observations of the spring-neap modulation of the gravitational circulation in a partially mixed estuary. Ocean Dynamics **54**: 299-306.

Roegner, G. C. and A. L. Shanks (2001) Import of coastally-derived chlorophyll a to South slough, Oregon. Estuaries **24**(2): 244-256.

Schoellhamer, D. H. (2002) Variability of suspended sediment concentration at tidal to annual time scales in San Francisco Bay , USA. Continental Shelf Research **22**: 1857-1866.

Simpson, J. H., J. Brown, J. Matthews and G. Allen (1990) Tidal Straining, Density Currents, and Stirring in the Control of Estuarine Stratification. Estuaries **13**(2): 125-132.

Stacey, M. T., J. R. Burau and S. G. Monismith (2001) Creation of residual flows in a partially stratified estuary. Journal of Geophysical Research-Oceans **106**(C8): 17013-17037.

Stommel, H. and H. G. Farmer (1952). On the Nature of Estuarine Circulation, Woods Hole Oceanographic Institute.

Uncles, R. J. and D. H. Peterson (1996) The long-term salinity field in San Francisco Bay. Continental Shelf Research **16**(15): 2005-2039.

Venrick, E. L. (2002) Floral patterns in the California current system off southern California: 1990-1996. Journal of Marine Research **60**(1): 171-189.

Walters, R. A., R. T. Cheng and T. J. Conomos (1985) Time Scales of Circulation and Mixing Processes of San-Francisco Bay Waters. Hydrobiologia **129**(OCT): 13-36.

Wilkerson, F. P., R. C. Dugdale, A. Marchi and C. A. Collins (2002) Hydrography, nutrients and chlorophyll during El Nino and La Nina 1997-99 winters in the Gulf of the Farallones, California. Progress in Oceanography **54**(1-4): 293-310.

Williams, P. B. (2001). Is there enough sediment? State of the Estuary, San Francisco, CA.